High Pressure and Low Temperature Equations of State for Aqueous Magnesium Sulfate: Applications to the Search for Life in Extraterrestrial Oceans, with Particular Reference to Europa.

Steven Vance

A dissertation submitted in partial fulfillment
of the requirements for the degree of

Doctor of Philosophy

University of Washington

2007

Program Authorized to Offer Degree: Department of Earth and Space Sciences

University of Washington
Graduate School

This is to certify that I have examined this copy of a doctoral dissertation by

Steven Vance

and have found that it is complete and satisfactory in all respects,
and that any and all revisions required by the final
examining committee have been made.

Chair of the Supervisory Committee:

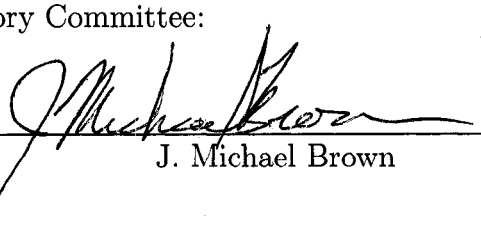

J. Michael Brown

Reading Committee:

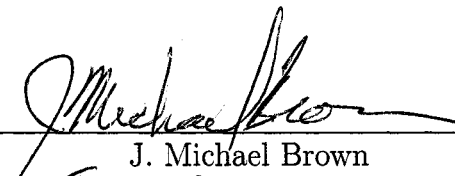

J. Michael Brown

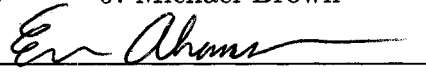

Evan Abramson

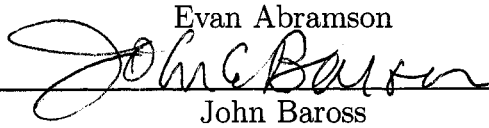

John Baross

Date: 11/30/07

In presenting this dissertation in partial fulfillment of the requirements for the doctoral degree at the University of Washington, I agree that the Library shall make its copies freely available for inspection. I further agree that extensive copying of this thesis is allowable only for scholarly purposes, consistent with "fair use" as prescribed in the U.S. Copyright Law. Requests for copying or reproduction of this dissertation may be referred to ProQuest Information and Learning, 300 North Zeeb Road, Ann Arbor, MI 84106-1346, 1-800-521-0600, to whom the author has granted "the right to reproduce and sell (a) copies of the manuscript in microform and/or (b) printed copies of the manuscript made from microform.

Signature 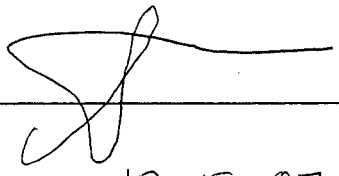

Date 12-5-07

University of Washington

Abstract

High Pressure and Low Temperature Equations of State for Aqueous Magnesium Sulfate: Applications to the Search for Life in Extraterrestrial Oceans, with Particular Reference to Europa.

Steven Vance

Chair of the Supervisory Committee:
Professor J. Michael Brown
Department of Earth and Space Sciences

A prevalence of cold, high pressure ($P > 100$ MPa) environments in the Solar System, and beyond, is discussed in the context of contemporary efforts to understand the origin and abundance of life in the Universe. Constraints on the depths of fluid circulation in extraterrestrial seafloors are explored through a model for the development of microfractures in olivine through cooling. For the example of Europa, we estimate a factor of four in per-unit-area hydrogen flux from serpentinization as compared with calculations for Earth's seafloor. Uptake of seafloor salt by an incipient thermal plume is suggested as a stay on buoyancy and a driver for stratification in the Europa's ocean. An apparatus for optical measurements in deep-ocean analogue materials is described. Laser-induced phonon spectroscopy is applied to the determination of the velocity of sound in water and in aqueous solutions of $MgSO_4$. The equation of state is deduced for concentrations from 0 to 2.0137 m for temperatures from -20 to 100 °C and pressures as high as 700 MPa. Debye Hückel theory is employed for calculating partial molal volume at infinite dilution. The volumetric contribution of $MgSO_4$ is less than expected above 200 MPa and at the extremes of temperature, indicating a change in ion-water interaction due to increased confinement under these conditions.

TABLE OF CONTENTS

LIST OF TABLES

LIST OF FIGURES

ACKNOWLEDGMENTS

I wish to express my gratitude to the people who volunteered their time and interest: Aaron Schilling in Summer 2004, Lars Gilmore from Fall 2005 to Summer 2006 and Virginia Player from Summer 2006 to Summer 2007.

Special thanks to Nicolas Castle and Hoku West-Foyle, who helped immensely in conceptualizing and executing the laboratory research.

Thanks are also owed to Bill Newhall of Harwood Engineering, Inc., and Pete Zieg at Newport Scientific, Inc., for generously sharing their time and expertise. Much help was received from the staff in the Physics Machine Shop and Chemistry Electronics Shop. Special thanks to Steven Domonkos of the Geophysics Machine Shop, who helped throughout and without whom nothing of use would have been built.

I'm grateful for the guidance and support I received from my advisory committee, and also from the staff and faculty in Astrobiology and Earth and Space Sciences, especially Dr. Michael Harrell.

I wish to thank Everett Shock and his laboratory group for hosting and advising me during a week-long visit early in my studies. Similarly, I wish to thank Prof. Tilman Spohn and the Institut für Planetologie in Münster, Germany for a uniquely stimulating Summer of research. I thank Jody Deming and her lab for a crash course in field microbiology, and for sending me as close to Europa as I'm likely to get.

Lastly, I am happy to acknowledge the support of family and friends, without whom I would not have persisted to this point.

Chapter 1

INTRODUCTION: THE DEEP COLD BIOSPHERE? COLD, HIGH PRESSURE ENVIRONMENTS AS ABODES FOR LIFE

This chapter discusses what is known about extraterrestrial environments in the Solar System and beyond. It identifies open questions in the planetary and astrobiological sciences. It ends with an outline of how the work presented in subsequent chapters adds to current thinking and strengthens the body of basic knowledge that can be brought to bear in future inquiries.

Deep-ocean drilling [D'Hondt et al., 2004], sampling of continental hot springs [Nealson, 2005] and exploration of deep mine shafts [Pedersen et al., 1997] provide evidence that Earth's subsurface supports a vast biosphere [Gold, 1992, Ventura et al., 2007, Whitman et al., 1998]. Hyperthermophilic archaea that inhabit these subsurface environments are among the most ancient of organisms, based on phyologeny [Pace, 1997, Reysenbach and Shock, 2002]. This evidence supports the hypothesis that life began below Earth's surface under conditions of elevated pressure and temperature [Hazen et al., 2002, Trevors, 2002]. A subsurface biosphere on Earth may be the best analog for long-lived extraterrestrial habitats on cold, dry planets like Mars, and in deep subsurface oceans like the one under Jupiter's moon Europa [Jakosky and Shock, 1998].

Hydrostatic pressure at great depths (up to 100 MPa in the Marianas Trench) may strongly affect prebiotic chemistry. These effects may be drastically different in the seafloors of putative icy-moon oceans. For example, hydrostatic pressure at the

seafloor of Europa's ocean may be greater than 200 MPa. In this regime, aqueous sulfate salts — thought to dominate Europa's ocean composition [Kargel et al., 2000] — have positive molar volumes. This fundamental change from "normal" environmental conditions has implications for fluid circulation [Vance and Brown, 2005] and indicates a potential for novel interaction with biotic material. Below Earth's surface, temperature rises rapidly with depth and likely limits the depth at which organisms can thrive. In colder objects like Europa, pressure may be the limiting factor to the persistence of life at great depths [Vance et al., 2007].

1.1 A Prevalence of Cold and Deep Aqueous Environments in the Solar System and Beyond

Of the more than 200 gas-giant planets known to circle other stars[1], those with orbits beyond the frost line for their parent star may harbor icy moons. In addition, a class of larger water-bearing planets, so-called ocean planets ($M_{Earth} < M < 8M_{Earth}$), may be common around other stars [Leger et al., 2004, Raymond et al., 2006]. Internal heating in these planets — primordial and radiogenic — would be sufficient to drive long-lived hydrothermal activity, assuming seafloor properties similar to Earth's.

Oceans may have existed in the inner solar system on Mars and Venus [Baker et al., 2005, Carr, 1996] and Ceres [McCord and Sotin, 2005]. Subsurface water may be abundant on Mars today [*e.g.* Lyons et al., 2005]. In the outer solar system, the icy satellites of the giant planets and the largest trans-neptunian objects are candidate ocean planets. These objects can be divided into two groups based on size. 1) The large satellites, in which pressures are sufficient to form high-pressure ices [*e.g.* Spohn and Schubert, 2003, Tobie et al., 2005a] at the seafloor. This group includes Titan, Ganymede, Callisto, and trans-neptunian objects larger than about 1300 km; and 2) The icy satellites and trans-neptunian objects, ranging in radius from several hundreds

[1] As of March, 2007;
http://vo.obspm.fr/exoplanetes/encyclo/catalog.php

of km up to about 1300 km may host oceans with rocky seafloors. Although Europa is larger, it belongs to this group because of its high rock content (~90%) and the resulting high heat production rate. Because of additional tidal heating, Europa is the most prominent known example of a small ocean planet. Other possible ocean candidates of this group include Triton, Eris (formerly 2003 UB_{313}), Pluto, Titania, and Oberon. Oceans may be present in these objects if they are fully differentiated — a characteristic not yet determined by space missions — and if small amounts of ammonia are present — as is expected in the outer solar system due to the increased abundance of volatiles in that region [Hussmann et al., 2006]. In the largest bodies, substantial ammonia-water oceans should persist even to the present time.

Following is a survey of locations in the solar system where high pressure aqueous environments may occur.

1.1.1 Mars

Surface geology indicates substantial aqueous alteration of the Martian crust has occurred [Squyres et al., 2004]. Interpretations of high-resolution remote sensing data [Russell and Head, 2007] suggest water ice glaciers exist on Mars, perhaps fed from sub-surface reservoirs [Okubo and McEwen, 2007]. The depth of these potential reservoirs is unknown. Montgomery and Gillespie [2005] propose that dewatering of hydrated minerals by heating and depressurization could have provided sufficient fluid to carve the extensive canyons of Vallis Marineris. In this case, the store of subsurface water might be extensive. Montgomery and Gillespie (2005) treat a column of evaporite minerals 4 to 6 km thick, producing 0.6 to 3.4 km of hydraulic head (Pmax 300 MPa). The pressure and temperature of dewatering is important in this application, and needs further investigation. Thus, chemistry of sulfate-bearing solutions at high pressures and low temperatures has applications to Mars.

1.1.2 Icy Jovian Satellites

On Europa and Callisto, induced magnetic field signatures measured by the Galileo probe are strong evidence for a conducting layer in the near surface [Zimmer et al., 2000], well within the icy layer as constrained by gravimetric measurements [Anderson et al., 1998]. In both cases, an aqueous ocean is the most likely interpretation, with sulfate salts expected as the dominant constituents as deep as 180 km [$P \sim 200$ MPa based on moment of inertia constraints obtained from the Galileo orbiter — Anderson et al., 1997], with liquid existing to temperatures as low as 250 K for a saturated eutectic ocean [Kargel et al., 2000, McKinnon and Zolensky, 2003]. Ganymede may have an ionic aqueous ocean as well, but the intrinsic magnetic field prevented measurement of an induced field [Stevenson, 2003].

Of the jovian subsurface oceans, Europa's is most promising in the search for life due to the strong tidal heat input implied by the orbital resonance of Europa with Io and Ganymede [Lipps and Rieboldt, 2005], as hinted at by the moon's young and geologically active surface [e.g. Figueredo and Greeley, 2004]. We discuss applications of solution chemistry to Europa's ocean in greater detail in the chapters that follow.

1.1.3 Icy Kronian Satellites

Saturns moons continue through Cassini spacecraft observations to reveal complex surface and subsurface activity driven by aqueous and hydrocarbon chemistry. The icy moons of Saturn may host aqueous ammonia oceans [Ross and Schubert, 1989, Hussmann et al., 2006, Ruiz and Fairen, 2005]. Saturn's moon, Titan, is of particular interest because of its dense methane atmosphere. Enceladus and Dione are also of interest because they are locked in a 1:2 orbital resonance, similar to the resonances of Io and Europa, and Europa and Ganymede, with attendant tidal dissipation. Enceladus' surface is heavily modified, suggestive of ammonia-water cryovolcanism [Kargel, 1996, Spencer et al., 2006]. Better knowledge of high pressure (100s of MPa in the

larger moons such as Titan and Dione) and low temperature [160 K for saturated NH^3 Hogenboom et al., 1997]) chemistry of ammonia—H_2O may be important for understanding processes in Saturn's moons.

Titan (Saturn's 15th Satellite)

Titan is expected to be mostly ice in composition. Methane in the moons dense atmosphere (1.5 atm at the surface) may be replenished by cryovolcanism from a liquid ocean in the 500 km of icy subsurface. There, the relevant solution chemistry is mixture of ammonium (NH_3^+) with other ions. A ~5% correction to the expected density for high pressure (¿50 MPa) and low temperature [160 K for saturated NH3, Kargel et al., 1991] aqueous ammonia the same order correction seen for concentrated MgSO4, as discussed in Chapter 6 would strongly affect the constraints on Titans internal structure from the inversion of moments of inertia obtained from Cassini-probe data (Sotin, personal communication).

Enceladus (Saturns 8th)

Encaladuss surface cracks are similar to those seen on Europa, and a striking paucity of craters indicates a young surface. South polar jets observed by the Cassini orbiter hint at subsurface aqueous activity [Porco et al., 2006], tidal stress along . The heavily modified surface hints at geologic processes comparable to those on Europa, caused perhaps by tidal heating driven by Enceladus 1:2 orbital resonance with Dione. Depending on the rheology of Enceladus, an interior icy mantle could be heated above the 173 K eutectic melting temperature for ammonia-water mixtures. In a satellite Enceladus size (radius 246 km), the internal pressure is on the order of 10 MPa below 100 km depth.

1.1.4 Uranus and Neptune

These large planets have significant inventories of heavy elements (atomic mass greater than 2), as indicated by the observed atmospheric deuterium to hydrogen ratios [de Bergh et al., 1990]. The interiors are expected to be composed of a hydrogen-rich atmosphere in the upper 20% of the planet possibly mixed with "ices" (H_2O, NH^3, CH_4), an icy shell to the lowest 20%, and a solid rocky core [Podolak et al., 1990].

Triton (7th moon of Neptune)

Triton is unique among large icy satellites in the solar system in that its orbit around Neptune is retrograde (angular momentum reversed from that of the solar system). Triton is thought to be $\sim$ 25% water ice, with the rest rocky material. Its surface is relatively uncratered (young), and features ridges similar to those that appear on Europa [Prockter et al., 2005] As a captured Kuiper Belt object, it likely experienced significant tidal heating in the past. The moon will experience significantly more tidal heating as its orbit degrades into Neptunes Roche limit and ultimately disintegrates [Chyba et al., 1989].

1.2 Prebiotic Chemistry in the Solar System

On Earth, and elsewhere, pressure effects on aqueous chemistry may have favored an origin of life at depth. One model for an origin of life envisions single strands of RNA as precursor organisms capable of metabolizing and reproducing, with Darwinian evolution achieved by concentrating molecules in a vesicle precursor to the modern cell membrane [Baaske et al., 2007, Monnard et al., 2002, Szostak et al., 2001]. Modern eukaryotic cell membranes composed of n-acyl chain molecules require "complex" sequential reactions to form, and so probably did not occur in prebiotic environments [Ariga et al., 2005]. Lipid vesicles form readily in the laboratory from a number of possible precursor molecules – decanoic acid forms vesicles in the range of [pH from

6 to 8 Deamer et al., 2002] similar to that for oleic acid and DPPC [2] (optimal at 9 and 6.25, respectively; Furuuchi et al. [2005]. Laboratory vesicles have properties analogous to modern cell membranes [Chen et al., 2005, 2004, Sacerdote and Szostak, 2005]. The decanoic acid molecule forms more readily in high temperature, high pressure environments (up to 300 °C and 200 MPa) than it does under standard conditions [Cody et al., 2000] — indication that deep-sea hydrothermal environments were well-suited to an origin of life in the membrane-first scenario.

The presence of divalent cations (e.g., Mg^{2+}) in aqueous solution inhibits vesicle formation, which could indicate a freshwater origin for life in the membrane-first scenario [Monnard et al., 2002]. If elevated pressures encourage the formation of vesicles despite the effect of dissolved salts, an oceanic origin of life may yet be consistent with the membrane-first scenario.

1.3 Pressure's Role in Planetary Processes as Revealed by the Present Contribution

This work adds to the scientific questions identified above by treating the prospects for life in cold, deep environments and considering novel energy sources that may occur in them. Chapter 2 comprises contributions from multiple authors. I contributed by developing the model framework for fluid percolation in extraterrestrial seafloors through time and by making the initial calculations of heat and hydrogen production from serpentinization in such systems. I acted as a principle investigator in the remainder of the effort, recruiting Jelte Harnmeijer for further development of the geochemistry, Jun Kimura for heat generation by viscous fluid flow through the porous seafloor, and Hauke Hussmann for estimates of tidal heating, ocean temperature and selection of the bodies considered. Chapter 3 proposes a mechanism for stratification in Europa's ocean due to pressure's effect on fluid chemistry. In the development of these ideas, it became clear that proper study of possible deep, cold biospheres requires

[2] dipalmitoyl-L-alpha-phosphatidylcholine

improvements in our understanding of aqueous chemistry at high pressures. Chapters 6 and 5 present new measurements in the aqueous magnesium sulfate system at relevant pressures, temperatures and concentrations, and in water, for which density measurements below zero ^{o}C and above 350 MPa (3500 atmospheres) have not been published to date. Expanded measurements in other aqueous systems and the above-described prebiotic chemical measurements are left for future work.

Chapter 2

DEEP HYDROTHERMAL SYSTEMS IN SMALL OCEAN PLANETS

[1]We examine means for driving hydrothermal activity in extraterrestrial oceans on planets and satellites of less than one Earth mass, with implications for sustaining a low level of biological activity over geological time scales. Assuming ocean planets have olivine-dominated lithospheres, a model for cooling-induced thermal cracking shows how variation in planet size and internal thermal energy may drive variation in the dominant type of hydrothermal system — *e.g.* high or low temperature, or chemically driven. As radiogenic heating diminishes over time, progressive exposure of new rock continues to the current epoch. Where fluid-rock interactions propagate slowly into a deep brittle layer, thermal energy from serpentinization may be the primary cause of hydrothermal activity in small ocean planets. We show that the time-varying hydrostatic head of a tidally forced ice shell may drive hydrothermal fluid flow through the seafloor, which can generate moderate but potentially important heat through viscous interaction with the matrix of porous seafloor rock. Considering all presently known potential ocean planets — Mars, a number of icy satellites, Pluto and other trans-neptunian objects — and applying Earth-like material properties and cooling rates, we find depths of circulation are more than an order of magnitude greater than in Earth. In Europa and Enceladus, tidal flexing may drive hydrothermal circulation and, in Europa, may generate heat on the same order as present-day radiogenic heat flux at Earth's surface. In all objects, progressive serpentinization generates heat on a globally averaged basis at a fraction of a percent of present-day

[1]This chapter was published as Vance et al. [2007].

radiogenic heating and hydrogen is produced at rates between 10^9 and 10^{10} molecules cm^{-2} s^{-1}.

2.1 Introduction

Ice-covered moons and planets are common in the solar system. Each of the outer planets has at least one icy moon, and the Kuiper Belt appears to contain many Pluto-sized minor planets [Brown et al., 2004]. Many of the larger icy moons show signs of extensive and prolonged geological activity, possibly indicating surface processes mediated by subsurface liquid water. In Mars, Europa, Callisto, Enceladus, and Titan, liquid water may persist to the present [Lyons et al., 2005, Zimmer et al., 2000, Kerr, 2005, Spohn and Schubert, 2003, Tobie et al., 2005b], raising the question of whether these planets host active hydrothermal systems similar to those found in Earth's oceans, and whether other planets may have also done so in earlier epochs.

Of the more than 200 gas-giant planets known to circle other stars[2], those with orbits beyond the frost line for their parent star may harbor icy moons. In addition, a class of larger water-bearing planets, so-called ocean planets ($M_{Earth} < M_{Planet} < 8M_{Earth}$), may be common around other stars [Leger et al., 2004, Raymond et al., 2006]. Internal heating in these planets — primordial and radiogenic — would be sufficient to drive long-lived hydrothermal activity, assuming seafloor properties similar to Earth's.

Seafloor spreading caused by mantle convection is the main driver for terrestrial hydrothermal activity; 60% of Earth's internal heat is presently dissipated at spreading centers [Sclater et al., 1980]. One might expect larger ocean planets ($M_{Planet} \geq M_{Earth}$) to drive hydrothermal systems predominantly by this mechanism as well. In ocean moons, primordial heat should be significantly less, and is not likely to drive plate tectonics [McKinnon and Zolensky, 2003]. In some cases tidal heating may drive

[2]As of March, 2007;
http://vo.obspm.fr/exoplanetes/encyclo/catalog.php

mantle convection in ocean moons, but on a more limited basis than occurs on Earth, owing to their lesser internal heating.

For the purposes of this paper — considering interior processes in a variety of objects — we use the term "ocean planet" to refer to icy moons hosting subsurface liquid water, reasoning that variation of formation history among similar-size planets and moons is probably more significant than differences in their subsequent physical evolution. We provide constraints on the depth to which fluid circulation and attending water-rock interaction occur, assuming long-term conductive cooling as the sole means for dissipating heat to the depths considered. Using these constraints, we examine the roles serpentinization- and tidally-driven circulation may play in regulating hydrothermal activity in ocean planets. We focus on small objects – those less massive than Earth, with seafloor hydrostatic pressures less than ~200 MPa. Our model predicts the rocky mantles of these cooler and lower-pressure objects will remain brittle, and thereby allow hydrothermal fluid penetration to depths greater than occur on Earth.

2.2 Ocean Planets in the Solar System

Oceans may have existed in the inner solar system on Mars and Venus [Baker et al., 2005] and Ceres [McCord and Sotin, 2005]. Subsurface water may be abundant on Mars today [*e.g.* Lyons et al., 2005]. In the outer solar system, the icy satellites of the giant planets and the largest trans-neptunian objects are candidate ocean planets. These objects can be divided into two groups based on size. 1) The large satellites, in which pressures are sufficient to form high-pressure ices [*e.g.* Spohn and Schubert, 2003, Tobie et al., 2005a] at the seafloor. This group includes Titan, Ganymede, Callisto, and trans-neptunian objects larger than about 1300 km; and 2) Smaller icy satellites and trans-neptunian objects, ranging in radius from several hundreds of km up to almost 1600 km in the case of Europa, which may host oceans with water-rock interfaces (seafloors). Europa belongs to this group because of its high rock

content (~90%) and the resulting high heat production rate. Because of additional tidal heating, Europa is the most prominent known example of a small ocean planet. Other possible ocean candidates of this group include Triton, Eris (formerly 2003 UB_{313}), Pluto, Titania, and Oberon. Oceans may be present in these objects if they are fully differentiated — a characteristic not yet determined by space missions — and if small amounts of ammonia are present to lower the melting temperature of the mixture — as is expected in the outer solar system due to the increased abundance of volatiles in that region [Hussmann et al., 2006]. In the largest bodies, substantial ammonia-water oceans should persist even to the present time.

Although we would not expect oceans on smaller objects today, they may have existed in the past due to the larger heating rates within the rocky component. Considering past heating adds Ariel, Umbriel, Dione and trans-neptunian objects like Charon, Ixion and Quaoar to the list of possible ocean planets. For Tethys and Iapetus the rock content is much smaller, making differentiation and oceans unlikely, even in the past. Recent Cassini spacecraft observations indicating significant internal heating in Enceladus [Spencer et al., 2006] highlight the possible importance of non-radiogenic energy in small icy bodies. Moment of inertia measurements for Rhea indicate the moon is nearly undifferentiated [Anderson and Schubert, 2007] and therefore unlikely to contain an ocean. Where oceans did exist, fluid-rock interactions may lead to production of heat and organic materials, as discussed below.

2.3 Depth of Fluid Circulation Below an Extraterrestrial Seafloor

The possibility of a deep sub-surface biota increases the space for potential habitation, especially in planets like Mars, where traditional surface environments are verifiably hostile to known organisms [Gold, 1992]. The abundance of Earth's subsurface biota is not well established, but could be comparable to the surface biomass [Pedersen, 2000]. Pressure, temperature, and nutrient access present challenges for putative subsurface organisms, but the ultimate limit to subsurface habitability may be access

to fluid.

For the present calculations, we favor a constraint on fluid circulation depth based on thermal cracking in olivine. This approach sets an upper limit on the depth to which permeability – necessary for fluid circulation – can occur. In the next section we consider what terrestrial rock permeability can say about possible extraterrestrial hydrothermal systems.

2.3.1 Constraints Based on the Permeability of Earth's Oceanic Crust

Estimates of permeability in hydrothermal systems span a range from 10^{-16} to 10^{-9} m^2 [Fisher, 1998]. At mid-ocean ridges and in other places where tectonic activity opens large flow channels in the seafloor, models of flow through hydrothermal systems constrain permeability to around 10^{-12} m^2 [Fisher, 1998, Fisher and Becker, 2000, Becker, 2000]. Moving away from mid-ocean ridges, permeability decreases to 10^{-17} m^2 in older seafloor basalt [age ~65-200 Myr Stein et al., 1995, Sinha and Evans, 2004].

Permeability in Earth's seafloor may diminish over time due to filling of pore spaces, either by silica that precipitates from ambient fluid [Stein et al., 1995], or by the accumulation of sediment [Martin and Lowell, 2000]. Kargel et al. [2000] suggest that Europa's seafloor may be covered with km-thick layers of sulfate precipitates, which might promote high temperature hydrothermal activity in a limited number of locations in the europan seafloor. Whatever the cause of diminished permeability in Earth's older seafloor, we emphasize that a broad range of permeabilities may be consistent with the other hydrothermal system parameters used by Lowell and DuBose [2005]. Applying a broad range to their previous calculation suggests a number of Earth-like hydrothermal systems in a europan ocean between 10^2 and 10^8 [the number of hydrothermal systems in Earth's seafloor is estimated at 10^9; Lowell and DuBose, 2005].

Permeability deeper beneath the seafloor is difficult to constrain. Laboratory

[Martin and Fyfe, 1970, Zimmerman et al., 1986] and bore-hole investigations [Anderson et al., 1985] to ~1 km depth in Earth's lithosphere indicate high temperatures and pressures tend to close pore spaces. In deep oceans like Europa's, where average pressure at the seafloor is ~2-7 times the average in Earth's oceans [Anderson et al., 1998], rock permeability may be limited by high pressures. Conversely, in small bodies like Enceladus, where core pressures approach a mere 20 MPa, and where the presence of ammonia may create ocean temperatures as low as ~ 180 K, rock permeabilities could be much higher than those found in Earth's oceanic crust.

2.3.2 Constraints Based on Thermal Cracking in Olivine

In regions of ocean-ridge systems where fracture-induced large-scale permeability is absent, fluid is expected to circulate through microfracture channels in mantle rock [Lister, 1974, Sinha and Evans, 2004]. A model treating the formation of microscale cracks due to thermal expansion anisotropy and mismatch [deMartin et al., 2004] predicts cracking depths consistent with seismic measurements indicating a transition from partially serpentinized (hydrated) to unaltered peridotite olivine at 3-4 km below the seafloor [Canales et al., 2000]. We apply the model to potential ocean planets in the solar system by estimating the depth to which thermal cracking might occur [deMartin et al., 2004].

The lithosphere is assumed to dissipate heat through conduction, with temperature beneath the seafloor increasing with depth in proportion to thermal conductivity of mantle material [$\lambda \simeq 3.0$ W m^{-1} K^{-1} for silicate rocks in Earth's upper mantle; Hofmeister, 1999] and H_{rad}, the internal radiogenic heat below seafloor depth d [following Schubert et al., 1986]. Pressure below the seafloor is assumed as for a two-layer planet [Turcotte and Schubert, 1982] with core-mantle and water layer densities ρ_{mc} and ρ_w, respectively. For simplicity and for consistency with previous models of dynamics in Europa's ocean [*e.g* Lowell and DuBose, 2005], we choose a value for the density of water $\rho_w = 1000$ kg m^{-3}. Where the majority of the H_2O layer is frozen,

ρ_w is closer to 900 kg m^{-3} (in which case we overestimate the pressure and therefore underestimate the cracking depth). In very deep oceans, near the ice III liquidus pressure, ρ_w can increase by as much ten percent. The presence of salts can increase the density by a comparable amount. We choose lower-layer densities consistent with known bulk densities of the bodies under consideration. For Earth and Mars we consider the increase in pressure (P) below depth d (where hydrostatic pressure is P_d) due to overlying rock, assuming constant rock density, $\rho_m = 3500$ kg m^{-3}, and gravitational acceleration equal to the average value at the surface ($P \simeq P_d + \rho_m g z$). This approach produces results for Earth's subsurface consistent with the preliminary reference Earth model [Dziewonski and Anderson, 1981].

Because we are interested in ocean planets likely to have a water-rock interface at their seafloors, we choose the lower layer density to be greater than or equal to the average density of olivine, $\rho_m \geq 3250$ kg m^{-3}. This eliminates larger icy bodies, including Ganymede, Callisto, and Titan. We admit Enceladus to this list, but only for the maximum plausible seafloor depth of 80 km based on orbital evolution constraints [Porco et al., 2006]; this approach is consistent with a fully differentiated moon with a hydrated rocky core [Barr and McKinnon, 2007]. Other candidates are selected as discussed in Section 2.2, consistent with a recent survey of possible oceans in the solar system based on thermal modeling [Hussmann et al., 2006].

The formation of microfractures is controlled by the development of residual stresses at grain boundaries. In a cooling aggregate, thermal expansion anisotropy between grains will increase stresses along grain boundaries. At high temperatures, residual stresses dissipate via viscous creep processes and cracking is inhibited. At low temperatures, where dissipative processes are sluggish, residual stresses accumulate along grain boundaries. Evans and Clarke [1980] derive the following relation for the evolution of mean stress $\langle\sigma\rangle$ along a grain boundary in an aggregate cooling at a

constant rate:

$$\frac{d\langle\sigma\rangle}{dT} = \frac{12\Omega\dot{\delta}_b D_o E}{\sqrt{3}k_b L^3 \dot{T}} \frac{e^{-Q/RT}}{T}\langle\sigma\rangle - \frac{\beta E \Delta\alpha}{(1+\nu)}. \tag{2.1}$$

The first term on the right hand side of (2.1) accounts for the relaxation of grain boundary stresses through viscous creep processes. The second term describes the elastic contribution of grain boundary stresses owing to thermal expansion anisotropy. Individual parameters are described in Table 2.1.

Residual stresses begin to accumulate along grain boundaries once temperature falls below the viscous-elastic transition temperature T'. In the numerical solution to Eq. 2.1, T' is defined as the temperature obtained by extrapolating the elastic (linear) portion of the curve of σ vs T to zero stress. The analytical expansion solution for T' is [Evans and Clarke, 1980]:

$$T' \approx \frac{Q/R_G}{\ln\left[\frac{12\Omega\delta_b D_o E}{\sqrt{3}nk_b L^3 \dot{T}}\right]}. \tag{2.2}$$

The limiting temperature T' decreases with

The normal stress σ_{yy} on a grain boundary where an elliptical flaw of size x occurs is dependent on T' and given by [Fredrich and Wong, 1986],

$$\begin{aligned}\sigma_{yy}(x) = \quad & \frac{E\Delta\alpha(T'-T)}{2\pi(1-\nu^2)}\left(\frac{4L^2}{4L^2+(2L-x)^2} - \frac{4L^2}{4L^2+x^2}\right. \\ & \left. + \ln\left[\frac{2L-x}{x}\right] - \frac{1}{2}\ln\left[\frac{4L^2+(2L-x)^2}{4L^2+x^2}\right]\right).\end{aligned} \tag{2.3}$$

Microfractures initiate along grain boundaries when tensile stress intensity K_I exceeds a critical factor K_{IC}, a material property (also called the fracture toughness) that is independent of cooling rate. For square grains of size $2L$ with flaws ranging to size a under confining stress P_c, [Fredrich and Wong, 1986],

$$K_I = \sqrt{\frac{2}{\pi a}}\int_0^a \frac{\sigma_{yy}(x)\sqrt{x}}{\sqrt{a-x}}dx - P_c\sqrt{\pi a}. \tag{2.4}$$

Variable	Variable Name	Value	Units	Reference
a	Flaw Size	$a < 2L$	m	
$D_o\delta_b$	Grain Boundary	$1.5 \times 10^{-0.8}$	$m^2\ s^{-2}$	[3]
	Diffusion Coefficient $\times$ Width			
d	Ocean Depth			
	Below Planet Surface			
E	Young's Modulus	197×10^9	Pa	[4]
H	Mantle Radiogenic Heating		W	
k_b	Boltzmann's Constant	1.38×10^{23}	$J\ K^{-1}$	
K_I	Stress Intensity		$Pa\ m^{1/2}$	
K_{IC}	Critical Stress Intensity	0.6 ± 0.3	$Pa\ m^{1/2}$	[5]
L	1/2 Grain Size		m	
n	Fitting Parameter	23		[6]
P_c	Confining Pressure		Pa	
Q	Activation Enthalpy for	3.75×10^5	$J\ mol^{-1}$	[7]
	Grain Boundary			
R	Planet Radius		m	
R_G	Universal Gas Constant	8.314	$J\ mol^{-1}\ kg^{-1}$	
T	Temperature		K or ^oC	
$\dot{T}$	Cooling Rate		$^oC\ s^{-1}$	
T'	Viscous-Elastic		K or ^oC	
	Transition Temperature			

Continued on next page

[3]Hirth and Kohlstedt [1995]

[4]Hirth and Kohlstedt [1995]

[5]deMartin et al. [2004]

[6]deMartin et al. [2004]

[7]Hirth and Kohlstedt [1995]

Table 2.1 – continued from previous page

Variable	Variable Name	Value	Units	Reference
x	Distance		m	
z	Cracking Depth		m	
	Below Seafloor			
$\Delta\alpha$	Thermal Expansion	3.1×10^{-6}	K^{-1}	[8]
	Anisotropy			
β	Boundary Angle	$\pi/6$	radians	
λ	Thermal Conductivity	3.0	W m^{-1} K^{-1}	[9]
ν	Poisson's Ratio	0.246		[10]
Ω	Atomic Volume	1.23×10^{-29}	m^3	
ρ_m	Density of Mantle Rock		kg m^{-3}	
ρ_w	Density of Water	1000	kg m^{-3}	
σ	Stress		Pa	

Table 2.1: Physical properties used in the model for thermal cracking in an olivine mantle below an ocean of depth d below a planet's surface.

Hardness tests and measurements of the onset of permeability in hot-isostatically pressed samples indicate the critical intensity in olivine is $K_{IC} = 0.6 \pm 0.3$ MPa $m^{1/2}$ [deMartin et al., 2004]. Fracturing depends on confining pressure P_c, temperature difference between mantle rock and the viscous-elastic transition $T' - T$, and grain size $2L$. We use this model to find the depth of thermal cracking, z, for grain sizes between 100 μm to 10 mm. We note that larger grain sizes may be expected in regions

[8] Bouhifd et al. [1996]

[9] Hofmeister [1999]

[10] Hirth and Kohlstedt [1995]

of extraterrestrial seafloors that have cooled more slowly than observed regions of Earth's seafloor.

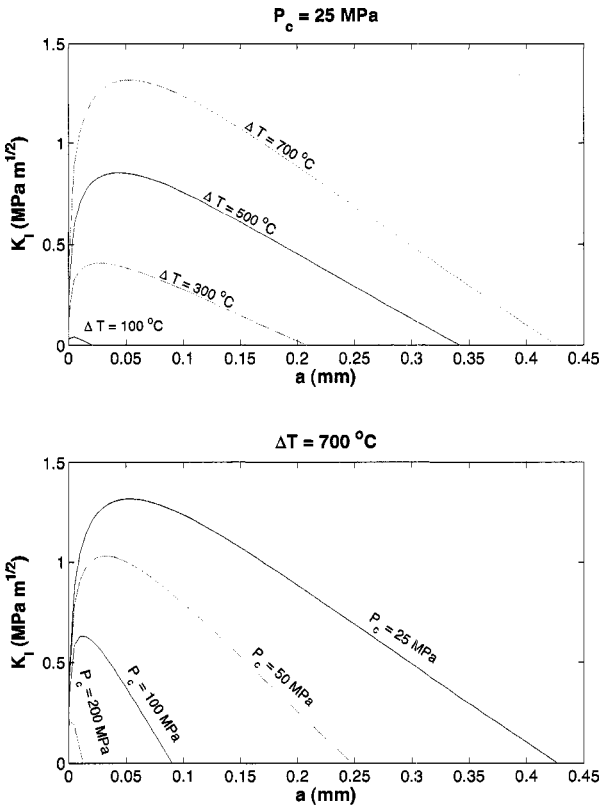

Figure 2.1: Stress intensity K_I in olivine with 1 mm grain size ($L = 0.5$ mm) as a function of maximum flaw size a for a range of temperatures at 25 MPa, and for a range of pressures at 700°C (corrected from deMartin et al. [2004], Fig. 6). For a given set of P_c and T, a is chosen from the maximum of the curve in the iterative calculation of P_c and T corresponding to the critical stress intensity (K_{IC}).

The cracking front is calculated for a given cooling rate ($\dot{T}$) and grain size ($2L$) by setting $K_I = K_{IC}$ and finding corresponding pressures and temperatures in Eq. (2.4). Maximum flaw size a is determined from the maximum of the curve of K_I versus a — that is, we assume once K_I exceeds K_{IC} for a given flaw size a a full grain boundary crack forms. Cracking is expected to occur to some extent for $K_I < K_{IC}$

due to factors not considered here [such as corrosion and non-standard rheology at high temperatures; Atkinson, 1984], and in this sense our model underestimates the depth of cracking. For the present application we assume a bulk cooling rate of $\dot{T} = 1\ ^{o}\mathrm{C\ yr}^{-1}$ where cracking occurs, consistent with cooling rates at mid-ocean ridges. Inhomogeneities in seafloor heating and composition will lead to variation in cooling rate, but the dependence on cooling rate is weak, as discussed below.

The method for finding cracking depths is illustrated in Fig. 2.2. Applying this analysis in regions of Earth's seafloor where mantle material is exposed (so-called metamorphic core complexes), with $\dot{T} = 1^{o}\mathrm{C\ yr}^{-1}$ yields a cracking depth of 0.5 km for 100 μm grains and 6 km for 1 mm grains, where seafloor depth d is taken to be 4 km and H_{rad} is 3.1×10^{13} W in the current era. This result is consistent with the depth of transition to unaltered peridotite in the MARK area of the Mid-Atlantic Ridge inferred from seismic measurements [Canales et al., 2000].

Earth's internal heat is predominantly dissipated at spreading centers driven by mantle convection; it is likely unique among ocean planets in the solar system in this respect. In cooler objects unable to sustain mantle convection, internal heat may be dissipated uniformly by conduction, or by localized melting in the mantle [Lowell and DuBose, 2005]. Cooling is likely slower in extraterrestrial lithospheres. The effect on cracking depth is difficult to determine; slower cooling reduces cracking depth (by roughly a factor of four going from $\dot{T} = 1\ ^{o}\mathrm{C\ yr}^{-1}$ to $\dot{T} = 1\ ^{o}\mathrm{C\ Gyr}^{-1}$) by allowing cracks to heal, but larger grain sizes increase cracking depth (by a factor of roughly two, dependent on planet size and ocean depth, going from 1 mm to 10 mm grains) by magnifying the accumulation of cooling-induced stress.

A lower bound on cooling rate is obtained from the change in a planet's geotherm as internal heating from long-lived radionuclides diminishes over time. In this model, water may be continuously exposed to fresh rock as a planet cools. Present rates of penetration (dz/dt) are given in Table 2.2 for fifteen potential and known ocean planets, assuming grain size 1 mm and cooling rate $\dot{T} = 1^{o}\mathrm{C\ yr}^{-1}$. During the first

$\sim$ 4 Gyr, dz/dt is initially lower by 50%, while the interior is very hot, and then higher by about 20%. In all objects considered, the rate of exposure of new rock is one to ten thousand times slower than present rates of seafloor spreading on Earth (45 mm yr^{-1}). Possible implications for hydrothermal activity are discussed below.

Also notable is the effect of diminished internal heating on the depth of cracking, z (Table 2.2). Where cooling rate, grain size and composition are identical to those for the regions of Earth's seafloor under consideration, fluid circulation is predicted to occur to orders of magnitude greater depth. Revised depths of fluid circulation would change previous estimates of the biopotential of extraterrestrial lithospheres (see Section 2.5.2).

2.4 Sources of Hydrothermal Energy

As on Earth, igneous rocks likely to dominate the ocean floors of icy planets may be rich in ferromagnesian silicates (olivine and pyroxene) that equilibrated at high temperatures. The characteristic temperature and cooling rates of a planet depend on the environment in which it formed — for example, whether the protoplanet thermally equilibrated in the insulating shroud of the solar nebula (or planetary subnebula for icy satellites) — and the initial inventory of radiogenic elements it incorporated. Table 2.2 lists estimates of present-day heating for eleven known and possible ocean planets in the solar system [Schubert et al., 1986]. In this section we discuss other sources of energy potentially important in extraterrestrial hydrothermal systems.

2.4.1 Tidal Heating

Tidal interaction between a satellite and its primary is relevant to the satellite's ocean-rock interface in two ways: 1) energy is dissipated due to tidal flexing, 2) the tidal bulge of the ice shell and ocean induces pressure changes at the seafloor because of mass loading. The first of these can in some cases contribute significantly to the satellite's energy budget. The latter process generates only modest heating

	R_P (km)	M_P ($\times 10^{20}$ kg)	d (km)	T_o (°C)	T_z (°C)	P_z (MPa)	z (km)	dz/dt ($\frac{mm}{yr}$)	H_{rad} ($\frac{mW}{m^2}$)	$\frac{H_{serp}}{H_{rad}}$ (%)	F_{H_2} ($\frac{F}{F_{Earth}}$)
Earth	6371	59742.00	4	0	114	237	6	0.000	60.59	0.00	1
Mars	3397	6420.00	0	0	88	243	12	0.000	22.87	0.01	1
Europa	1565	487.00	100	-10	62	250	25	0.001	8.77	0.05	4
Enceladus	252	0.73	80	-90	0	45	172	0.000	0.61	6.56	32
Titania	789	35.27	269	-69	14	262	91	0.004	2.75	0.43	12
Oberon	761	30.14	280	-79	6	264	106	0.005	2.41	0.52	13
Pluto	1195	131.40	365	-21	-10	268	6	0.000	5.10	0.02	1
Charon	604	16.20	159	-90	97	241	256	0.027	2.19	0.91	21
Eris	1300	172.00	386	-90	-80	285	6	0.000	5.50	0.02	1
Sedna / Orcus	800	40.00	238	-90	31	258	108	0.007	3.38	0.51	17

Table 2.2: Thermal cracking depth and related hydrothermally relevant properties for Earth and other possible ocean planets (past and present). R_P and M_P are equatorial radius and best-known mass, respectively. Seafloor depth (d) is chosen from best presently known values compatible with the existence of an olivine mantle. For potential ocean planets in the outer solar system (lower portion), depths are taken from Hussmann et al. [2006] for a minimum initial ammonia concentration consistent with the existence of a liquid layer at temperature T_o. Depth of thermal cracking (z) below the seafloor in the current era is given for an olivine matrix composed of 1 mm grains cooling at a rate of 1 ^{o}C yr^{-1}. T_z and P_z are temperature and pressure at depth z. dz/dt represents the rate of increase in cracking depth (in mm yr^{-1}) in the current era (seafloor spreading on Earth is currently 45 mm yr^{-1}). Corresponding surface heat flux (H_{serp}) is given as a percent of radiogenic heating (H_{rad}). Per-unit-area molecular hydrogen flux (F_{H_2}) is normalized to Earth's value of 10^9 molecules cm^{-2} s^{-1}. For Enceladus, fluid access is predicted to occur to the deepest interior in the earliest period. Heat and H_2 fluxes for Enceladus are averaged over the moon's presumed 4.5 Gyr history. Fluid rock interactions may continue to the present in Enceladus where low-temperature kinetics limit rapid reaction, or if tidal processes cause episodic high-temperature alteration of the interior (see Section 2.4.1

for generous estimates of rock porosity. However, tidally enhanced fluid flow may be important where thermal gradients are not steep enough to drive vigorous convection.

Heat from Tidal Deformation

Tidal deformation and corresponding dissipation rates will be high for large satellites on eccentric orbits close to their primaries. In the case of synchronously rotating satellites in low-eccentricity orbits, the heating rate is given by [Segatz et al., 1988]

$$H_{tidal} = \frac{21}{2} R^5 n^5 \frac{e^2}{G} Im(k_2), \tag{2.5}$$

where R is the satellite radius, n is the orbital mean motion, e is the orbital eccentricity, and G is the constant of gravitation. $Im(k_2)$ is the imaginary part of the potential tidal Love number k_2 evaluated at the surface. The latter is defined as the ratio of the tidal potential due to the displacement of mass inside the satellite (formation of the bulge) to the potential due to the external perturber. The imaginary part of k_2 is a measure for the tidal phase lag or, equivalently, the relaxation time due to inelasticity of the satellite's material (ice or rock). Here we assume a viscoelastic Maxwell model to calculate the tidal response of the satellites, assuming dissipation occurs only in an ice layer overlying a liquid water ocean.

We calculate the heating rates according to Eq. 2.5 for all the satellites that may contain oceans. For the rigidity and viscosity of ice-I we assume 3.3 GPa, and 5×10^{15} Pa s, respectively. Exceptions are Enceladus and Europa. For Enceladus we adjusted (lowered) the viscosity in order to match the internal heating constraint of 6 GW, which was derived from Cassini data [Spencer et al., 2006] as Enceladus's energy release in the south polar region. For Europa we assumed an ice thickness of 30 km and a viscosity of 5×10^{14} Pa s, which would be consistent with previous structure and tidal heating models. Dissipation in all the models is assumed to occur due to inelasticity of the ice shell. The results are given in Table 2.3.

The height of the tidal bulge (radial displacement u_r) can be calculated from the radial Love number h_2, as

$$u_r = \frac{h_2 \phi}{g}, \tag{2.6}$$

where g is the gravitational acceleration at the satellite's surface and ϕ is the potential due to the primary, evaluated at the satellite's surface. The potential depends on the longitude and co-latitude of the point considered at the surface, and on time, because of the varying distance of the satellite resulting from its orbital eccentricity. Expressions for the potential are given by Segatz et al. [1988] and Moore and Schubert [2000]. Inserting the potential into Eq. 2.6 and calculating the maximum height of the tidal bulge (which will be located at the equator) yields the values given in Table 2.3.

If heated by radiogenic heating alone, Enceladus is not predicted to host an ocean presently. Recent Cassini measurements suggesting strong internal activity [Porco et al., 2006, Spencer et al., 2006] indicate an ocean may exist in this moon. We thus assume a typical internal structure model including an ocean (see caption, Table 2.3) to calculate the tidal deformation and dissipation for Enceladus. Note that a heat production rate based on our simple choice of ice thickness and ice viscosity may not necessarily represent a steady state in which the heat production will be in equilibrium with the heat flow through the ice shell. To search for equilibrium states requires detailed modeling of possible temperature profiles and the resulting heating rates, which would be beyond the scope of this paper. In the case of Enceladus the values are chosen to be consistent with the heat release observed by Cassini. They do not describe a thermal equilibrium state of Enceladus.

As shown in Table 2.3, significant tidal heating can be expected on Europa and Enceladus. For all other bodies considered here, heating will be less than 1% of the total heat budget. Radial displacement at the satellites' surfaces (u_r) is about 27 m on Europa and a few tens of cm for Enceladus and Triton. With an order of only a

few cm or less, u_r is negligible (but non-zero) for the other objects considered here.

Tidal heating rates mainly depend on the orbital eccentricity. That value is in general expected to be even greater in the past because it is usually damped by dissipation within the satellite, a process occurring on a time-scale of billions or, at a minimum, millions of years. Thus, the present-day value for tidal dissipation may be representative of most of a satellite's history. One exception occurs when the orbital eccentricity of a satellite is forced by that of another due to a mean motion resonance. Io, Europa, and Ganymede, share a 4:2:1 resonance. Enceladus is locked in a 2:1 resonance with Dione. Where resonances occur, orbital eccentricities may be forced to non-zero values depending on the nature of the resonance. Coupling with the satellites' thermal states may lead to oscillation of the orbital elements with time. The phenomenon may have important consequences for the heat budgets of satellite systems [Hussmann and Spohn, 2004], but full consideration in the present context is left for future work.

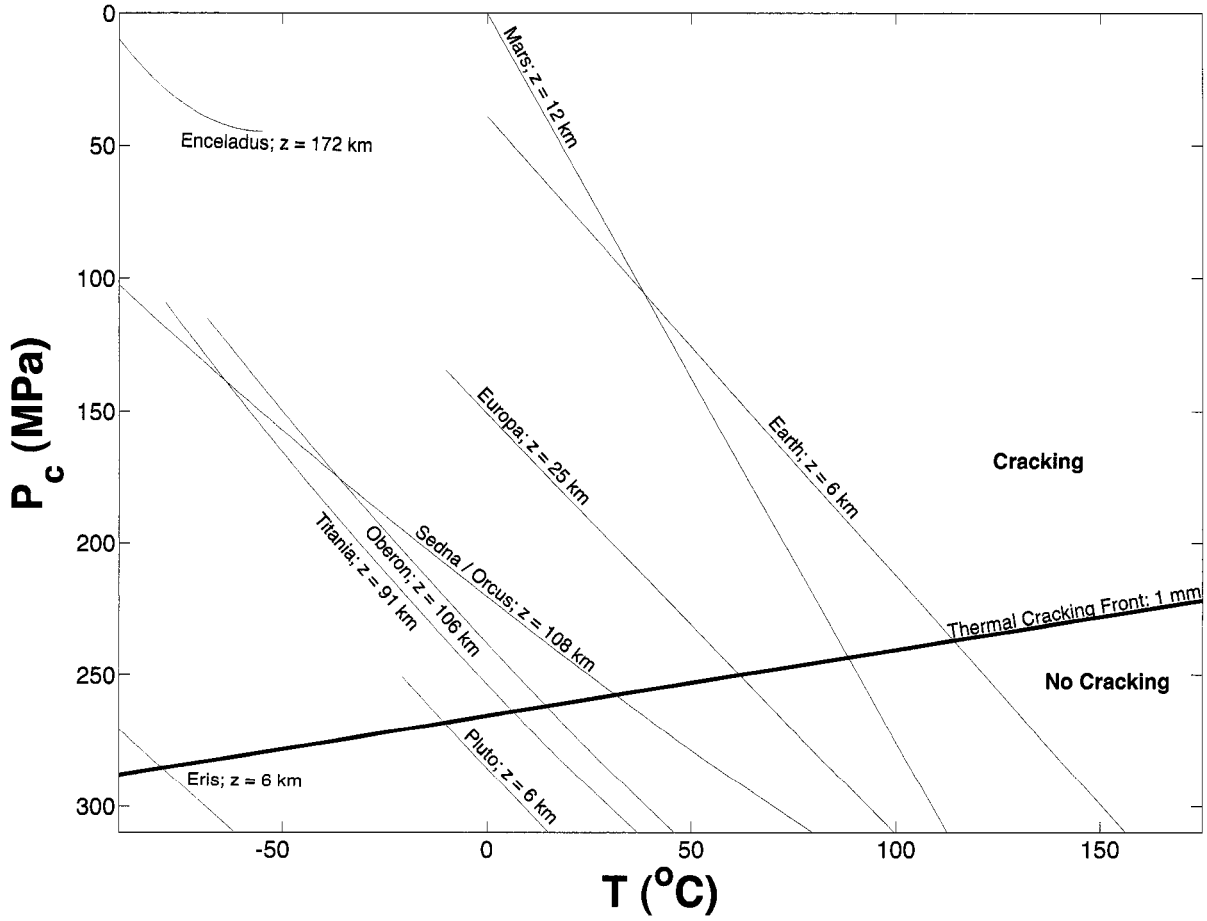

Figure 2.2: Pressure-temperature profiles in planetary seafloors. Temperature (in ^{o}C) is plotted versus confining pressure P_c for a two layer object starting at seafloor depth z shown next to each object's name. Thermal cracking is predicted to occur to critical pressures and temperatures depicted here for olivine with 1 mm grain size, assuming a critical stress intensity of 0.6 MPa m$^{1/2}$ and a cooling rate of 1 ^{o}C yr^{-1}. Corresponding cracking depths are noted for each object, as determined by locating the intersection of a given geotherm with the cracking front. Estimates for Earth, Mars, Europa and Enceladus are based on available constraints on mass distribution (ocean depth, density and moment of inertia; see text and Figs. 2.3 and 2.4). Cracking depths are estimated for other candidate water-bearing objects in the solar system as determined by Hussmann et al. [2006], assuming the minimum ammonia concentration (which determines T at the seafloor) necessary to support an ocean.

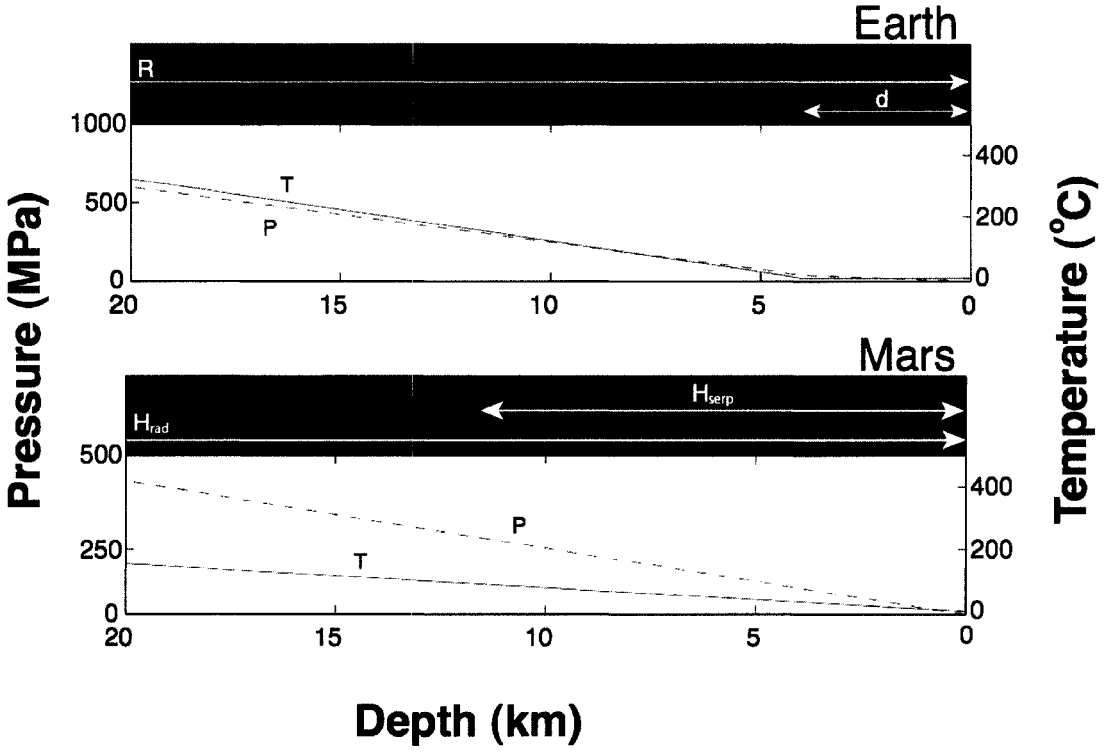

Figure 2.3: Near-surface pressure, temperature, and cracking depth profiles for Earth and Mars. Cracking occurs to depth z in an olivine mantle below the ocean of depth d (for Mars, $d = 0$), assuming material parameters as given in Table 2.1. For these two objects, pressure is calculated from surface gravity. Temperature is calculated for a conducting seafloor based on estimated radiogenic heating H_{rad}. For any choice of cooling rate and grain size, a martian crust of the same composition as Earth's has twice the cracking depth. Further results and implications are presented in Sections 2.4 and 2.5 for the current epoch, assuming nominal grain size and cooling rate for mid-ocean ridges on Earth.

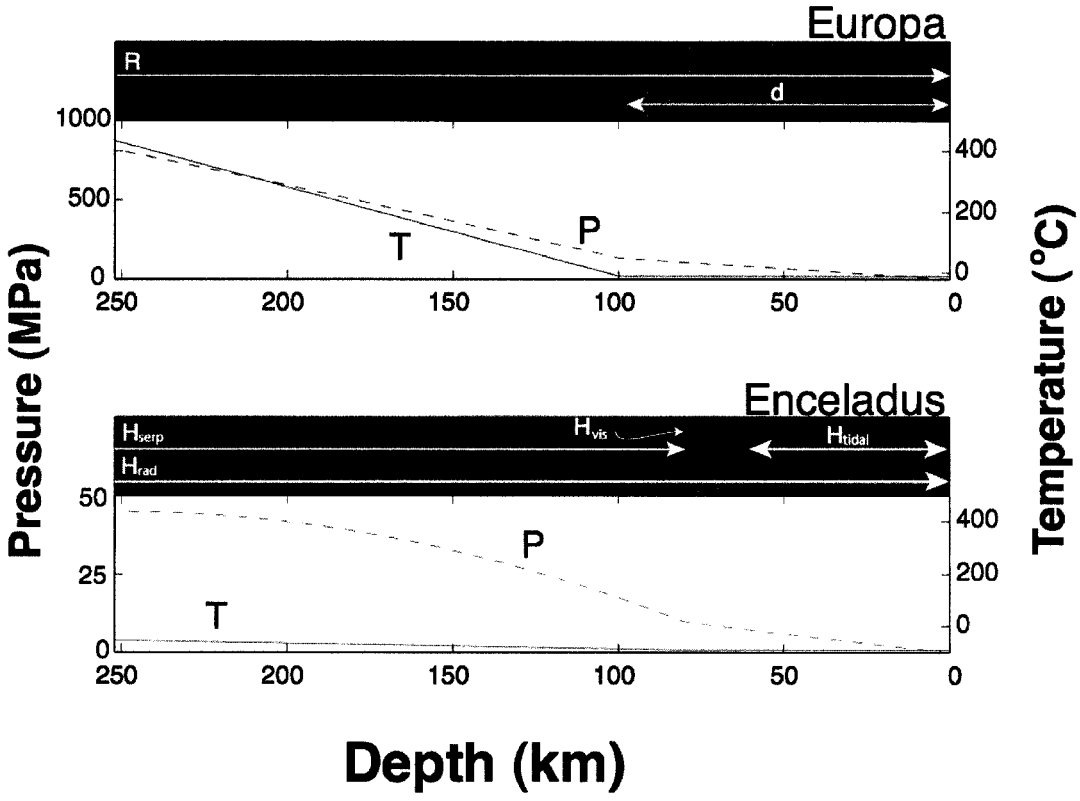

Figure 2.4: Pressure, temperature, and cracking depth profiles for Europa and Enceladus. Cracking occurs to depth z in an olivine seafloor below the an ocean of depth d, assuming material parameters as given in Table 2.1. For all icy planets considered, pressure is calculated for a two-layer object with an upper layer of depth d and density $\rho_w = 1000$ kg m^{-3} and lower layer density consistent with available bulk planetary value. Temperature is calculated for a conducting seafloor based on estimated radiogenic heating H_{rad}. Seafloor temperature is assumed to be at melting temperature of a likely ocean composition – salt water for Europa and ammonia/water for Enceladus. Varying seafloor depth for Europa over the range of present constraints [Anderson et al., 1998], z changes from 31 km for $d = 80$ km to $z = 5$ km at the maximum depth of $d = 170$ km. Shown above is the cracking depth for $d = 100$ km, for which $z = 25$ km. For very deep oceans, hydrostatic pressure limits the extent of cracking. Thus, Ganymede, Callisto, Titan and Triton are not considered here. Further results and implications are presented in Sections 2.4 and 2.5 for the current epoch, assuming nominal permeability, grain size and cooling rate for mid-ocean ridges on Earth.

	k_2	h_2	$Im(k_2)$	H_{rad} ($\times 10^9$ W)	H_{tidal} ($\times 10^9$ W)	H_{tidal}/H (%)	u_r (m)
Europa	0.242	1.169	0.0054	198	2870	94	27.4
Enceladus	0.066	0.177	0.0036	0.256	5.00	95	3.8
Titania	0.034	0.096	0.0025	9.26	0.0024	0.25	0.07
Oberon	0.028	0.076	0.0032	7.34	$\sim 10^{-4}$	~ 0	0.008
Triton	0.163	0.555	0.0052	69.40	0.17	0.25	0.24

Table 2.3: Tidal dissipation rate (H_{tidal}) and maximum radial displacement at the surface (u_r) for satellites in which oceans might exist. The internal structure models and the radiogenic heating rates due to long-lived isotopes H_{rad} are taken from Hussmann et al. [2006]. H_{tidal} and u_r are calculated from Eqs. 2.5 and 2.6, respectively. H_{tidal}/H is the ratio of tidal heating and the total heating rate $H = H_{tidal} + H_{rad}$. Values for Enceladus are calculated assuming an ice thickness of 5 km and an ice viscosity of 10^{15} Pa s, yielding the Cassini-derived output of energy [Spencer et al., 2006] of about 6 GW. For Europa, we assume an ice layer thickness of 30 km and an ice viscosity of 5×10^{14} Pa s. For the remaining satellites we assume an ice viscosity of 5×10^{15} Pa s. For Triton we assume an eccentricity of e = 0.0004 [Murray and Dermott, 1998].

Heat Generated by Tidally Induced Porous Flow

Tidal deformation of the ice shell covering a liquid water ocean acts as a time-varying hydrostatic head. This pumping action may induce fluid-rock interactions at the seafloor. Pressure at the seafloor varies with the periodic change in tidal loading. This drives fluid circulation through fractures in the mantle rock. Depending on the physical characteristics of the seafloor, viscous interaction between the fluid and the rock may generate heat sufficient drive chemistry important for life. The amount of dissipation depends on the elastic properties of fluid and rocky matrix, the tidal period, and the amplitude of the tidal deformation. From the values for the tidal deformation given in the previous section, only Europa's ice layer experiences the significant tidal deformation (Table 2.2). Here, we estimate the heat generated by this tidally induced porous flow for Europa.

Wang and Davis [1996] estimated the Earth's tidal dissipation by fluid flow in subsea formations for an M2 tide with an amplitude of one meter and period of twelve hours. We follow their model, applying the tidal amplitudes and periods given in Section 2.4.1. The dissipation energy is the product of the Darcy flow velocity and pressure gradient. Fluid velocity through a porous matrix, or Darcy velocity, is given by

$$w = -\frac{\kappa}{\mu}\frac{\partial p}{\partial z}. \tag{2.7}$$

where κ is the permeability, μ is the fluid viscosity, taken to be 10^{-3} Pa s, p is the incremental pressure change, and z is the depth. The pore pressure change below the seafloor is governed by the following equation, assuming that a seafloor medium consists of L layers and the flow is mostly vertical,

$$\frac{\partial^2 p_j}{\partial z^2} = \frac{1}{\eta_j}\left(\frac{\partial p_j}{\partial t} - \gamma_j \frac{\partial \sigma_B}{\partial t}\right), \tag{2.8}$$

where $j = 1, \cdots, L$, p is the incremental pressure change, z is the depth, and t is the time. $\sigma_B = \sigma_b \cos(2\pi t/\tau)$ is the loading function for the ocean tide, where $\sigma_b = \rho_w g u_r$, and τ is the tidal period (for Europa, $\tau = 3.55$ days). The elastic properties of seafloor material are described by the bulk modulus of the matrix frame, pore water, and solid grains, denoted by K, K_f, K_s, respectively, and the Poisson's ratio ν of the frame. Transport properties depend on the permeability κ, the porosity n, and the fluid viscosity μ which is taken to be 10^{-3} Pa s. The pressure wave due to tidal fluctuation propagates to a characteristic depth controlled by the hydraulic diffusivity $\eta = \kappa/\mu S$ during the tidal period. The depth of cracking to which the water can percolate is greater than this characteristic scale (as illustrated in Fig. 2.4 and Table 2.2). S is the storage coefficient of the saturated porous medium, which describes the effect of compressibility of the seafloor components. The storage coefficient is $S = (1/K') + (n/K_f)$ if the solid materials are assumed incompressible compared to the matrix frame and pore fluid ($1/K_s \simeq 0$) [Van der Kamp and Gale, 1983]. In this case

, the loading efficiency is given by [Jacob, 1940],

$$\gamma = \frac{1}{1 + n\,(K'/K_f)}, \tag{2.9}$$

where K' is the horizontally confined bulk modulus of the matrix frame related to K and ν. Details of other parameters are described in Wang et al. [1999]. In a single near-surface layer ($L = 1$ in Eq. 2.8), the energy generated by tidally-driven viscous dissipation can be approximated as,

$$H_{vis} = \frac{\sigma_b^2}{2}\sqrt{\frac{\pi\kappa}{\mu\tau K'\gamma}}\,(1-\gamma)^2. \tag{2.10}$$

Material parameters are taken to be same as Earth's — that is, we use $\nu = 0.25$, $K_f = 2.2$ GPa [Turcotte and Schubert, 1982]. For the present calculations we choose a range of values for Earth's seafloor: frame bulk modulus K' is between ~0.1 GPa for the seafloor sediments and ~10 GPa for solid rock [Crone and Wilcock, 2005]. Figure 2.5 shows energy dissipation per unit area as a function of the confined frame bulk modulus K' and permeability κ for a porosity of $n = 0.1$ as a maximum value, consistent with drill hole measurements in the upper 1000 m of Earth's oceanic crust [Becker et al., 1982]. For permeability ranging from 10^{-16} to 10^{-9} m^2, as mentioned in Section 2.3.1, and $K' = 10$ GPa, heating from viscous dissipation (H_{vis}) is on the order of $0.001 - 1$ mW m^{-2}. Heat generation varies by roughly an order of magnitude in the range of porosities between 0.1 to 0.9 (Figure 2.6). Assuming these material properties for the bodies under consideration, this heating mechanism is significant only in Europa because the height of the tidal bulge in other satellites is quite small (Table 2.3). For example, even assuming unrealistically high porosity of $n = 0.5$ and $\kappa = 10^{-10}$ m^2, the heat generation due to tidally induced porous flow in Enceladus, Titania, Oberon, and Triton are 5.02×10^{-4}, 1.99×10^{-6}, 1.78×10^{-8}, and 1.20×10^{-4} mW m^{-2}, respectively, which are one or more order of magnitude smaller

than radiogenic heating rates (see Table 2.2). The same values of K', n, and κ yield heat generation in Europa of about 5.8 mW m^{-2}, comparable with the radiogenic heating rate.

In reality, the seafloor has spatially heterogeneous elastic properties. Where interfaces separate vertical seafloor layers with different bulk moduli, additional porous flow is induced by the difference in instantaneous response of the pore pressure across the interfaces. This effect can be approximated as a two–layer system ($L = 2$ in Eq. 2.8) — an interface dividing two uniform half-spaces with contrasting frame bulk moduli. Around the interface, the same order of magnitude of energy dissipation as the case of a single near surface layer ($L = 1$ in Eq. 2.8) is generated. If the seafloor has multiple layered structure with different bulk moduli, the amplitude of generated heat may become several times larger Wang et al. [1999]. Although this effect deserves further investigation, the relative paucity of data and the large uncertainties in the parameters suggest that more detailed discussions are unlikely to be important here. The present discussion illustrates a potential importance of viscous dissipation in generating heat in Europa's seafloor.

2.4.2 Serpentinization

At the off-axis mid-Atlantic hydrothermal systems Trans-Atlantic Geotraverse (TAG), Rainbow, and Lost City, the geological process of serpentinization provides a significant source of thermal energy. In the Lost City system it very likely constitutes the dominant source [Kelley et al., 2005]. We consider the potential for serpentinization processes in extraterrestrial oceans lacking mid-ocean-ridge tectonics, with implications for astrobiology.

Ferromagnesian silicate minerals are dominant in unfractionated igneous rocks (*e.g.*, peridotites) that comprise Earth's upper mantle, and may typify subseafloor lithologies on small ocean planets. The abundance of peridotite in a planetary lithosphere is largely governed by the temperature of formation, which depends on the

timing of formation relative to the body's ability to dissipate heat [Schubert et al., 1986, McKinnon and Zolensky, 2003]. Even later, slower radiogenic heating can be intense enough to form peridotite, but eventually cooling takes over and the system turns retrograde – at lower temperatures, thermodynamic equilibrium favors a transformation back to the hydrated mineral form, in this case serpentine. In the event of an early period of peridotite-forming intense heating, the subsequent formation of ocean(s) could give rise to an epoch of serpentinization-driven hydrothermal activity.

The process of serpentinization essentially acts to re-equilibrate peridotitic assemblages from a nascent water-deficient high-temperature state to the water-saturated low-temperature state characterising planetary seafloor environments. In the presence of water, the common rock-forming silicate minerals olivine and clinopyroxene, at the pressures under consideration (10-200 MPa) and at temperatures less than $\sim$ 700 K, occur within the stability field of the serpentine minerals (antigorite, lizardite and chrysotile). The resultant metamorphic hydration reaction is termed "retrogressive" as it accompanies a decrease in metamorphic grade. Such reactions are typically accompanied by both a large molar solid volume increase ($\Delta V_{solids} > 0$) and the release of heat energy ($\Delta H_{reaction} < 0$). The heat so-released is appreciable: at 300 K and pressures between 10 and 200 MPa, for example, $\sim$ 83 kJ of heat is released per mol of serpentine produced. Within the P-T window pertinent to serpentinization on small ocean planets, which lies entirely within the stability field of serpentine, the exothermic nature of the reaction increases with temperature, and decreases weakly with pressure.

Of additional significance is the large positive solid volume change associated with serpentinization. This is of particular interest to the crusts of ocean planets because of the potential feedback resulting from increased exposure of serpentinizable peridotitic material, through crack propogation and kernel formation [O'Hanley, 1992], following the initial onset of serpentinization. The change in volume of the solid during serpentinization (ΔV_{solids}) is a function of pressure and temperature, and in the

pressure-temperature window considered lies between 45 and 60 cm^3 per mol of serpentine produced. An important consideration on the volumetric expansion, however, is the rate of peridotite dissolution relative to serpentine precipitation. If dissolution is fast relative to precipitation and to the rate of migration of the alteration fluid, volumetric expansion and heat production may be inhibited [Nesbitt and Bricker, 1978]).

An estimate of the heat generated by serpentinization is obtained by considering the energy released in hydrating available material in the volume of rock to depth z below the seafloor. The per-unit-area heat for a reaction penetrating to depth z is determined from an estimate of the amount of olivine produced by the reaction $H_{hydration} = n_{oliv}\Delta H / A_{seafloor}$. In our heat calculations, we consider the reaction for the Mg-end member,

$$\begin{aligned} 2Mg_2SiO_4 + 3H_2O &\leftrightarrow \\ &\qquad Mg(OH)_2 + Mg_3Si_2O_5(OH)_4 \\ \text{forsterite} + \text{water} &\leftrightarrow \quad \text{brucite} + \text{serpentine}. \end{aligned} \tag{2.11}$$

Although the thermodynamics of the reaction will differ along the geothermal gradients considered, the dependence on pressure and temperature is trivial compared to other considerations. For simplicity we assume an average enthalpy of reaction of $\Delta H = -83$ kJ per mol serpentine. We assume a lherzolitic bulk composition consistent with Earth's primordial mantle: 70% olivine, with an Fe/Mg ratio of 0.1. We assume all of the olivine is hydrated to serpentine.

Our estimates for presently known and candidate ocean planets are given in Table 2.2, with tidal and radiogenic heating for comparison. Heat due to serpentinization comprises less than a percent of radiogenic for all bodies considered. However, as we discuss in the following sections, centers of serpentinization may drive the production of bionutrients. The slow release of this form of energy allows it to sustain gradients in

chemical potential over long periods of time. These factors make even minor amounts off serpentinization important when assessing habitability.

2.4.3 Longevity of Serpentinizing Systems

The rate at which serpentinization reactions proceed potentially plays a large part in determining the longevity of hydrothermal systems on small ocean planets. Many factors affect the rate of serpentinization. These include pressure, temperature, fluid composition (as indicated by, *e.g.*, pH, Eh, CO_3^{2-}– and silica activity), fluid access to serpentinizable rock, and the Fe/Mg ratio of the peridotitic material undergoing serpentinization. Reaction rate constants determined in the laboratory [*e.g.*, Martin and Fyfe, 1970, Wegner and Ernst, 1983] are on the order of 10^{-7} to 10^{-8} sec^{-1}. Such rapid rates would preclude the persistence of hydrothermal systems on geological timescales. However, rates so-determined apply to experimental systems with very fine grain sizes and a high fluid/rock ratio, conditions that become increasingly unrealistic with depth of fluid penetration. Under conditions more relevant to the crusts of small ocean planets, fluid delivery to the rock is more likely to be rate-determining factor. In such cases, a much slower reaction rate between 10^{-11} and 10^{-13} sec^{-1} is applicable [Skelton et al., 2005]. In the absence of crustal rejuvenation, these reaction rates imply longevities of hydrothermal systems on the order of 10^6 years. Accordingly, serpentinizing systems may have been short-lived phenomena in planetary systems lacking tectonism and crustal rejuvenation, as all available serpentinizable material would have hydrated within the first million years of ocean/crust interaction. Given that the inception of life on Earth likely occurred rapidly after the formation of a stable lithosphere [Rosing, 1999], and the possibility of a hydrothermal cradle for life [Brasier et al., 2002, Van Kranendonk, 2006], such early periods of serpentinization may be of considerable interest to astrobiology.

There are two reasons why serpentinizing systems may survive for extended periods in ocean planet crusts: 1) serpentinization may occur at lower temperatures on

small ocean planets than those applicable to terrestrial systems. At 298.15 K, the rate of olivine dissolution in the laboratory ranges from 10^{-11} to 10^{-17} mol cm^{-2} s^{-1} [Wogelius and Walther, 1992]; 2) our estimates suggest that crack propagation and resulting exposure of fresh serpentinizable peridotitic material to fluid proceed at rates on the order of 1 km Ga^{-1}. This slow serpentization can proceed provided fluids can reach deep, fresh rock through the already serpentinized layer.

2.4.4 Serpentinization as a Source of Nutrients and Metabolites

Irrespective of their potential as a source of thermal energy, serpentinizing systems are of considerable astrobiological relevance to small ocean planets. The interaction of seawater with peridotite leads to significant change in fluid compositions, with potentially important implications for astrobiology. Unfortunately, flux measurements of potential metabolites in systems on Earth are hampered by the difficulty of distinguishing serpentinization-derived solutes from those of a magmatic origin.

In addition to heat, H_2 and CH_4, serpentinizing systems may also provide a source of biologically important trace-metals. On Earth, elevated fluid concentrations of Mn, Fe, Co, Ni, Cu, Zn, Ag, Cd, Cs and Pb have been ascribed to the serpentinization of ultramafic rocks [Douville et al., 2002], although the pH dependence of such leeching processes is not well-constrained.

Water in equilibrium with serpentinizing peridotite is characterized by a high pH and highly reducing conditions [Schroeder et al., 2002, Wetzel and Shock, 2000]. This theoretical finding is not always compatible with observations in the environment [*e.g.* Moody, 1976, Seyfried and Dibble, 1980, Janecky and Seyfried, 1986, Allen and Seyfried, 2003]. Allen and Seyfried [2004] argue that this unexpectedly high pH is a transient phenomenon resulting from the preferential hydration of the relatively siliceous pyroxene component following the initial onset of serpentinization. Lower pH increases concentrations of Fe, Ni, Cu, Zn, Ca and K [Charlou et al., 2002] in hydrothermal fluids.

H_2 generation

The highly reduced nature of molecular hydrogen (H_2) makes it a candidate electron donor in chemotrophic metabolic processes such as methanogenesis. The production of H_2 is of further astrobiological interest due to the potential, in the presence of CO and/or CO_2 and an appropriate catalyst, for the abiological production of another important electron donor, CH_4 [Berndt et al., 1996, Charlou et al., 1998] by the overall reaction:

$$4H_2+CO_2 = CH_4 + 2H_2O \tag{2.11}$$

H_2 generation in serpentinizing systems has been demonstrated in the field [Neal and Stanger, 1983, Abrajano et al., 1990, Kelley and Fruh-Green, 2001], in the laboratory [Janecky and Seyfried, 1986, Berndt et al., 1996, McCollom and Seewald, 2001] and theoretically [Wetzel and Shock, 2000, Sleep et al., 2004].

The release of H_2 in serpentinizing systems results from Mg and Fe^{+2} partitioning in the products of serpentinization reactions that is markedly different from that in the protolith ferromagnesian silicates. This occurs because serpentine and brucite tend to incorporate relatively lower amounts of Fe(II) into their structures than do the reactants olivine or pyroxene. Oxidation of the unincorporated Fe(II) originally hosted in fayalite and/or ferrosilite, via dissociation of water, produces magnetite and hydrogen gas, giving rise to the net reactions [Allen and Seyfried, 2003]:

$$3Fe_2SiO_4 + 2H_2O = 2Fe_3O_4 + 3SiO_2(aq)+2H_2(aq) \tag{2.12}$$

$$\text{fayalite} + \text{water} = \text{magnetite} + \text{silica} + \text{hydrogen}$$

$$3FeSiO3+H_2O = 2\ Fe_3O_4 + 3SiO_2(aq)+H_2(aq) \tag{2.11}$$

$$\text{ferrosilite} + \text{water} = \text{magnetite} + \text{silica} + \text{hydrogen}$$

The amount of H_2 released through serpentinization thus depends upon the degree

of Fe-incorporation into the secondary assemblage. Of central importance to evaluating H_2 fluxes on small ocean planets, therefore, is the composition of the protolith assemblage that undergoes serpentinization. Ultramafic (peridotitic) versus basaltic assemblages, and higher Fe/Mg ratios in the protolith assemblage, favor higher H_2 production during serpentinization.

In terrestrial systems, approximately two-thirds of the Fe(II) originally present in fayalite is oxidized to magnetite [Berndt et al., 1996]. The stoichiometry of the main H_2-producing reaction (Eq. 2.12) suggests that 3 moles of fayalite produces 2 moles of hydrogen. Hydrogen from subseafloor serpentinization may be a limiting nutrient in ocean moons that support life. For the reaction of forsterite (Eq. 2.11) Allen and Seyfried [2003] observe 2.3 mmol kg^{-1}. The reaction of fayalite (Eq. 2.12) produces ~500 mmol kg^{-1}, as estimated for the Coast Range ophiolite [Schulte et al., 2006].

2.5 Implications for Life in Ocean Planets

We estimate rates of heat and hydrogen production through time using our constraints on circulation depths based on thermal cracking (Section 2.3.2). After one billion years, rates are nearly constant; everywhere, the global heat generated by hydrating to the cracking depth is at most a percent of radiogenic heating. Hydrogen production is $\sim 10^9$ molecules per cm^2 per second for Pluto, Eris, Earth, Mars and Europa, and $\sim 10^{10}$ molecules per cm^2 per second for the other bodies listed in Table 2.2. Our estimates of heat and hydrogen production in small ocean planets can be compared with emerging evidence of methane in the solar system and with previous calculations of potential extraterrestrial biomass production.

2.5.1 Organics in the Solar System

Cosmochemical observations are beginning to reveal a plethora of organic molecules in gaseous nebulae outside the Solar System [Pendleton and Allamandola, 2002]. To date, only methane has been observed on any of the objects discussed here (not

counting Earth). However, there is reason to expect larger organic molecules where methane is found. In this section, we highlight some recent observations of methane in the solar system as a possible indication of other organic molecules. We wish to emphasize that the processes outlined in this work may aid in the production of organics in small ocean planets.

Methane has been detected in the atmosphere of Mars [Formisano et al., 2004]. Calculated residence times point to a source from isolated locations on the martian surface [Krasnopolsky, 2005]. The majority of the martian CH_4 is likely created by abiotic Fischer-Tropsch reactions associated with serpentinization [Oze and Sharma, 2005]. In the case that all of the observed methane is abiogenic, the observation CH_4 is nevertheless an important indication of possible nutrients for life on Mars [Fisk and Giovannoni, 1999, Weiss and Ingersoll, 2000].

Pluto and Eris are the first trans-neptunian objects with measured methane reflectance spectra [Delsanti and Jewitt, 2006]. The four-hour rotation rate of recently discovered trans-neptunian object 2003 EL_{61}, as revealed by light curve measurements, constrains the object's density to between 2600 and 3340 kg m^{-3} [Rabinowitz et al., 2006], implying it is primarily a rocky body with a superficial covering of ices. As with other trans-neptunian objects, the tidal-orbital evolution of 2003 EL_{61} and its satellites is not yet constrained [Brown et al., 2005], and may be a source of energy to drive chemical weathering of the body's interior.

Methane observed on distant icy objects may derive partially from retrogressive metamorphism. The rocky components of trans-neptunian objects and small icy satellites like Enceladus may be fully accessible to water owing to their small sizes. Tidal interactions in binary and multiple-object systems provide an additional source of energy and possibly a means for driving fluid flow. As such, trans-neptunian and other icy "dwarf planets" should not be dismissed as targets of potential astrobiological interest.

2.5.2 Potential Extraterrestrial Biomass

Estimates of the potential for supporting life geochemically on Earth or elsewhere vary depending on the temperatures, pH, and reactions considered [Shock, 2004, McCollom and Shock, 1997, 1998, McCollom et al., 1999]. For Mars and Europa, estimates of biologically available energy from volcanic activity and from weathering reactions indicate that the the number of bacteria that could be supported over a 4 Gyr period is $\sim$8.6 g cm^{-2} on Mars – at least a hundred times less than on Earth in one thousand years – and far fewer on Europa [Jakosky and Shock, 1998, Link et al., 2005]. Based on material presented here, we suggest there is reason to rethink these estimates. First, the cited estimates do not account for subsurface weathering as a source of energy. Jakosky and Shock [1998] suggest that weathering $\sim$5% of crustal material to 10 km depth would contribute an additional factor of 20 to potential biomass production, but they choose to neglect this factor because at such depths permeability sufficient to support fluid circulation is deemed unlikely. We advocate that it is at least plausible that weathering not only occurs at depth, but at depths even greater than the 10 km suggested for Mars.

Second, additional energy from the sources considered here must also be taken into account, assuming that some portion of the heat they produce is converted to bioavailable nutrients. Viscous tidal dissipation could be an important source of additional heat in ice-covered moons like Europa and Enceladus if tidal flexing occurs primarily in an ice shell overlying a liquid ocean. Serpentinization ultimately derives from other sources of energy via initial dehydration of parent rock, much of it likely coming from an early stage in a planet's history when conditions may have been too hot to support life. In this way, serpentinization-driven systems may offer a way for organisms to reclaim primordial heat energy.

2.6 Conclusion

Owing to a greater depth of hydrothermal circulation from thermal cracking in brittle mantle material, small ocean planets in the solar system may have the capacity to support ecosystems that are stable on geologic time scales, with greater amounts of bio-available energy than previously suggested. Unreacted rock may be exposed at a steady rate as the thermal cracking front moves deeper into the lithosphere due to the decrease in internal radiogenic heating. Based on this constraint, present-day depth of water penetration for Mars may be roughly an order of magnitude greater than previous estimates. If oceans exist in Europa, Enceladus, Titania, Oberon, and Triton, the tidal bulge of their ice shells may drive hydrothermal fluid flow if sufficient permeability exists below their seafloors. In Europa, an estimate of viscous heating from fluid flux through a porous matrix indicates heating by this mechanism may be on the same order as present radiogenic heating. In Enceladus, the presence of a subsurface ocean may facilitate tidal heating in ice shell on the same order as present-day radiogenic heating, a result consistent with heat release derived from Cassini spacecraft measurements [Spencer et al., 2006]. It should be noted that there is no evidence for a global ocean from present Cassini data. However, to obtain high heating rates within the ice shell of Enceladus, a decoupling from the interior is required. Whether local liquid reservoirs would allow for sufficient tidal heating remains to be investigated.

In satellites locked in tidal resonances, crustal rejuvenation is possible if orbital resonance oscillations occur. Without such rejuvenation, the slow deepening of cracks over time, as outlined above, provides a steady source of thermal and chemical energy that may be sufficient to maintain stable, if limited, ecosystems to the current era.

Acknowledgments This project was supported by the National Science Foundation's IGERT program, grant number DGE-9870713, "IGERT: Astrobiology: Life in and beyond Earth's Solar System," NSF award EAR-0337796, the NASA Astro-

biology Institute and NASA award NNG06GF81G. We thank Tim Crone for helpful comments on tidal dissipation and William Brazelton for discussion on the biochemistry of hydrothermal systems. We thank the reviewers for their helpful critiques.

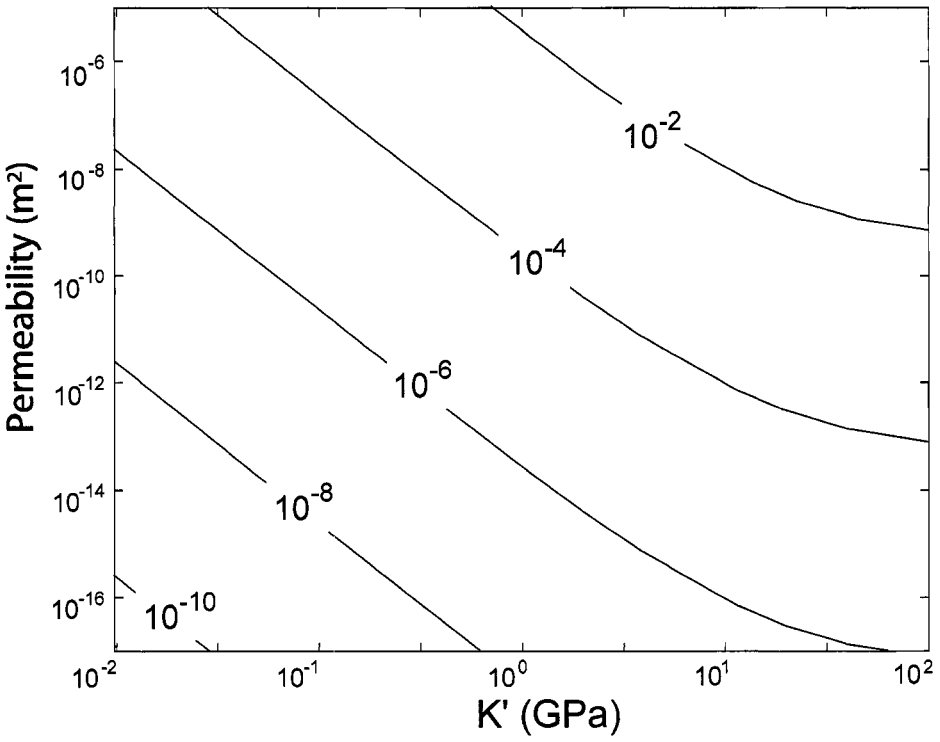

Figure 2.5: Rates of tidal energy input ($\mathrm{W\,m^{-2}}$) from viscous dissipation in the near subsurface of an Europa's seafloor as a function of the permeability and the confined bulk modulus of the matrix frame K' with a reference porosity of $n = 0.1$ [Becker et al., 1982].

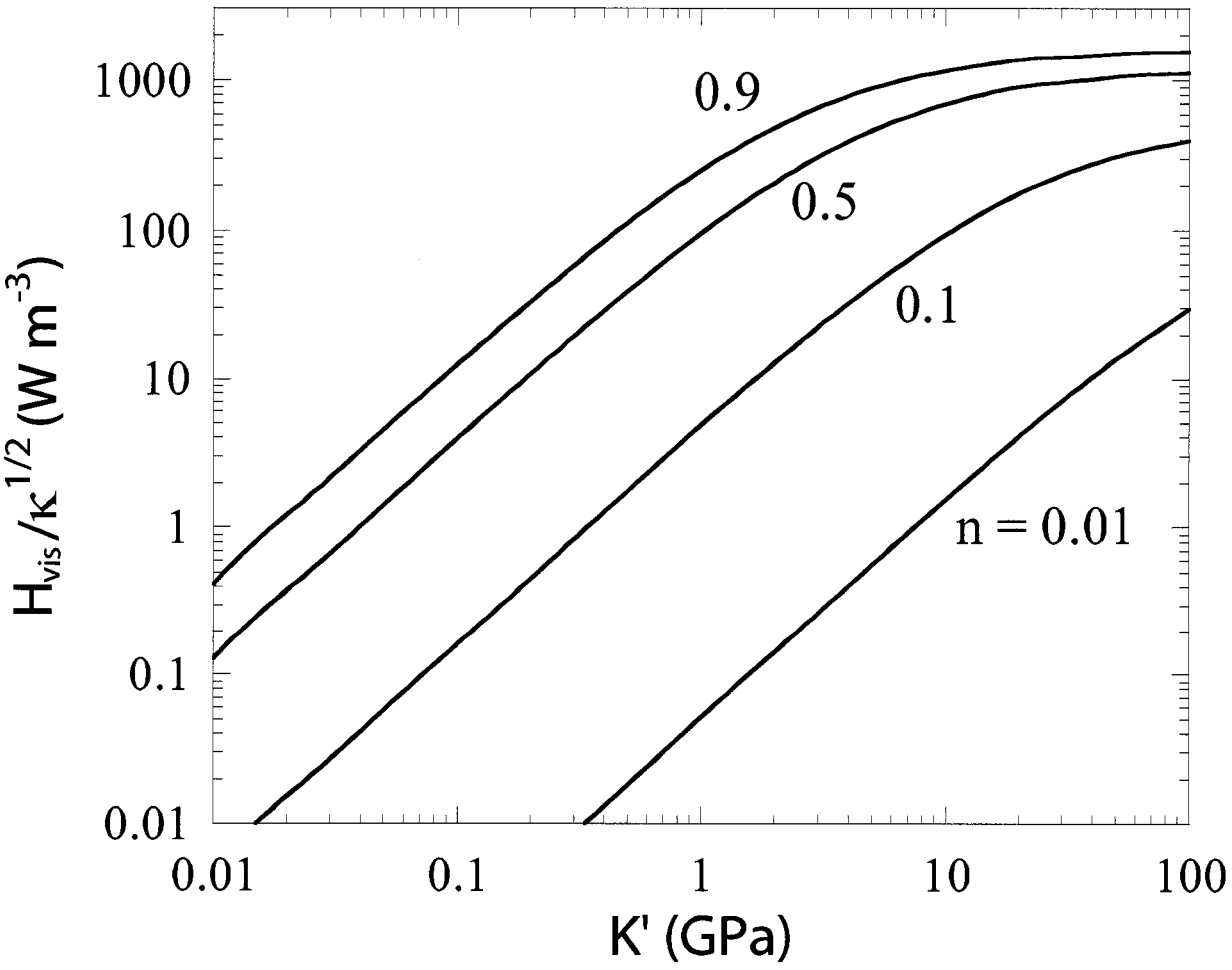

Figure 2.6: Viscously dissipated energy H_{vis} normalized to permeability in a europan seafloor with tidal height $u_r = 27.4$ m, and Poisson's ratio $\nu = 0.25$, for a range of porosities from $n = 0.01$ to 0.9.

Chapter 3

STRATIFICATION AND DOUBLE-DIFFUSIVE CONVECTION IN EUROPA'S OCEAN

[1]Fluid dynamics in Europa's ocean have been described in terms heat input (radiogenic and tidal) to Europa, its overall size and rate of rotation, and the depth of its ocean [Collins et al., 2000, Thomson and Delaney, 2001, Goodman et al., 2004]. Assuming the ocean salinity is homogeneous, Goodman et al (2004) describe a buoyant plume originating from the floor of Europa's ocean. The plume remains buoyant over entire depth of the ocean and reaches the base of the ice shell as a rotationally confined column with diameter on the order of tens of kilometers, comparable to the size of observed melt-through features on the surface. Melosh et al. [2004] point out that, in a dilute ocean, a rising plume would lose buoyancy just before reaching the surface, due to water's anomalous thermal expansion properties (at low temperature and pressure, water has negative thermal expansion). Specifically, the effect would occur in the 23 km below Europa's surface, but only if the ice shell is thinner than 23 km and if the water is sufficiently dilute – salinity less than 3.4 Wt% for seawater, figures that are only poorly constrained by limited data pertaining to low temperature, high pressure thermochemistry. To date, no one has considered the effect of a salinity anomaly in a rising plume.

Pressure at the base of a 70-180 km ocean [Anderson et al., 1998] is 100-200 MPa. Until recently [Marion et al., 2005], researchers modeling chemical and physical properties of Europa's ocean have treated solution properties only at 0.1 MPa (1 atm), largely due to a lack of experimental data at low temperature and high pressure

[1]This chapter was published as Vance and Brown [2005]

[Kargel et al., 2000, Melosh et al., 2004]. We emphasize that the literature pertaining to high pressure (Na^2,Mg)SO^4 is indeed sparse [*e.g.* Hogenboom et al., 1995, Abramson et al., 2001]. Our model calculations were performed using a model that extrapolates to high pressures and low temperatures. Using a simple calculation for the density anomaly of a thermal upwelling (hereafter referred to as a plume) versus pressure, we show that a small uptake of salt at the seafloor causes an initially buoyant upwelling to lose buoyancy at a height dependent on temperature and salinity of the plume and of the ambient ocean.

Here we assess the effects of fluid composition and depth-dependent hydrostatic pressure on dynamics in a Europan ocean primarily composed of aqueous Na_2SO_4 and $MgSO_4$, for both a saturated and a dilute ocean. We observe a salinity- and pressure-dependent check on buoyancy in putative upwellings, which could act as a mechanism for storing heat in the ocean's base. Uptake of salt to a warmed parcel of water from the seafloor environment causes upwellings to lose buoyancy before reaching the base of the overlying ice, implying a tendency toward ocean stratification. We make an analogy to double-diffusive convecting systems observed in the Red Sea and elsewhere in Earth's waters. Using currently understood parameterizations for onset and stability, we estimate a range of temperatures and salinities for which double-diffusive convection may occur in Europa's ocean. In the Red Sea, boundary layers separating convecting zones have been observed to move upward as the lower layer acquires heat and salt. We examine the possibility of stratification and double-diffusive convection as mechanisms for heat storage in Europa's ocean, and possible correlation with recently inferred changes in ice surface alteration style over the last 30-80 Myr.

We test the buoyancy of a plume at all depths in Europa's ocean by calculating the density anomaly, B, with plume buoyancy occurring when

$$B \equiv \frac{\rho_{ocean} - \rho_{plume}}{\rho_{plume}} > 0. \tag{3.0}$$

For the calculation of densities, we model volumes of aqueous solutions using apparent molal volumes from Marion et al. [2005] and specific volume of water from Wagner and Pruss [2002].

3.1 The Influence of Pressure Thermochemistry on Buoyancy in Europa's Ocean

As pointed out by Melosh et al (2004) an unstratified, fully convective europan ocean is nearly isothermal. In an initially fully circulating ocean, fluid temperature increases adiabatically with depth happens because it is compressed with more rapidly than it can exchange heat with the environment. It follows [*c.f.* Turcotte and Schubert, 1982] that the incremental increase in temperature with depth is,

$$\left(\frac{\partial T}{\partial z}\right)_S = \frac{\alpha_V g T}{C_P} \tag{3.0}$$

where z is depth. α, is the coefficient of thermal expansion, for water $O(2\times10^{-4})$ K^{-1}. Europa's gravity is 1.31 m s^{-2}, increasing to roughly 1.5 m s^{-2} approaching the rocky mantle [Turcotte and Schubert, 1982]. $T$is the temperature, in K, at the depth of concern. $C_P$is the heat capacity of the fluid at the pressure and temperature of concern, and is about 4 kJ kg^{-1} K^{-1}. The adiabatic increase in temperature is in the neighborhood of 0.002 K km^{-1}, or 0.2 K over the entire depth of a 100 km ocean.

For a rotationally confined plume with a thermal anomaly of 0.2–1 mK [Goodman et al., 2004], we assess plume buoyancy in a dilute $MgSO_4$ ocean and a saturated eutectic ocean. Choosing a dilute Na_2SO_4 ocean instead, the ocean composition and plume enrichment for which a specific critical rise height is observed vary by no more than 10%, respectively. For the saturated ocean, we estimate the saline enrichment of the plume from Marion et als (2005) saturation profile in Mg^{2+}, Ca^{2+}, Na^{-}, SO_4^{2-}, and Cl^{-} at 146.0 MPa (~100 km depth).

In the saturated eutectic ocean, there should be ample precipitate at the seafloor

for the uptake of brine precipitate as the plume forms. If uptake is commensurate with the increase in solubility with temperature, enrichment leads to negative buoyancy at the seafloor, and the ocean will tend to stratify from the bottom up. In our calculations, we do not consider precipitation from the plume, but the effects of precipitation are discussed below.

In the more dilute ocean, enhanced salinity comes about through interaction with surrounding rock, perhaps via hydrothermal circulation [Kargel et al., 2000, McKinnon and Zolensky, 2003]. We test a range of plume enrichment in a dilute $MgSO_4$ ocean from a calculation of the density anomaly, B (3).

3.1.1 Results

Density anomaly profiles are presented in Figure 3.1 for 0.28 molal $MgSO_4$, the minimum composition for which an unenriched plume ($n_{plume} = n_{ocean}$) is buoyant at all depths. The density anomaly versus europan ocean depth is shown for three cases: 1) pure water plume and ocean 2) saline ocean and plume with the same composition 3) plume with excess salinity in the same ocean. The density anomaly decreases as a plume rises, due to the pressure dependence of water's thermal expansion profile. Neutral buoyancy occurs where the density anomaly is zero.

The pure water and homogeneously saline systems have been treated [Collins et al., 2000, Thomson and Delaney, 2001, Goodman et al., 2004, Melosh et al., 2004]. For pure water, the plume reaches neutral buoyancy at around 20 km depth; possibly well below the ice ceiling. In the case of homogeneous composition ($n_{plume} = n_{ocean}$), the positive temperature derivative of V_o (illustrated in Figure 3.2) makes the plume even less dense, moving the profile in the direction of greater buoyancy. As noted by Melosh et al. [2004], this causes the plume to remain buoyant up to the ice ceiling of Europa's ocean.

Saline enrichment of the plume, due to uptake at the seafloor, shifts the density anomaly profile in the direction of neutral buoyancy ($B = 0$). The magnitude of the

T_{ocean} (K)	n_{ocean} (molal $MgSO_4$)	Δn (molal $MgSO_4$)	$d_{neutral}$ (km) $T = 0.2$ mK	$d_{neutral}$ (km) $T = 1.0$ mK
271.15	0.28	5×10^{-7}	80	12
271.15	0.28	1×10^{-7}	12	5
271.15	0.28	6.5×10^{-7}	100	12
271.15	0.28	2×10^{-6}	100	60
271.15	1.00	1×10^{-6}	65	5
265.15	0.28	5×10^{-7}	80	27
265.15	1.00	1×10^{-6}	15	10

Table 3.1: Depth (below Europa's surface) of neutral buoyancy for a 100 km deep ocean with average temperature 271.15 K and 265.15 K. Loss of buoyancy at depth occurs for a small saline anomaly in a ring plume, over a range of 1-2 orders of magnitude. Increasing ambient salinity or plume thermal anomaly for a given ambient temperature decreases the depth of neutral buoyancy. Lowering ocean temperature appears to increase the depth of neutral buoyancy, though it is difficult to discern a change for the smaller thermal anomaly

density anomaly shift depends on both ambient and plume salinity, but the primary effect occurs over the entire range of ambient concentration of 0-1 molal MgSO4 that we have considered. For the range of ocean salinities considered, the effect occurs for saline enrichment in the range 10^{-7} to 10^{-6} molal, ~3 orders of magnitude less than the increase in solubility commensurate with ΔT_{plume}. Critical rise heights are illustrated in Table 1 for a range of ocean salinities and enrichments, for $\Delta T_{plume} =$ 0.2 mK and $\Delta T_{plume} = 1$ mK.

Whether plume buoyancy can be maintained over the entire depth of Europa's ocean depends on the ocean's depth, temperature profile, and composition. The degree to which a plume at the seafloor acquires excess salinity and, thereby, the height to which its rise is limited depend on the change in solubility and dissolution rate with temperature, the existence of a reservoir of salt to draw from, the dimensions of the reservoir, and the residence time of the plume at the seafloor.

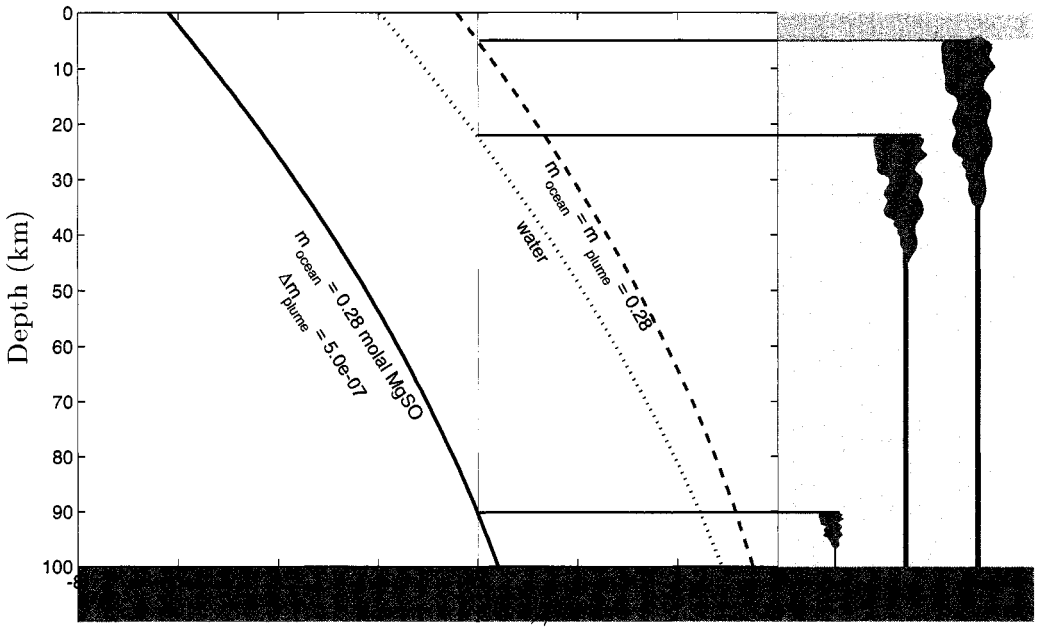

Figure 3.1: Density anomaly in a Europan ocean for a plume with thermal anomaly of 0.2 mK. Ocean temperature is set to 271.15 K at the seafloor, with an adiabatic temperature decrease to ~270.85 K near the surface. A pure water plume in a pure water ocean (small dots) loses buoyancy around 20 km below the surface, where thermal expansion changes from positive below to negative above. A plume in a 0.28 molal $MgSO_4$ ocean (large dots) is less dense than the pure water plume with the same thermal anomaly, due to the increasing $MgSO_4$ molal volume with temperature (Figure 3.2). The convergence of V^o values at high pressure (Figure 3.2) accounts for the convergence with the pure water plot at the seafloor. Adding salt to the plume (solid) via uptake at the seafloor increases the density anomaly of the plume, such that the plume loses buoyancy 20 km above the seafloor.

3.1.2 Double-Diffusive Convection in Europa's Ocean

Loss of plume buoyancy at a height determined by saline enrichment suggests that Europa's ocean is stratified to some degree. This contrasts with the assertion [Thomson and Delaney, 2001, Goodman et al., 2004] that the ocean has a large Rayleigh number, and convective heat and fluid transport are ubiquitous. Here, we explore the

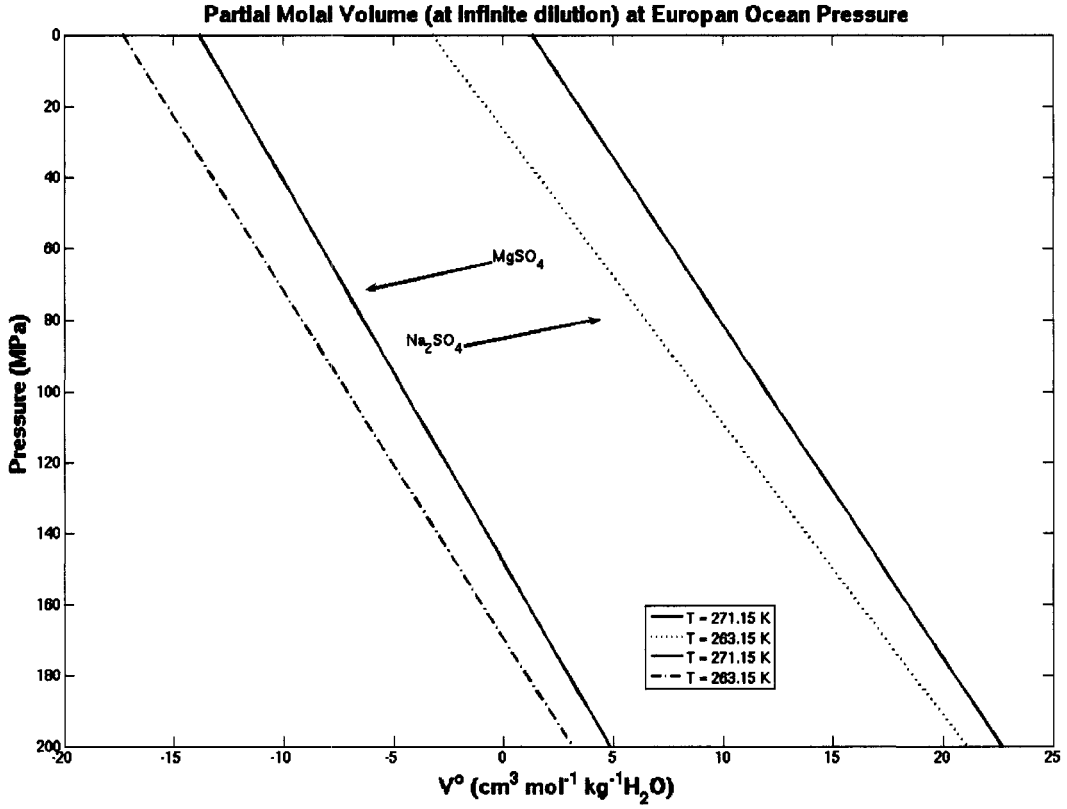

Figure 3.2: Partial molal volumes for Na_2SO_4 and $MgSO_4$, obtained using Millero [1983]. V_o increases with pressure and temperature.

possibility of convection in a lower layer that is warm and saline, with convection also occurring above, in a cooler, more dilute layer, with a diffusive boundary between them.Generally, the stability of a non-convecting, or stagnant, layer will be determined by its ability to transport heat to the overlying water, either by advection or diffusion. If there is a gradient in both temperature and salinity, double-diffusive convection can occur, in which the magnitudes of the two gradients determine the style of heat and material transport. In the simplification that density scales linearly with temperature and salinity [Turner and F., 1973], one arrives at two non-dimensional numbers that characterize the double-diffusive system:

$$Ra = \frac{g\alpha\Delta T d^3}{\kappa\nu} \tag{3.1}$$

$$Rs = R_\rho Ra = \frac{g\beta\Delta S d^3}{\kappa\nu} \tag{3.2}$$

$$R_\rho \equiv \frac{\beta\delta S\delta z}{\alpha\delta T\delta z} \tag{3.3}$$

Ra is the Rayleigh number and convection occurs for $Ra > O(10^3)$. d is the characteristic scale length for the system (here, the height of Europa's ocean). Rs is the salinity Rayleigh number, in which $\beta = \delta \ln \rho / \delta S$ is the coefficient of saline contraction, analogous to α in Ra.

When $1 \leq R_\rho < 10$ a double-diffusive system is observed [Fernando, 1989], in which a well-mixed (convecting) lower layer is separated from a well-mixed upper layer, with a step profile in salinity and temperature between them. The better-studied regime of salt fingering [Merryfield, 2000] occurs when salinity and temperature decrease with depth. In this situation, saltier fluid from above enters the lower, more dilute layer, and begins to rapidly descend in characteristic "finger" plumes. The subtler, less studied, diffusive regime, in which heat and salt diffuse upward, occurs when salinity and temperature increase with depth, with $1 \leq R_\rho < 10$, and has been observed in cold and isolated systems on Earth [Kelley et al., 2003, see below].

3.1.3 Feasibility of Double-Diffusive Convection in Europa's Ocean

Here, we assess the feasibility of double-diffusion in Europas ocean based on the above discussion, assuming the range of relevant R_ρ is the same. We assume properties of water as mentioned in previous sections. R_ρ is defined in Equation 3.3. For the aqueous $MgSO_4$ system at 271.15 K [Hogenboom et al., 1995], the coefficient of saline contraction is $\beta \sim 0.1$ mol^{-1}. For a range of difference in potential temperature between the top and bottom of Europa's ocean $\Delta T = 10^{-4}$ to 10^1 K, the salinity

change over the entire ocean to attain $1 \leq R < 10$ is: $\Delta S \sim 10^0 - 10^{-6}$. ΔS over the entire 100 km ocean depth is 0 to 7 orders of magnitude greater than the salinity difference chosen to illustrate the stagnation (Figure 3.1; Table 1).

If double-diffusive convection occurs in an ocean near saturated composition, precipitation from a rising plume would cause salt to "rain down" into the ocean below. Rain out would enhance the salinity of the ocean below while to transferring heat upward rather than keeping it at the level of neutral buoyancy. The resulting disturbance to the relative thermal and saline gradients would increase R_ρ above the range where double-diffusive convection is observed in laboratory experiments.

3.1.4 Double-Diffusive Convection in Earth's Waters

The existence of stable double-diffusion systems in Earth's waters has been inferred from the step, or staircase, nature in salinity profiles in the Weddel Sea, in the Greenland Sea, below ice island T-3 in the Arctic [all so far mentioned: Kelley et al., 2003] in ice-covered Lake Vanda in Antarctica [Hoare, 1966], and in the Black Sea [Kelley et al., 2003, Ozsoy and Unluata, 1997].

In the Black Sea, where temperature and salinity increase with depth and the bottom is heated geothermally, the bottom convecting layer is stable and nearly isothermal, 300-400 m thick, O(1000) years old, and perhaps 0.5 K warmer and 3 Wt% more saline than the overlying water [Ozsoy and Unluata, 1997], Double diffusive convection is observed directly above (and possibly below) hydrothermal systems in the Red Sea [Blanc and Anchutz, 1995, Anschutz et al., 1998]. Convective layers in the Red Sea moved upward in the thirty years since they were first observed in the 1960's [Anschutz et al., 1998]. No such change has been noted for Lake Vanda. Kelley et al. [2003] speculate that high-latitude regions on Earth may be largely susceptible to diffusive regime double-diffusive convection, based on analysis of R_ρ in areas where salinity and temperature profiles have been measured.

3.2 *Implications for Europa's Geologic History*

Layer evolution could be indicated by the relatively recent occurrence of melt-through features in Europa's surface history. Surface stratigraphy of the icy lithosphere [Figueredo and Greeley, 2004] suggests melt-through rather than tectonic processes dominate Europa's surface dynamics in the current epoch. If we take this to indicate a trend toward complete resurfacing of a the ice shell, the spread of a warm salty layer to the surface may be key to explaining the time scale of the process. If the warm layer moves upward with the addition of heat and salt, as in the Red Sea [Anschutz et al., 1998], chaos features could indicate intrusion of a warm plume after the layer reaches some critical height.

Might storage of heat be responsible for catastrophic melt-through and resurfacing of Europa's ice? The minimum ocean temperature above freezing needed to melt the entire ice shell can be estimated by solving for ΔT_{ocean} in

$$M_{ocean} C_P \Delta T_{ocean} = M_{ice} Q_{ice} + M_{ice} C_P \Delta T_{ice}, \tag{3.3}$$

the equation of heat transferred from the ocean in order to melt the entire volume of the ice shell. T_{ocean} is the amount, in K, by which the ocean temperature exceeds the freezing temperature of the ice shell. Q_{ice} is the latent heat of melting, 334 kJ kg^{-1}. M_{ocean} and M_{ice} are the masses of the ocean and ice layers, $M \sim \frac{4}{3}\pi(R^3_{top} - R^3_{bottom})\rho_{water}$, respectively. ΔT_{ice} is the increase in temperature necessary to reach to the melting temperature. We take ΔT_{ice} to be $\sim$ 86 K, the average difference between Europa's surface temperature ($T_{surface} \sim$ 100 K) and an ocean ceiling at 273 K. With C_P of 4 kJ kg^{-1}, the ocean temperature above freezing needed to melt a 2 km ice shell is around 5 K. Fig. 5 illustrates how the ocean temperature above freezing scales with ice thickness.

The time scale to heat the ocean by O(1) K can be estimated as .

$$t \sim \frac{M_{ocean} C_P \Delta T}{F}. \tag{3.3}$$

$F = 4\pi R^2_{seafloor} H$ is the total heat flux from the seafloor, in W. The time scale to heat a 100 km ocean by $T = O(1)$K is $t \sim 10^2 - 10^1$ Myr for the lower and upper estimates of heat inputs used in this paper (H = 0.15 to 4 mW m^{-2}), respectively (for other assumed values, see Appendix). Thus, resurfacing of the ice shell by heat stored in Europa's ocean is possible on the time scale of Europa's 30-80 Myr surface age [Zahnle et al., 2003] if the ice shell is thinner than 1 km or heat storage is effective enough to heat the ocean to O(1) K above the melting temperature of the ice shell. Neither of these possibilities is ruled out by current knowledge of Europa or studies of double-diffusive convection to date.

Upward progress of convecting layers is not the only possibility. For instance, if tidal and radiogenic heat inputs are dissipated effectively, perhaps through a thin ice shell and thin diffusive layers separating convecting zones, double-diffusive layers could actually move downward. Future work should examine heat balance in Europa's ocean.

3.3 Conclusion

We have demonstrated the possible existence of a layered system analogous to double-diffusive convection systems on Earth. Saline enrichment in nascent upwellings provides a depth-dependent stay on buoyancy similar to the effect pointed out by Melosh et al. [2004]. The effect implies stratification of the ocean, and may indicate a means for the onset of layered convection. As a test of the feasibility of double-diffusive convection, we find mild saline stratification consistent with parameters expected for layering systems [Kelley et al., 2003].

Heat storage and release via stratification, mediated perhaps by double-diffusive

convection, may be the temporal link between surface and subsurface processes, only if the ice shell is very thin (< 1 km) or the mean ocean temperature significantly higher (> 1 K) than the freezing temperature of the ice shell. Further quantitative treatment of compositional effects in Europa's ocean is necessary, pending the contribution of more experimental data on sulfate salts, and investigation of double-diffusive phenomena, both in the lab and via exploration of systems in Earth's waters.

Chapter 4

SETUP AND OPERATION OF THE ICY SATELLITE INTERIOR SIMULATOR

In its original conception, the Icy Satellite Interior Simulator (ISIS) operated schematically in identical fashion to the system developed by Surya Wiryana. This system included three subcomponents: hydraulic, fluid, and loading. The loading portion was subsumed into the hydraulic component during the development of the new system after it was determined that a rubber capped glass cuvette served as an effective sample container (fluid component). In the description of ISIS's components that follows, we relate details of some of the original components, which serves to highlight some principles of high pressure design. A manual for operating ISIS concludes this section.

4.1 A Description of ISIS

4.1.1 Hydraulic Component

The hydraulic component consists of equipment for pressure generation and measurement: a pressure generator (PG), a 10x intensifier (I), a fluid reservoir (R), a low pressure gauge (LG), a high pressure gauge (HG), and a number of valves the, as described below.

The Pressure Medium

To avoid corrosion in the system and to aid in obtaining a high pressure seal, we chose as a hydraulic medium the diester fluid di(2-ethylhexyl) sebacate (known also as dioctyl sebacate, and by its trade name, Monoplex DOS or simply DOS), which

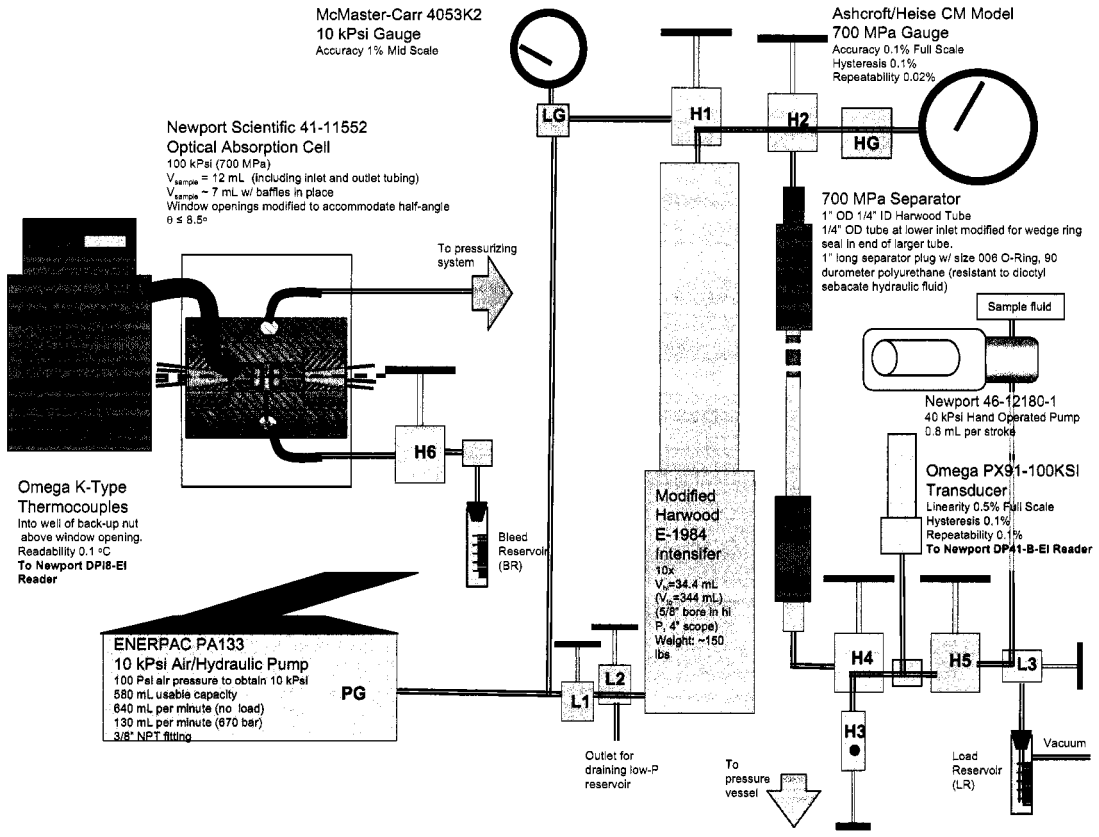

Figure 4.1: Schematic of the apparatus for obtaining high hydraulic pressure in aqueous solutions.

has been found to be well suited for the range of pressures considered, with viscosities that change by only three orders of magnitude between 0 and 500 MPa (O(1) to O(4) μm MPa^{-1} s^{-1}; Vergne [1990]) at room temperature.

The final version of the system employs a five percent by volume mixture of fuel-grade kerosene and DOS. Contrary to previous claims that the fluid remains clear to -35 °C and 300 MPa [Gagnon et al., 1988], we found pure dioctyl sebacate clouded below $\sim$ 10 °C at the lowest pressures employed (50 MPa). This may have been due to

the presence of the silicone grease used to seal the sample cuvette. Pure 50 cS silicone fluid, when used as a pressure medium, was found to gel irreversibly at moderate pressures when loaded in pure form, and at the lowest pressure at temperatures below the freezing point of water. With the hypothesis that clouding was due to the formation of wax particles, kerosene was added to the sebacate oil to act as a solvent. Pure kerosene was tested as a hydraulic fluid, but was found to absorb the incident infrared light, thereby attenuating the ISS signal.

It was occasionally necessary to flush with fresh fluid, as the sebacate oil took on a greenish color over time. Placing a nitrile o-ring in a 10 mL flask of DOS for about a week produced the same effect, so the discoloration was attributed to prolonged exposure to nitrile rubber present in the air-hydraulic pump and in the o-ring seals of the pressure vessel. This tinted fluid weakened the ISS signal, presumably by absorbing the frequency-doubled (green) laser pulses. Placing a 1 cm path length cuvette in front of the water standard eliminated the signal, but putting the same cuvette in the path of the infrared light had no effect on the signal.

Generation of Moderate Pressure

The first version of the system incorporated a High Pressure Equipment 30,000 psi (330 MPa) model 37-6-30 screw piston pressure generator with a capacity of 11 mL per stroke. The reservoir consisted of a 500 mL vacuum flask sealed with a two-hole stopper, with 1/4" ID brass tubes connected to rubber tubing to allow movement of hydraulic fluid from the base of the flask to two valve inlets in the hydraulic component of the system. For ease of use, this system was replaced with an ENERPAC model PA133 air/hydraulic pump capable of producing 10,000 psi of pressure with 100 psi of air, with an internal reservoir of 580 mL. A Newport model 12182 hand-operated pump, contributed by Ivan Getting, was also connected directly to the high pressure side of the system at H5, allowing for direct application of up to 280 MPa without the use of the pressure intensifier.

Pressure Intensification

Elevated pressure is generated using a 10x intensifier, a modified Harwood, Inc. model E-1984 donated by George Shaw, of Union College in New York. The intensifier operates by the transmission of pressure across a ratio of areas that defines the pressure multiplier. Low and high pressure reservoirs are of equal length, and the low pressure reservoir in the modified E-1984 has ten times the volume of the high pressure reservoir. The piston transmits pressure by pushing a plug in the high-pressure cylinder. The plug uses a teflon washer and brass wedge ring on both sides to obtain a Bridgman seal. Another Bridgman seal is obtained at the outlet end of the high-pressure cylinder with lead and teflon washers, and another brass wedge ring. The high- and low-pressure cylinders have capacities of 34 and 340 mL, respectively.

Pressure Measurement

A low-pressure gauge, McMaster-Carr catalog number 4053K2, rated to 10,000 psi (70 MPa), was used to indicate operation of the low-pressure side of the system.

A high-pressure Heise CM model dial gauge traceable to a National Institute of Standards and Technology dead-weight standard, allowed measurement of pressure to 700 MPa with a precision of 0.1 %. The gauge is temperature-compensated and includes physical stops to protect against loss of calibration in the event of rapid depressurization.

Plumbing

Low-pressure valves used in the 700 MPa system are rated to a minimum of 10,000 psi. For the purpose of this description, only their functional roles are important. Low-pressure valves L1-L4 perform the following functions. L1 allows uptake of fluid from the reservoir into the pressure generator; L2 and L3 allow isolation of the pressure generator when taking up fluid, and when resetting the intensifier; L4 allows

reinsertion of fluid into the reservoir when resetting the intensifier.

High-pressure valves are rated to 100 kpsi (700 MPa). These were purchased from Newport Scientific, Inc. H1 separates the low- and high-pressure sides of the intensifier. H2 can be used for isolating the hydraulic system. H3 opened when bleeding fluid from the top outlet of the pressure vessel.

4.1.2 Fluid Component

The fluid component consists of a separator (S), fluid reservoir (FR), the pressure vessel (PV), and four valves.

Separator

The original design of the Icy Satellite Interior Simulator required a means for isolating the corrosive sample from the hydraulic medium. A separator was build for this purpose (Fig. 4.2). The separator tube and connector remain in use in the final version of the system as the additional high pressure volume serves to slow leaks and allows for finer control of pressure.

The separator is constructed from Harwood 16F tubing (1/4" ID, 1" OD, cold-drawn 304 SS in a jacket of 17-4 PHS). To separate hydraulic from sample fluid, a 1" long cylindrical plug was fit to the interior of the tube, with an o-ring groove for a size 006 o-ring at one third it length. Nitrile was initially used as the o-ring material, but was found to swell and corrode under pressure. Durometer 90 viton was tested but an acceptable seal was not obtained. Durometer 90 polurethane was found to provide an acceptable fit, consistent with findings of Paterson [1964]. O-rings were obtained locally from O-Rings West, Inc. With the plug in place, the separator volume was 9 mL.

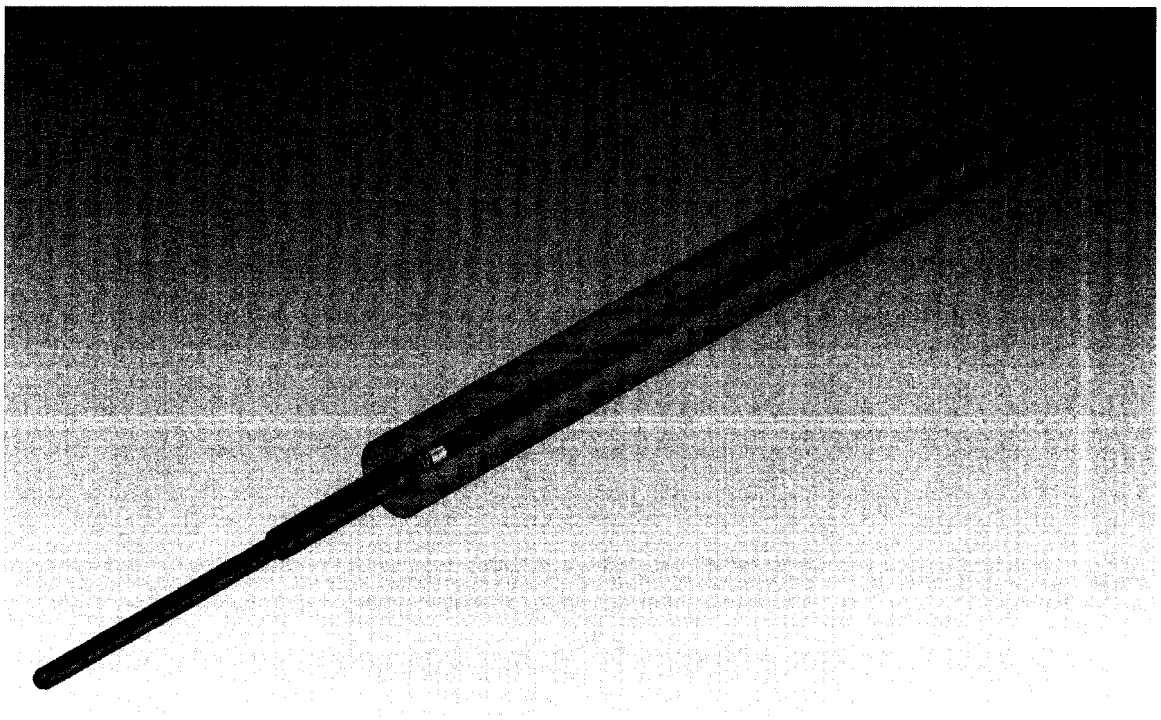

Figure 4.2: Separator assembly. A Harwood type M 1" diameter tube, honed to 0.259", accomodates a Bridgman-sealing piston plug with unsupported areas provided by a sealed interior volume. The separator connector tube (lower left) also employs a Bridgman unsupported-area seal in the interior space of the separator tube, allowing for the application of corrosive fluids in the sample region. The other end of the separator is sealed with a Harwood M-type compression fitting, adapting to a standard 1/4" high pressure tube.

Separator Connector Tube

The Harwood M-type fitting is a compression fitting that should not be regularly reopened. It was therefore necessary to find a means to reliably open and reseal the separator tube. Bill Newhall (President of Harwood, Inc.) designed a Bridgman sealing system on the end of a turned portion of a 1/4" 100 kPsi (700 MPa) tube. The separator end fitting (modified version depicted in Fig. 4.3; Harwood drawing number

B11729) was remade a number of times in the process of obtaining a reliable seal and finding an optimal means for extracting the device. The original design incorporated a conical washer to accomodate the 45° bevel of the steel wedge ring. This was apparently done to keep the Bridgman seal away from the threaded portion of the tube that was needed for a retaining nut. After it was determined that teflon and lead washers might be needed for sealing in the 150-250 MPa regime, we undertook to machine a proper mating bevel on the new tube. The threaded portion of the end fitting was eliminated by making the 1/4" OD piece from a 3/8" 150 kPsi tube (Figs. 4.3-4.5).

Separator Piston Plug

The piston plug, suggested by George Shaw of Union College and shown in Figs. 4.6-4.8, was fabricated on a lathe from a rod of 304 stainless steel. A mushroom-cap cylinder was made to fit into a second piece with a slotted interior volume. This second piece was itself made of two pieces, the slotted portion and a smaller capping piece with a circular through-hole, that were silver-brazed together at $\sim$ 1100°C. Brass wedge rings were fabricated that would seal on the inner surface of the separator tube on two outer wedges, and on an interior wedge. The allowance for interior volume allows the plug to compress under the application of hydraulic pressure. Pre-loading of the plug on insertion seats the teflon ring for operation of the plug up to the $\sim$250 MPa sealing pressure of the brass wedge rings.

For greater ease of machining and brazing, and for more precise pre-loading, subsequent designs of the plug were built in a manner that allowed the mushroom cap to be inserted after brazing the mating piece. A 0-64 nut was fashioned that could slide freely in the slot. This was captured in the interior volume after the bottom pieces were brazed together. The mating slot on the mushroom plug was replaced with a thread, which eliminated the need to for delicate filing of the slotted end during fabrication.

The plug was tested in the separator assembly on three occasions. In the first two cases it was apparent that a satisfactory seal had been achieved, but leakage occurred on the third test. The plug was removed after we developed a method for isolating the sample fluid within the pressure vessel in a spectrophotometric cuvette.

Pressure Vessel

The pressure vessel is a Newport Scientific model 41-11552 Optical Absorption Cell, rated to 100 kPsi (700 MPa). The cell body is a cylinder of type 403 stainless steel with a 4" OD and 6 3/8" length. High pressure inlets for 1/4" tubing are positioned at the center of the wall, 120^o apart. One inlet is positioned vertically to allow displacement of air on loading of hydraulic fluid.

4.1.3 High-Pressure Plumbing

High-pressure valves H3 and H5 isolate the separator from the pressure vessel. H4 was originally intended to separate the loading component from the fluid component. In the absence of the separator component of the system, H4 is useful for confirming high pressure operation using the Bourdon-tube gauge, and for tracing leaks.

4.2 Operating Instructions for the High Pressure System

Loading, operation and disassembly may be performed as follows (pages formatted for copying and posting). The description assumes a starting condition of a disassembled (though not necessarily clean) system.

Cleaning Sample and Window Pieces

- Rinse DOS from the outside surfaces of the sample cuvette using acetone.
- Wipe any silicone oil from the polurethane stopper using a lint-free wipe wetted with acetone.
- Wash sample cuvette and stopper with de-ionized water and place in a 10 mL flask with 3-4 drops Starna cleaner.
- Clean window pieces (window holders, back-up-rings and windows) and sample holder by rinsing all surfaces and wiping with lint-free cloths (Kimwipes).
- Transfer from the original aluminum foil lined bin to another, newly lined, bin.
- Repeat if necessary.
- Clean optical sapphire window surfaces with lense tissue and acetone.

Assembling Window Pieces

- Inspect windows to insure cleanliness. If window appears slightly pocked, a high pressure seal may still be obtained. It is important in this case to choose the smoothest of the two window faces for the metal-facing side.

- Place window holder with polished face upward.

- Install back-up ring and polurethane durometer 90 o-ring.

- Gently position sapphire window so it is centered on the aperture in the holder. If the holder and window are clean, a single, concentric, diffraction pattern appears at the metal-sapphire interface. If a finely spaced linear pattern appears instead, the window is slightly elevated on one due to a piece of contaminant. Pushing the window down in this case will most likely provide a high pressure seal, but repeated loading in this manner may damage the window surface.

- Place the window holder clip over the window so it holds the window firmly against the metal surface. The holder clip is matched to the window holder. The clip may be refit to the window by squeezing it in a one inch (25.4 mm) lathe collett or opening it using a hammer and a screwdriver handle or other round-ended cylinder of the appropriate size.

Loading Sample

- Apply a thin, barely visible, layer of silicone grease to the walls of the polyurethane stopper and set aside.
- Fill a short 100 mL container with sample fluid sufficient to drown the sample cuvette.
- Rinse the cuvette with sample fluid then place in pre-filled container.
- Position stopper in top of cuvette, taking care not to get grease on outer optical surfaces.

Resetting Intensifier

- Valve settings: H1 and L1 closed, H5 and L2 opened.
- Apply pressure using the hand pump, with a regular pumping motion, until the fluid level of the piston indicator tube is at the minimum marked.

Loading the pressure vessel

- Valve positions: H4 closed, H5 and H3 open.
- Load fluid using the hand pump until ~10 mL of fluid escapes from bleeder. A slow, regular, pumping action seems to ensure laminar escape of air contained in the system, which seems to correlate with a minimum chance for leaking sample fluid.
- Close H6 and H5 while applying moderate pressure with the hand pump (this prevents leakage from depressurization of the windows).

Run-time Operation

- Note: contact of the thermocouple with window face should be verified by the adiabatic change in temperature ($\sim 0.5-1\ ^{o}$C for a 50 MPa change in pressure).

  Low Pressure Operation

  - Valve positions: L3 and H4 closed, H5 and H3 open.
  - Use the hand-operated pump to apply pressure up to 280 MPa.

  High Pressure Operation

  - Valve positions: H5 closed; L3, H4 and H1 open.
  - Use the hand-operated pump to apply pressure up to 700 MPa (going higher may affect the linearity of the pressure transducer).

Unloading

- Valve settings: H3 closed, H5 open
- Unscrew the window retainer nuts by hand. If necessary, obtain additional torque by inserting 1/4" bolts into bleed holes.
- Extract each window assembly by screwing a 3/8-16 rod into the thread of the window holder opening and pulling while gently rocking. Have a paper towel ready to absorb leaked fluid.
- If it did not come out with one of the window pieces, reach into the vessel bore and remove the sample holder.
- Set aside the window pieces and sample holder in a plastic bin lined with aluminum foil in order to protect the windows from damage and keep oil off of instrumentation.
- If necessary, remove a stuck back-up ring by tapping against its inner surface with a brass rod, alternating to opposite inner sides to avoid deforming the ring.

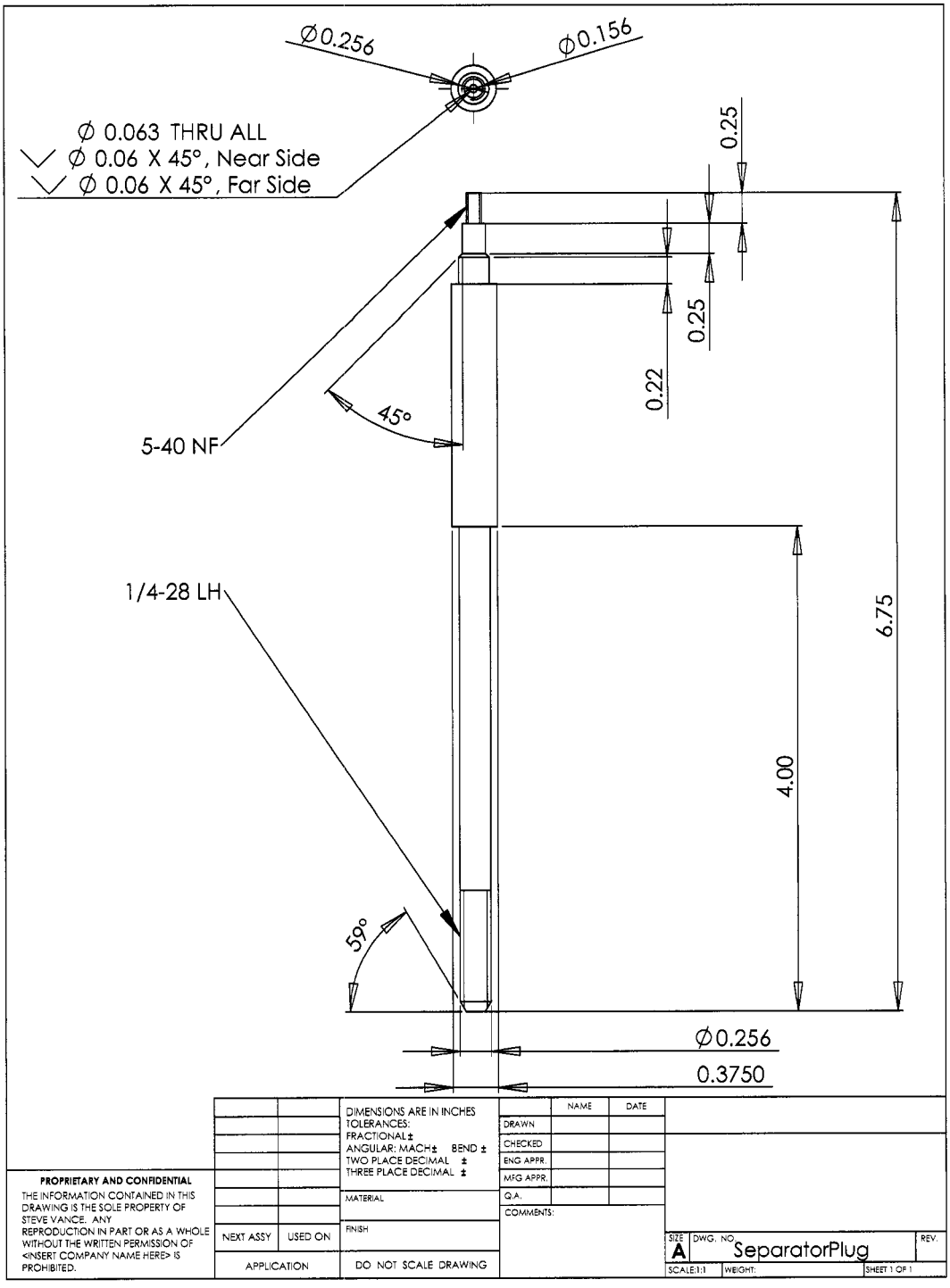

Figure 4.3: Detail of separator connector tube. Modified from Harwood drawing number B11729.

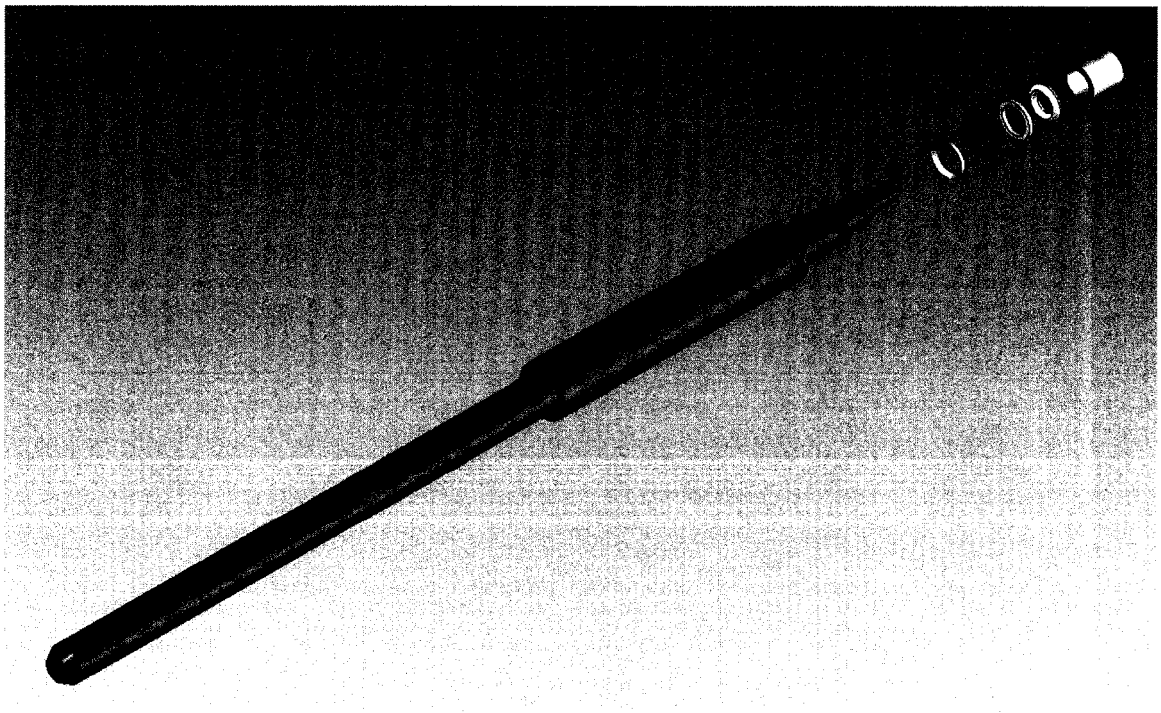

Figure 4.4: Exploded view of separator connector tube.

Figure 4.5: Assembled separator connector

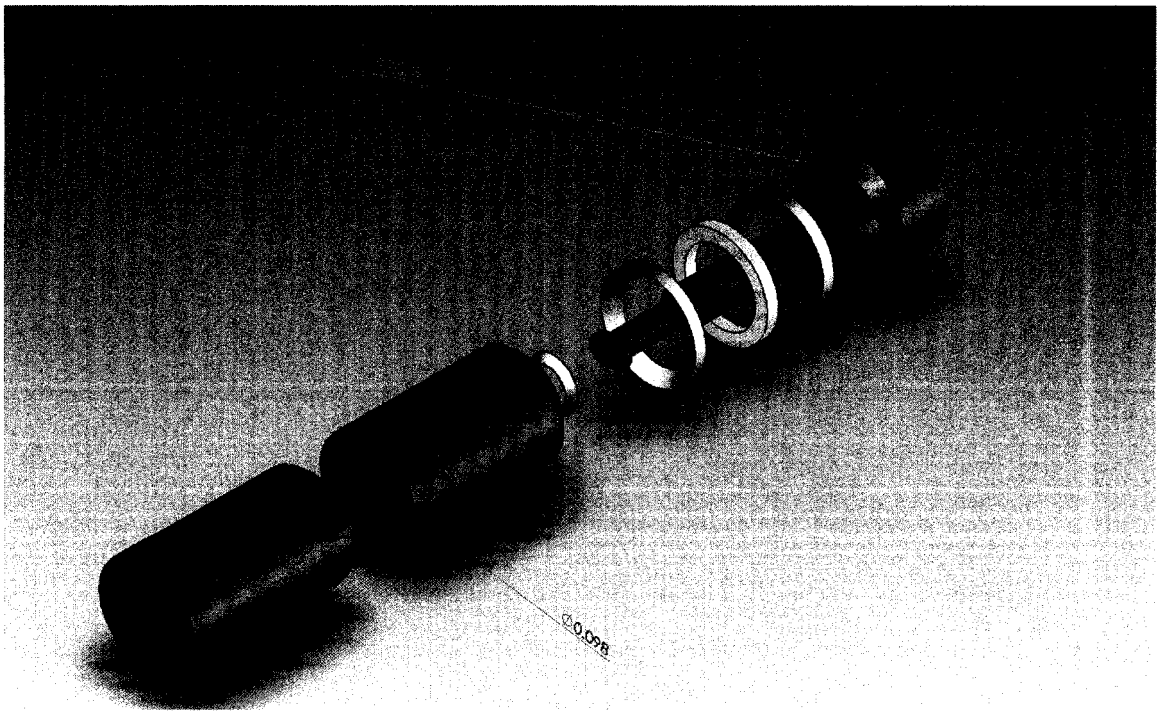

Figure 4.6: Exploded view of separator piston plug. Three Bridgman unsupported-area seals allow the plug to properly seat and seal to 700 MPa.

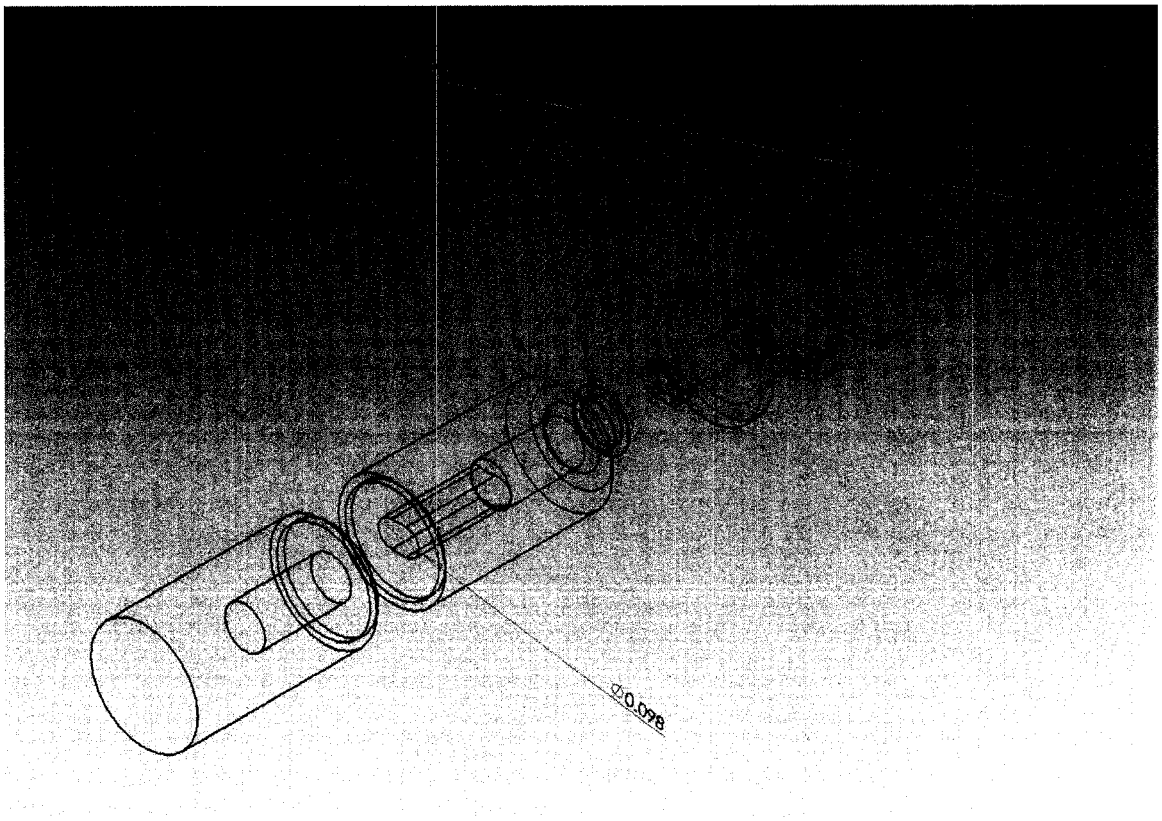

Figure 4.7: Exploded wireframe view of separator piston plug.

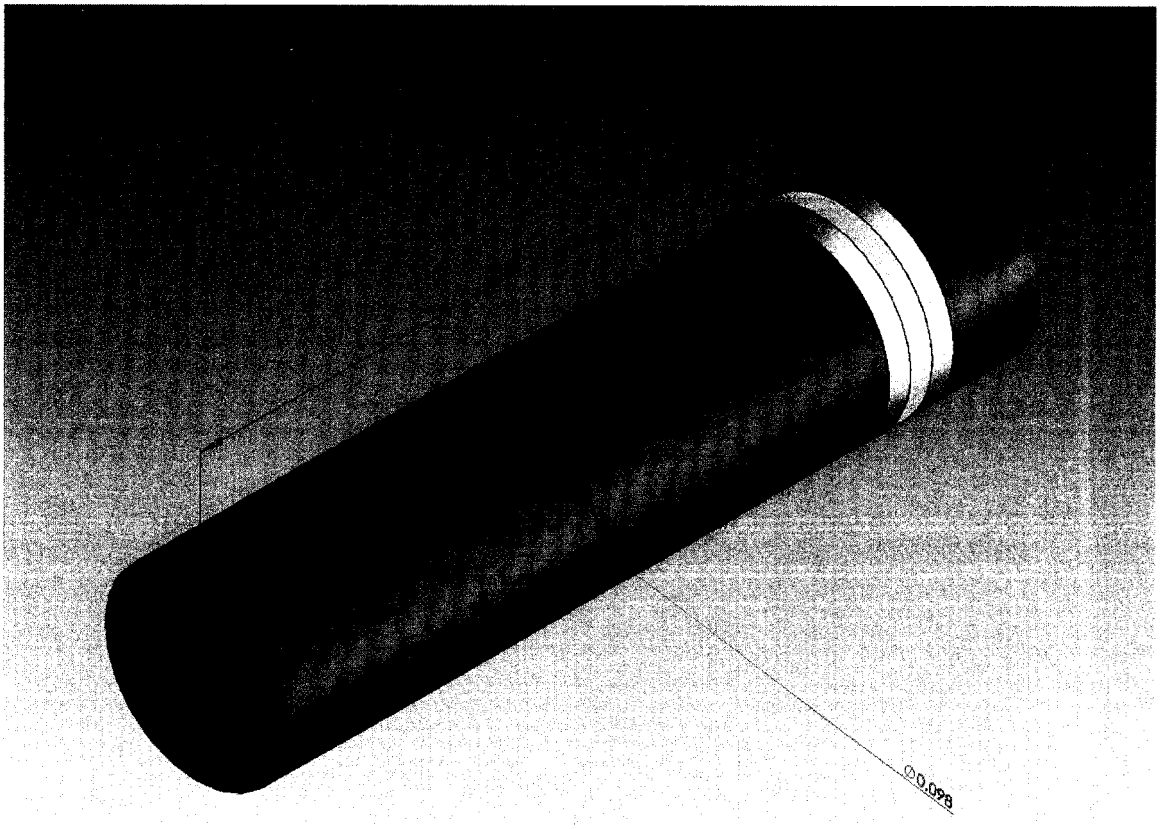

Figure 4.8: Assembled separator piston plug.

Chapter 5

SOUND VELOCITIES IN WATER TO 700 MPA AND -20 TO 100 ^{O}C

5.1 Introduction

To test for systematic errors in the Icy Satellite Ocean Simulator (Chapter 4), sound velocities in pure water were measured by impulsive stimulated scattering, an optical method for generating an acoustic excitation and tracking its evolution [Abramson et al., 1999]. These measurements extend coverage of previous ultrasonic measurements at subzero temperatures to 700 MPa. The new measurements also provide improved coverage of the sub-GPa range of pressure.

5.2 Equipment and Methods

Impulsive stimulated scattering (ISS) was used to measure velocities [Abramson et al., 1999]. The identical instrumentation was used as in previous experiments. A Quantronix model 416 Nd:YAG laser was used to generate $\sim$ 100 ps infrared pulses (θ_{IR} = 1064 nm). In this experiment, the convergence in the sample of split pulses at a known angle causes an instantaneous change in index of refraction where constructive interference causes heating. Impulsive expansion of the heated regions sets up a standing acoustic mode on the time scale of tens of nano-seconds. The interference pattern acts as a diffraction grating, the modulation of which can be tracked by the diffracted portion of a frequency-doubled pulse, delayed by time-of-flight, to give the sound frequency.

For the present study, the whole angle of the incident infrared beams was θ_{IR} = 15.2^{o} to accommodate the apparatus described below. The nominal wavelength of

the resulting grating in index of refraction, determined from the Bragg condition for interference, is $\lambda = \lambda_{IR}/2\sin(\frac{\theta_{IR}}{2})$. The precise wavelength was inferred from ISS measurement of the sound frequency in de-ionized water at one bar and ambient temperature, for which the sound velocity is known to high precision. Sound velocity in water was determined from the IAPWS equation of state [Wagner and Pruss, 2002].

5.2.1 The Icy Satellite Interior Simulator: An Apparatus with Optical Access for In-Situ Measurements to 700 MPa from -20 to 100 °C

The Icy Satellite Interior Simulator (ISIS) was constructed for the investigation of phenomena in simulated ocean planet environments. The system (Fig. 4.1) employs a Newport Scientific optical absorption cell modified to accept beams incident at an included angle of up to twenty degrees. The cell's standard sapphire windows were replaced with c-axis oriented windows purchased from Guild Optical Associates, Inc.

Samples were contained in a Starna 10 mm glass spectrophotometric cell cut to fit in the 25 mm opening of the pressure vessel and sealed using a piece of durometer 70 polyurethane cut to roughly 1x1x0.5 cm. The edges of the plug were coated with silicone grease to insure against leakage. The sample cuvette was then placed in a brass holder machined to fit in the cylindrical opening of the pressure vessel and to prevent breakage of the cuvette from over-tightening of the window retainer nuts. Dioctyl sebacate was used as the hydraulic fluid. Contrary to previous claims that the fluid remains clear to -35 °C and 300 MPa [Gagnon et al., 1988], we found pure dioctyl sebacate clouded below $\sim$ 10 °C at the lowest pressures employed (50 MPa). This may have been due to the presence of the silicone, which was found to gel irreversibly at moderate pressures, and at the lowest pressure at temperatures below the freezing point of water. To prevent clouding 5% kerosene was added by volume. Pure kerosene was tested as a hydraulic fluid, but was found to absorb the incident infrared light, thereby attenuating the ISS signal. The sebacate oil took on a greenish coloration after prolonged exposure to nitrile rubber present in the air-hydraulic pump and in

the o-ring seals of the pressure vessel. This discolored fluid weakened the ISS signal by absorbing the frequency-doubled (green) laser pulses, so it was occasionally necessary to flush with fresh fluid.

5.2.2 Control and Measurement of Pressure

Pressure was generated with a 70 MPa pressure source connected to a Harwood 10x intensifier. Pressure was measured using an Omega 700 MPa transducer cross-calibrated to a Heise CM model 700 MPa Bourdon-tube gauge. Precision in the measurement of pressure is estimated at 0.2%. In the worst cases, pressure fell by up to 20 MPa when leakage occurred. It was observed that this drop was usually linear in time. In such cases, it was deemed prudent to take as the measured value the average of pressure readings at the start and end of the ISS measurement. Under normal operating conditions, pressure was stable to within about 0.3 MPa, well under the 0.7 MPa error equivalent to the error in the ISS measurement.

5.2.3 Control and Measurement of Temperature

Temperature was controlled to within 0.1 °C on the time scale of measurement using a Lauda 107 chiller, which circulated a fluid (ethylene glycol) copper tubing brazed to a bronze cylinder fitted to the outside of the pressure vessel. Temperature was measured to ±0.1 °C with a chromel-alumel thermocouple in contact with the sapphire window. Contact with the outside of the window was verified from the adiabatic change in temperature on pressurization of the sample, which was immediately discernible as a change of roughly one °C per 100 MPa. This responsiveness was taken to indicate our measurement of the outside window temperature correlated well with the temperature of our sample. Thermocouples were occasionally calibrated to the melting and boiling temperatures of water at atmospheric pressure.

The effect of temperature on the ISS signal was appreciable. At the lowest temperatures and pressures, the reduced thermal expansivity of water limited the strength

of the diffracted signal used to measure the sound velocity. Conversely, at temperatures greater than the ambient temperature of the calibration standard, the diffracted signal was often much stronger than in the standard.

5.3 Results

Systematic errors in the measurement of velocity were estimated to be 0.2% under optimal conditions due to drift in temperature, pressure, and the alignment of optics. Under the worst conditions, errors are conservatively estimated to have been as high as 1%. These estimates are consistent with comparisons of our data with previous measurements and equations of state (see 6.4).

Results of velocity measurements are summarized in Table ??. Dates, measured frequencies and filenames are given for archival purposes. Calculation of densities is discussed in Chapter 6.

5.4 Discussion

Velocity measurements along six isotherms are displayed in Fig. 5.1. These describe a smooth surface in P and T. Individual measurements along six isotherms are shown in panels to the right of the main window along with curve fit.

Residuals between our velocity measurements and the reference equation of state [Wagner and Pruss, 2002] are shown in Fig. 5.2. Where comparison is made with individual points from published data, velocities are within three degrees of each isotherm. Our data are grouped by pressure within 10 MPa and by temperature within the range printed above for each isotherm.

Measurements by Holton et al. [1968] at 50 °C, which are incorporated into the IAPWS equation of state, tends to be lower than the equation of state and its other reference data at the same temperature [Fujii and Masui, 1993, Wilson, 1959] by as much as 5%. This trend occurs at all temperatures in our data set in the range of their measurements, which may indicate a systematic bias in the measurements of

Holton and coworkers (1968). Where larger numbers of measurements are available, our velocities are in good agreement with the reference data. This suggests that our apparatus is well calibrated and our measurements free from major systematic error.

Residuals of velocity with the reference equation of state at 0 °C follow a similar trend in pressure as the reference data used in the database [DelGrosso and Mader, 1972]. At 0 and -10 °C, our measurements confirm those of DelGrosso and Mader [1972] and extend them to 700 MPa.

5.5 Conclusion

New impulsive stimulated scattering measurements of velocity for pure water extend coverage of previous ultrasonic measurements at subzero temperatures to 700 MPa. The new measurements provide improved coverage of the sub-GPa range of pressure. This analysis also provides assurance that our system is free from major systematic errors.

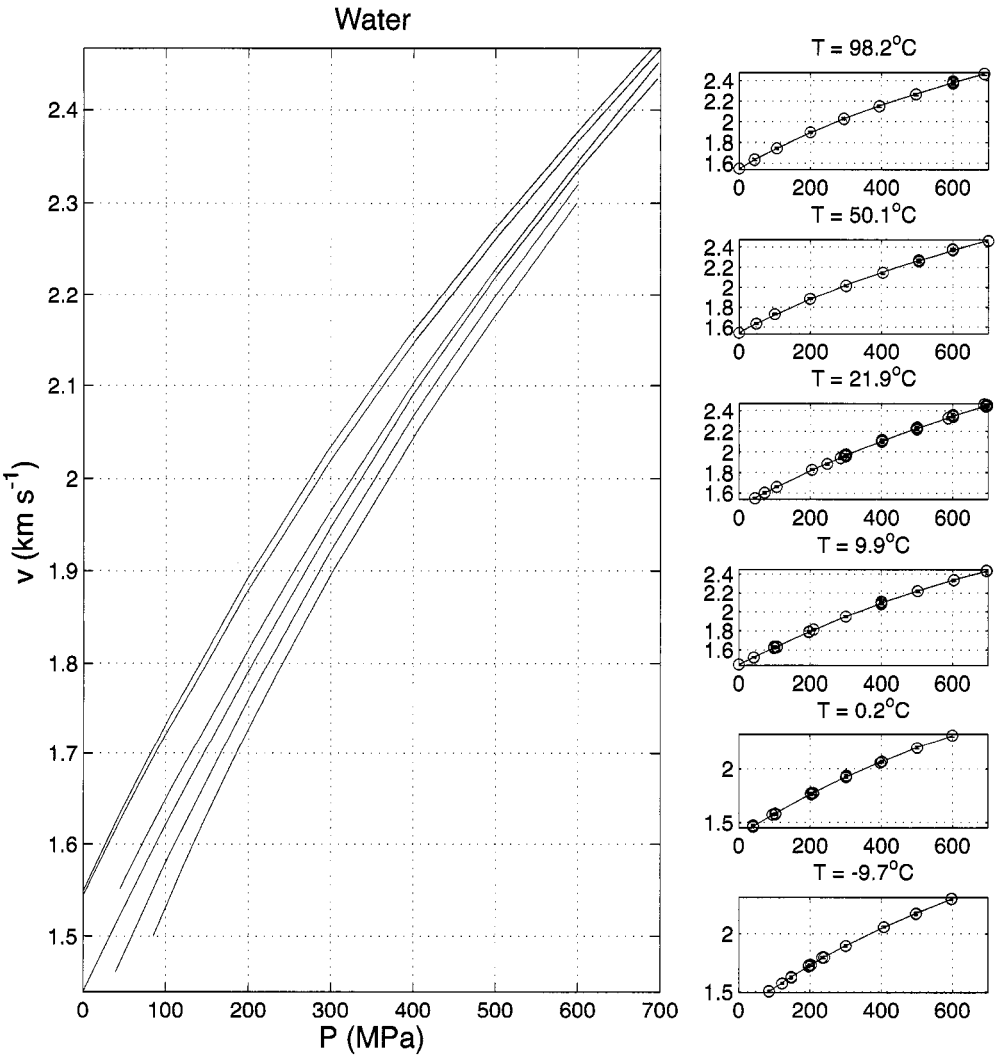

Figure 5.1: Sound velocities in water to 700 MPa from 0 to 95 °C. Velocities are plotted on the vertical axis (in km s^{-1}) as a function of pressure (in MPa) on the horizontal axis. The panels at the right show measurements (circles) along the isotherms noted. For each temperature, a third degree polynomial fit in pressure is displayed (lines). The fitted velocities are shown together in the large panel at the left to illustrate a smooth surface in pressure and temperature.

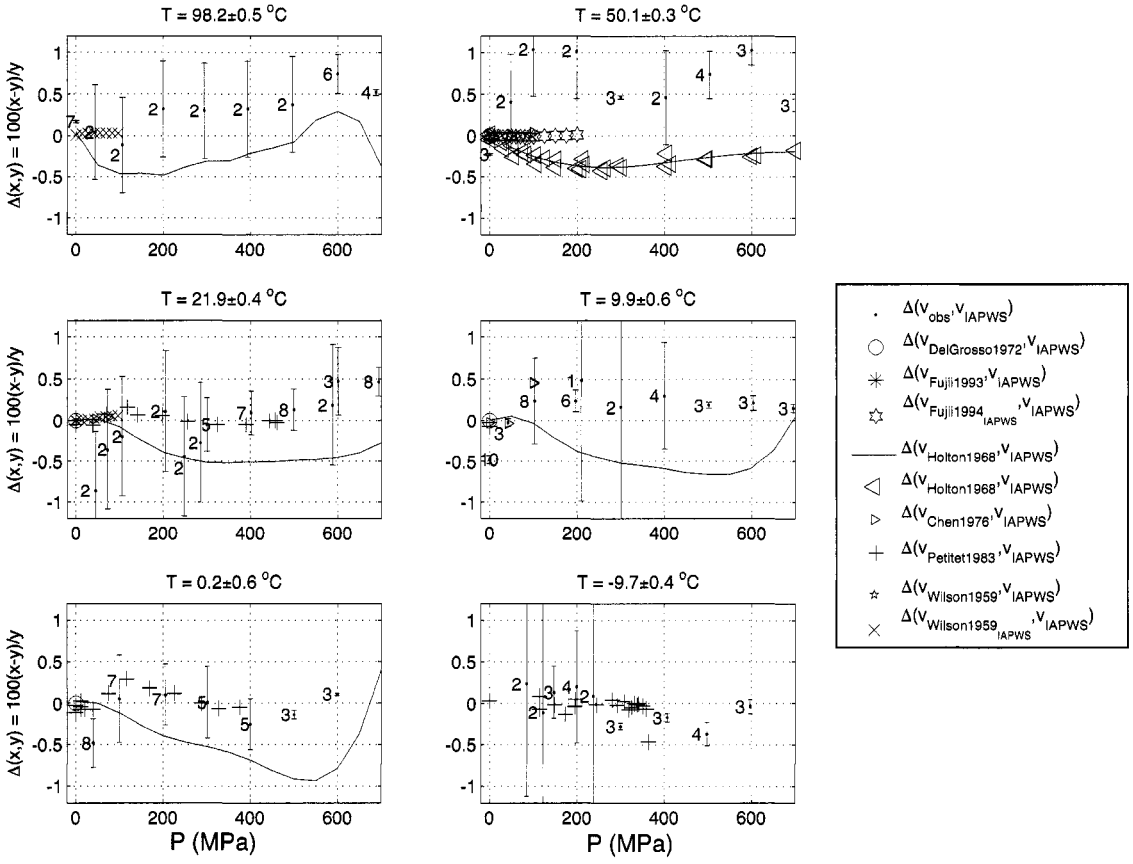

Figure 5.2: Comparison of sound velocities from this study with previously published values. Residuals are referenced to the equation of state from the International Association for Properties of Water and Steam [IAPWS; Wagner and Pruss, 2002]. For statistical purposes, grouped data are corrected using the reference equation of state to lie on the isotherm and on the mean pressure for each bin. Where more than two measurements were made, error bars indicate two standard errors; otherwise, error bars are the twice the maximum standard deviation for scaled measurements on the isotherm.

Chapter 6

EQUATION OF STATE FOR CONCENTRATED AQUEOUS $MGSO_4$ TO 700 MPA AT TEMPERATURES FROM -20 TO 100 ^{O}C FROM MEASURED SOUND VELOCITIES

6.1 Introduction

The previous chapters motivate a study to improve the equation of state for solutions relevant to deep icy satellite oceans such as Europa's. In this chapter, we describe new measurements of sound velocity in magnesium sulfate to high concentration (2.0137 m) and pressure (700 MPa). From these we calculated solution densities, which differ from theoretical prediction [Marion et al., 2005] by as much as 5% at the highest pressures and at the highest and lowest temperatures. From our densities we inferred excess volumes and partial molal volumes at infinite dilution, which are needed for accurate predictions of solubility at elevated pressures. Our results indicate that predictions of solubility using the present state of the art [Marion et al., 2005] are accurate for low concentrations up to about 200 MPa and at 20 ^{o}C, but may fail at significantly higher or lower temperatures, or at higher pressures.

Sound velocities were measured in aqueous magnesium sulfate ($MgSO_4$) by the method of impulsive stimulated scattering, an optical method for generating an acoustic excitation and tracking its evolution [Abramson et al., 1999]. Densities were calculated from the adiabatic relation for the bulk modulus and apparent and partial molal volumes were inferred based on the equation of state for water.

Density data for aqueous systems are scarce or non-existent at concentrations, temperatures and pressures relevant to subsurface aqueous reservoirs in icy satellites.

There is a particular need for more work in the range of high salinity ($m \gtrsim 1$ molal (10%) in the $MgSO_4$ system) and in multi-component systems, though recent studies have begun to address that issue [Abdulagatov et al., 2007, Hogenboom et al., 1995, Motin, 2004]. Until now, measurements at both low temperature and high pressure (> 100 MPa) were non-existent. We know of only one other study of $MgSO_4$ densities at high pressures [Chen et al., 1977, at 273.15, 298.15, and 323.15 K, to 1 m and 100 MPa]. Studies of solubility and freezing in the $MgSO_4$ (aq) system [Fig. 6.1 Hogenboom et al., 1995] reveal a lower temperature liquidus at 390 MPa, encompassing the pressure range relevant to depths in Europa's ocean, and oceans in other icy satellites and planets. While this work extended several hundred MPa above the highest pressures in Europa's ocean and possibly above the highest pressure in oceans in other satellites low-temperature density data were published only at 0.1 MPa.

6.2 Equipment and Methods

Impulsive stimulated scattering (ISS) was used to measure velocities [Abramson et al., 1999]. The identical instrumentation was used as in previous experiments. A Quantronix model 416 Nd:YAG laser was used to generate $\sim$ 100 ps infrared pulses (θ_{IR} = 1064 nm). In this experiment, the convergence in the sample of split pulses at a known angle causes an instantaneous change in index of refraction where constructive interference causes heating. Impulsive expansion of the heated regions sets up a standing acoustic mode on the time scale of tens of nano-seconds. The interference pattern acts as a diffraction grating, the modulation of which can be tracked by the diffracted portion of a frequency-doubled pulse, delayed by time-of-flight, to give the sound frequency.

For the present study, the whole angle of the incident infrared beams was $\theta_{IR} = 15.2^o$ to accommodate the apparatus described below. The nominal wavelength of the resulting grating in index of refraction, determined from the Bragg condition for interference, is $\lambda = \lambda_{IR}/2\sin(\frac{\theta_{IR}}{2})$. The precise wavelength was inferred from ISS

measurement of the sound frequency in de-ionized water at one bar and ambient temperature, for which the sound velocity is known to high precision. Sound velocity in water was determined from the IAPWS equation of state [Wagner and Pruss, 2002].

6.2.1 The Icy Satellite Interior Simulator: An Apparatus with Optical Access for In-Situ Measurements to 700 MPa from -20 to 100 °C

The Icy Satellite Interior Simulator (ISIS) was constructed for the investigation of phenomena in simulated ocean planet environments. The system (Fig. 4.1) employs a Newport Scientific optical absorption cell modified to accept beams incident at an included angle of up to twenty degrees. The cell's standard sapphire windows were replaced with c-axis oriented windows purchased from Guild Optical Associates, Inc.

Samples were contained in a Starna 10 mm glass spectrophotometric cell cut to fit in the 25 mm opening of the pressure vessel. The cuvette was closed using a piece of durometer 70 polyurethane cut to roughly 1x1x0.5 cm. The edges of the plug were coated with silicone grease to insure against leakage. The sample was help vertically upright so that buoyancy limited the infiltration of hydraulic fluid. The sample cuvette was then placed in a brass holder machined to fit in the cylindrical opening of the pressure vessel and to prevent breakage of the cuvette from over-tightening of the window retainer nuts. Dioctyl sebacate was used as the hydraulic fluid. Contrary to previous claims that the fluid remains clear to -35 °C and 300 MPa [Gagnon et al., 1988], we found pure dioctyl sebacate clouded below $\sim$ 10 °C at the lowest pressures employed (50 MPa). This may have been due to the presence of the silicone, which was found to gel irreversibly at moderate pressures, and at the lowest pressure at temperatures below the freezing point of water. To prevent clouding 5% kerosene was added by volume. Pure kerosene was tested as a hydraulic fluid, but was found to absorb the incident infrared light, thereby attenuating the ISS signal. The sebacate oil took on a greenish coloration after prolonged exposure to nitrile rubber present in the air-hydraulic pump and in the o-ring seals of the pressure vessel. This

discolored fluid weakened the ISS signal by absorbing the frequency-doubled (green) laser pulses, so it was occasionally necessary to flush with fresh fluid.

6.2.2 Control and Measurement of Pressure

Pressure was generated with a 70 MPa pressure source connected to a Harwood 10x intensifier. Pressure was measured using an Omega 700 MPa transducer cross-calibrated to a Heise CM model 700 MPa Bourdon-tube gauge. Precision in the measurement of pressure is estimated at 0.2%. In the worst cases, pressure fell by up to 20 MPa during measurement when leakage occurred. It was observed that this drop was usually linear in time. In such cases, it was deemed prudent to take as the measured value the average of pressure readings at the start and end of the ISS measurement. Under normal operating conditions, pressure was stable to within about 0.3 MPa, well under the 0.7 MPa error equivalent to the error in the ISS measurement.

6.2.3 Control and Measurement of Temperature

Temperature was controlled to within 0.1 °C on the time scale of measurement using a Lauda 107 heater/chiller, which circulated fluid (ethylene glycol) through copper tubing brazed to a bronze cylinder fitted to the outside of the pressure vessel. Temperature was measured to ±0.1 °C with a chromel-alumel thermocouple in contact with the sapphire window. Contact with the outside of the window was verified from the adiabatic change in temperature on pressurization of the sample, which was immediately discernible as a change of roughly one °C per 100 MPa. This responsiveness was taken to indicate our measurement of the outside window temperature correlated well with the temperature of our sample. Thermocouples were occasionally calibrated to the melting and boiling temperatures of water at atmospheric pressure.

The effect of temperature on the ISS signal was appreciable. At the lowest temperatures and pressures, the reduced thermal expansivity of water limited the strength

of the diffracted signal used to measure the sound velocity. Conversely, at temperatures greater than the ambient temperature of the calibration standard, the diffracted signal was often much stronger than in the standard.

6.3 Results

Results for all of our measurements are summarized in Tables ??–??. Dates, measured frequencies and filenames are provided for archival purposes. Measurements are listed in ascending order in nested subcategories by concentration, temperature, pressure, respectively. Velocity and density are listed for all concentrations. Apparent molal volumes, partial molal volumes at infinite dilution, and excess volumes are listed for aqueous solutions of magnesium sulfate.

6.3.1 Velocities

Systematic errors were estimated to be 0.2% under optimal conditions due to drift in temperature, pressure, and the alignment of optics. Under the worst conditions, errors are conservatively estimated to have been as high as 1% (see 6.4).

Measurements were made in the ranges of pressure and temperature mapped in Fig. 6.1 for pure water (also see Chapter 5), 0.0800, 0.5103, 0.9965, 1.5062 and 2.0104 m. A majority of the measurements were made along isotherms. A polynomial fit in pressure (for an example, see Fig. 6.2). The fits were evaluated visually during acquisition in an attempt to insure a proper description of the shape of the isotherm in pressure.

Some adiabatic measurements were made during cooling for the purpose of improving the two-dimensional fits in P and T that were used in the inversion of velocity data for densities (see Section 6.4).

6.3.2 *Volumetric Properties*

Grid-interpolated data (see Section 6.4) were used for the calculation of density by recursive integration of,

$$\left(\frac{\partial \rho}{\partial P}\right)_T = \frac{1}{v^2} + \frac{T\alpha^2}{C_P} \qquad \text{and} \qquad \left(\frac{\partial C_P}{\partial P}\right)_T = -T\frac{\partial^2 V_{sp}}{\partial T^2}. \tag{6.0}$$

Thermal expansion (α) and specific heat capacity (C_P) were calculated from the model densities described above. The constant of integration (specific heat at 0.1 MPa and all temperatures of interest) was estimated as:

$$C_P^o = C_{P,water} + \sum_i m_i C_{P,i}^o. \tag{6.0}$$

We used IAPWS95 [Wagner and Pruss, 2002] for the specific heat capacity of water. We obtained the ionic contribution to the specific heat at infinite dilution from supcrt92 using the slop92 database. For temperatures below zero ^{o}C the ionic contribution ($C_{P,i}^o$) was approximated by extrapolation in a cubic polynomial fit to the lookup data. The calculation of density is relatively insensitive to the initial specific heat; substituting standard values for water changes the calculated densities by a maximum of 0.003 kg m^{-3}.

Apparent molal volumes (ϕ; Fig. 6.12) were calculated in the same manner as was done by Chen et al. [1977], by subtracting specific volumes for water [in the present case, from Wagner and Pruss, 2002] from the specific volumes of the solution:

$$\phi \equiv mV^o + V^{ex} = V_{sp} - V_{water} = \frac{1 + 0.001mW}{\rho_{obs}} - \frac{1}{\rho_{water}}. \tag{6.0}$$

For the calculation of the partial molal volume at infinite dilution V^o, we assumed that the lowest order terms in ϕ as a function of concentration are those given by

Pitzer [1973]:

$$\phi = mV^o + V_{DH}(m) + V_2 m^2 + V_3 m^3, \tag{6.0}$$

where V_2 and V_3 are empirical coefficients and V_{DH} is the Debye-Hückel term that describes the ion-water interaction in terms of the dielectric constant of water, D:

$$V_{DH} = 6RT\frac{I\ln(1+b\sqrt{I})}{b}A_\phi\Big(\frac{\partial \ln D}{\partial P} - \frac{\beta}{3}\Big) \tag{6.0}$$

The volumetric formulation of this interaction is the pressure derivative of the more compact expression for the excess Gibbs free energy:

$$G^{ex} = \frac{RT}{1000}\Big(\frac{-4A_\phi}{b}I\ln(1+b\sqrt{I}) + 2m^2\nu_+\nu_-\beta\Big), \tag{6.0}$$

The osmotic coefficient, A_ϕ, is

$$A_\phi = \frac{1}{3}\sqrt{\frac{2\pi N\rho_{water}}{1000}}\Big(\frac{e^2}{Dk_BT}\Big)^{3/2}, \tag{6.0}$$

in which N is Avogadro's number, ρ_{water} is the density of water [Wagner and Pruss, 2002], e is the charge of the electron and k_B is Boltzmann's constant. I is the ionic strength, given by,

$$I = 0.5(m^+(z^+)^2 + m^-(z^-)^2) \tag{6.0}$$

$I = 4\ m$ for 2:2 electrolytes such as $MgSO_4$. The empirical constant, b, is a constant 1.2 $kg^{1/2}\ mol^{-1/2}$ [Phutela and Pitzer, 1986].

6.3.3 Excess Volumes

Partial molal volume at infinite dilution V^o is the coefficient of the first term — that is, the linear term — in the expansion of apparent molal volume ϕ in concentration. The remainder is expressed by the excess volume, V^{ex}. We calculated from V^{ex} from our data based on $\phi = mV^o + V^{ex}$.

6.4 Discussion

6.4.1 Evaluation of Velocity Measurements

Figures 6.3-6.5 display residuals of velocity isotherms with polynomial fits in pressure from 0.0800 to 0.9965 m, the range of concentration in which comparison with other velocity measurements is possible. For fitting and statistical purposes, measurements were made to lie along the isotherm by applying a small correction based on velocities for water [Wagner and Pruss, 2002]. Measurements within 10 MPa were corrected to lie on the mean in pressure.

Comparison with the one available published equation of state to significant pressure [Chen et al., 1978, 0 to 1 m, 0 to 100 MPa, 0 to 50 °C] shows agreement to within 0.5% at 10 °C and above approaching atmospheric pressure. There appears to be a general trend in pressure of increasingly positive misfit, reference velocities becoming greater than the fit to the isotherm. It is also interesting to note that the reference velocities tend to be smaller than our values at low temperature and below $\sim$ 50 MPa by as much as 1%.

The possibility of sample contamination can be examined using Figures 6.3-6.5. None of the materials used in the hydraulic system – dioctyl sebacate, kerosene nor silicone oil – is soluble in water under standard conditions, but there was some concern about contamination over time or at elevated pressure or temperature. As mentioned in Section 6.2.1, the stopper plug used to close the sample container served as an imperfect barrier. In a few cases, a droplet of fluid was sometimes observed on the underside of the plug after changing the pressure. These usually went away with time, and subsequent measurements on returning to the same conditions of pressure and temperature were consistent with those made prior to the droplet's arrival and departure.

Precipitation was a concern at low temperatures, and was noted to occur on cooling in the more concentrated solutions on a few occasions. These were anticipated from

the phase diagram of [Hogenboom et al., 1995], and were noted as a sharp drop in velocity. Subsequent heating allowed for reliable repetition of velocity measurements made prior to precipitation.

No major bias is observed in the plot for hysteresis (triangles) for the concentrations shown in the figures, nor for similar comparisons (not shown here) for velocity measurements at 1.5062 and 2.0137 m.

6.4.2 Calculation of Densities

The calculation of densities from velocity measurements requires a two-dimensional grid in P and T at each concentration. This necessitated extrapolation of our data in regions of P and T where measurement is not possible due to freezing or precipitation of salt. In order to obtain a representation of our velocity measurements that extrapolates well in pressure and temperature, we used a fitting scheme similar to that employed by Wiryana [1998]. For each concentration, an offset parameter b and fitting function in $P_{tx} = 1/(P + b)$ and T were chosen that produced nearly linear representations of the inverse-squre of velocities along an isotherm (for an example, see Fig. 6.6). Residuals of the two-dimensional fits with the original data are gaussian (Fig. 6.8). The distribution of errors in pressure and temperature is nearly uniform. At all concentrations more than two-thirds of individual points fall within one standard deviation and the standard error of the fit is roughly one tenth of the error in measurement (σ and S_E in Fig. 6.8).

6.4.3 Densities

Solution densities computed from measured velocities compare well with direct measurements by Hogenboom et al. [1995] (Fig. 6.9). Densities (Fig. 6.10) compare favorably with theoretical predictions below 100 MPa, but are markedly higher at greater pressures, by nearly five percent at the highest pressures and concentrations

(Fig. 6.11). The greatest disparity occurs at the highest pressures and the highest and lowest temperatures.

6.4.4 Apparent Molal Volumes

For the calculation of apparent molal volume ϕ, V_{water} is taken from measurements made in our laboratory (Chapter 5). Comparison of ϕ with predicted values [Marion et al., 2005] illustrates how linear extrapolation from previous measurements of ϕ below 100 MPa [Chen et al., 1977] fails above $\sim$ 200MPa. The contribution of magnesium sulfate to the overall solution volume deviates from predictions by up to 100% at the highest pressures and the lowest and highest temperatures (Fig. 6.13).

6.4.5 Partial Molal Volumes at Infinite Dilution

Partial molal volumes at infinite dilution are compared with predictions from Marion et al. [2005] in Fig. 6.14. As is also seen with apparent molal volumes (ϕ, Fig. 6.12), a positive slope in pressure decreases sharply above $\sim$200 MPa. Calculated values for V^o are in agreement at atmospheric pressure (0.1 MPa) with the input values from Marion et al. [2005] within $\sim$ 5 mL. The misfit remains within this range up to 200 MPa at 10 ^{o}C. The deviation at elevated pressure is least at 20 ^{o}C and greatest at the highest and lowest temperatures.

The downward curvature of V^o with increasing pressure indicates that extrapolations from available high pressure data [Chen et al., 1977] are not valid for $P >$ 200 MPa. At these elevated pressures, the configuration of ions and water in the solution is sufficiently compressed to noticeably impede further compression. In past work on electrolyte chemistry [Krumgalz et al., 1999, Marion et al., 2005], partial molal volume at infinite dilution were calculated as: $V^o(P,T) = V^o(P = 0,T) - \kappa^o(T)\Delta P$. Partial molal compressibilities κ^o were assumed constant in pressure [Millero, 1983], resulting in the linear representations plotted in Fig. 6.14. In the calculation of the

change in activity coefficients with pressure,

$$\frac{\gamma_i^P}{\gamma_i^{P0}} = \exp\left(\frac{(\bar{V} - V^o)(P - P^o)}{RT}\right), \tag{6.0}$$

compressibility terms in V^o were ignored due to an inability to evaluate their accuracy [Krumgalz et al., 1999, Marion et al., 2005, $\bar{V} = \phi/m$ is the partial molal volume]. Our measurements suggest a pressure dependence in κ^o is necessary. These more accurate compressibilities may then be accounted for in the calculation of activity coefficients.

As a difference quantity derived from fits to apparent molal volume (itself a difference quantity), partial molal volume at infinite dilution is subject to errors introduced by the gridding of velocity data. Choosing a lower order polynomial for the functional fit to the inverse-square of velocity allows for a representation of V^o that shows similar phenomenology, but at the cost of diminished confidence in the accuracy of the input velocity surface.

There is some history of difficulty in the calculation of V^o for magnesium sulfate. Phutela and Pitzer [1986] noted that that the slope of density with concentration is much steeper for $MgSO_4$ than for other electrolytes. They chose to infer V^o indirectly based on their measurements in other solutions, namely: $V^o(\mathrm{MgSO4}) = V^o(MgCl_2) + V^o(Na_2SO_4) - 2V^o(\mathrm{NaCl})$.

6.4.6 Excess Volumes

Figure 6.15 compares the contribution to the apparent molal volume (ϕ) from excess volumes (V^{ex}) and partial molal volumes at infinite dilution (V^o). At all temperatures in the range of our measurements, our results agree with predictions from Marion et al. [2005] below 200 MPa, but show an enhanced contribution from V^{ex} at high pressure as compared.

6.5 Conclusion

Densities of aqueous $MgSO_4$ derived from sound velocity measurements to 2 m and 700 MPa are found to be in agreement with prior literature to 100 MPa and 1 m in the range 0 to 100 ^oC [Chen et al., 1977], and with the few measurements to higher pressures [1 and 2 m to 400 MPa at 25 ^oC Hogenboom et al., 1995, see Table 6.1] .

The new measurements show that theoretical predictions of solution density, which are based on extrapolation from compressibilities to 100 MPa [Chen et al., 1977], overestimate density by as much as 4% at 2 m and 700 MPa. The linear compressibilities of Chen et al. [1977], though adequate up to 100 MPa, fail to capture the actual contribution of the solute to the total solution volume at higher pressures. The smaller pressure derivative in compressibility at higher pressures may be attributed to more strongly repulsive ion-ion and ion-water interactions with increasing density as the mean free path between constituent atoms and molecules decreases.

Partial molal volumes at infinite dilution are inferred from the velocity measurements using conventional Debye-Hückel theory [Bradley and Pitzer, 1979]. Results are in agreement with predicted values [Marion et al., 2005] within 5 mL up to 200 MPa, indicating magnesium sulfate solubility is reasonably predicted by the Pitzer framework for ionic species in the range of pressures relevant to Europa's ocean.

Our measurements indicate accounting is needed for pressure dependence in the compressibility term in the partial molal volume at infinite dilution V^o above 200 MPa and at non-standard temperatures above ~100 MPa. This information may be estimated from our measurements, but a more accurate description awaits further measurements in magnesiums sulfate and other electrolyte solutions.

The velocities and inferred volumetric properties of aqueous $MgSO_4$ presented here extend the accumulated knowledge of such properties into hitherto unexplored regions of pressure and temperature. The ability accurately calculate solution density and solubility under conditions of pressure, temperature, and composition relevant to deep

oceans like Europa's allows for increased confidence in the interpretation of satellite remote sensing data of subsurface properties. These improvements in the chemical data also enable simulation of ocean circulation and chemical evolution needed to interpret Europa's surface geology and assess its habitability.

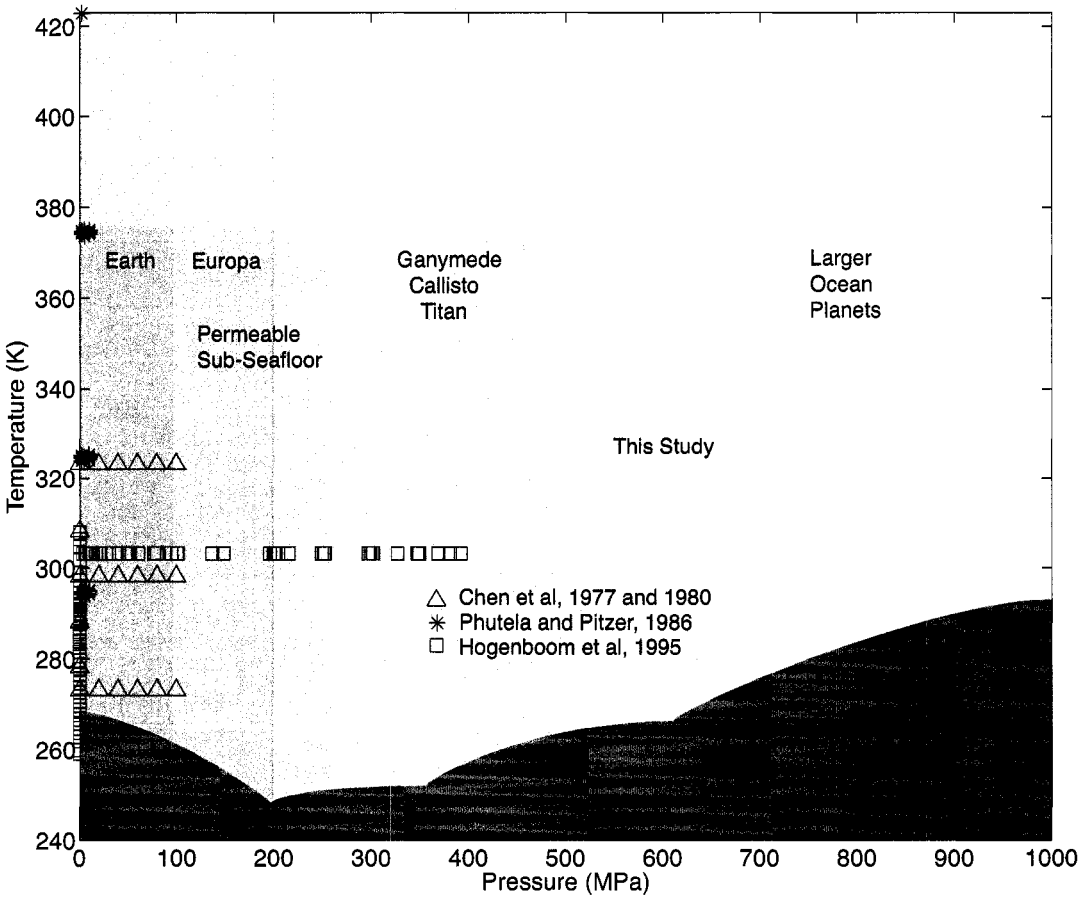

Figure 6.1: Experimentally accessible temperature and pressures. The heavy curve roughly follows the liquidus for the aqueous $MgSO_4$ system [estimated from Hogenboom et al., 1995]; above 400 MPa, the curve follows the liquidus for water. Relevant pressures for oceans in the large icy satellites are as high as 200 MPa, and O(1) GPa if fluids penetrate into the lithosphere. The upper temperature range is relevant to hydrothermal systems and "ionic oceans" in the interiors of Neptune and Uranus. Plotted symbols are pressures and temperatures where densities have been measured in the aqueous magnesium sulfate system. To our knowledge, these data comprise the entire body of published work on pressure's effect on aqueous magnesium sulfate.

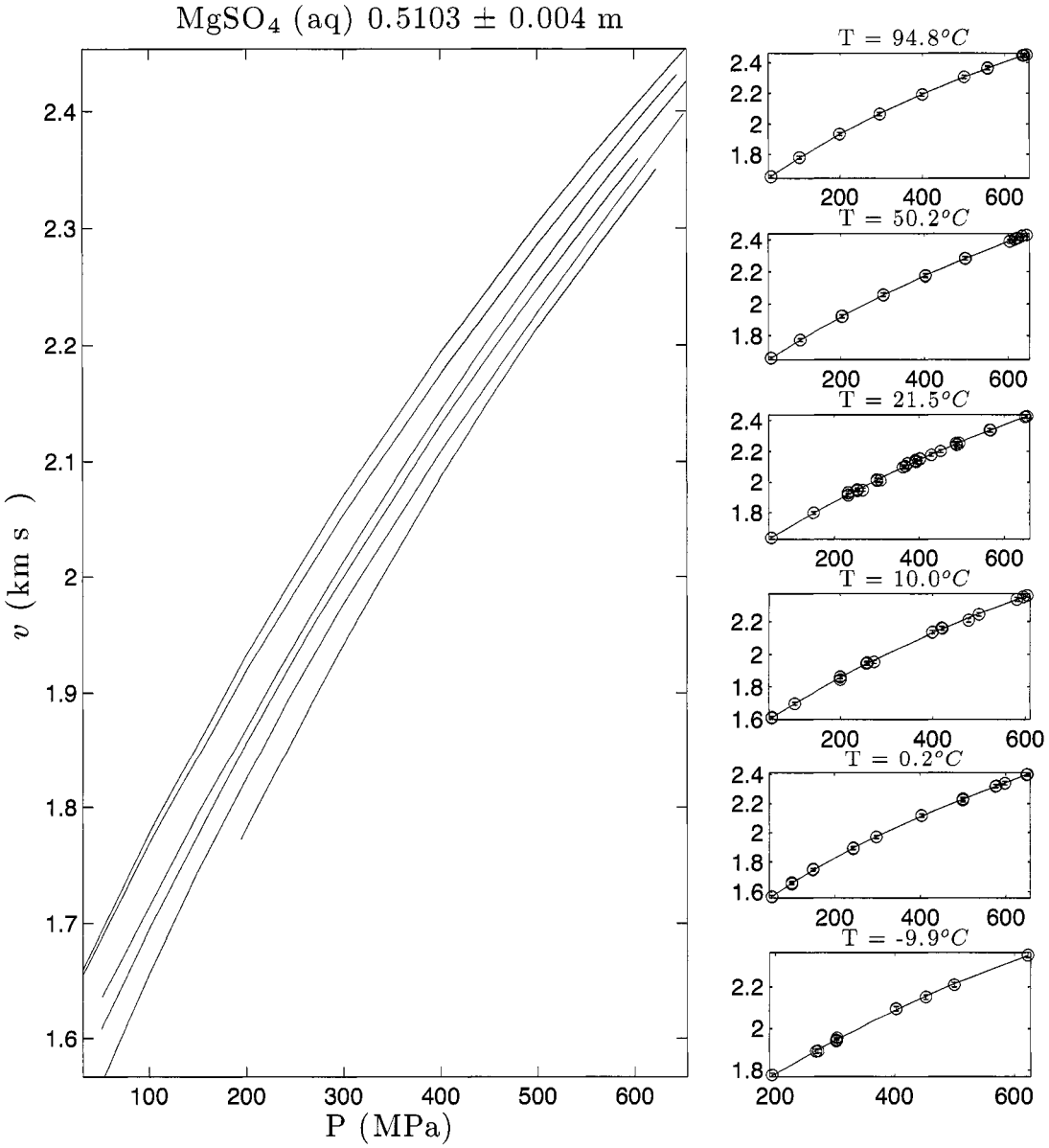

Figure 6.2: Sound velocities in 0.5103 molal $MgSO_4$ (aq) to 700 MPa from -10 to 95 ^oC. Velocities are plotted on the vertical axis (in km s^{-1}) as a function of pressure (in MPa) on the horizontal axis. The panels at the right show measurements (circles) along the isotherms noted. For each temperature, a second degree polynomial fit in pressure is obtained (lines).

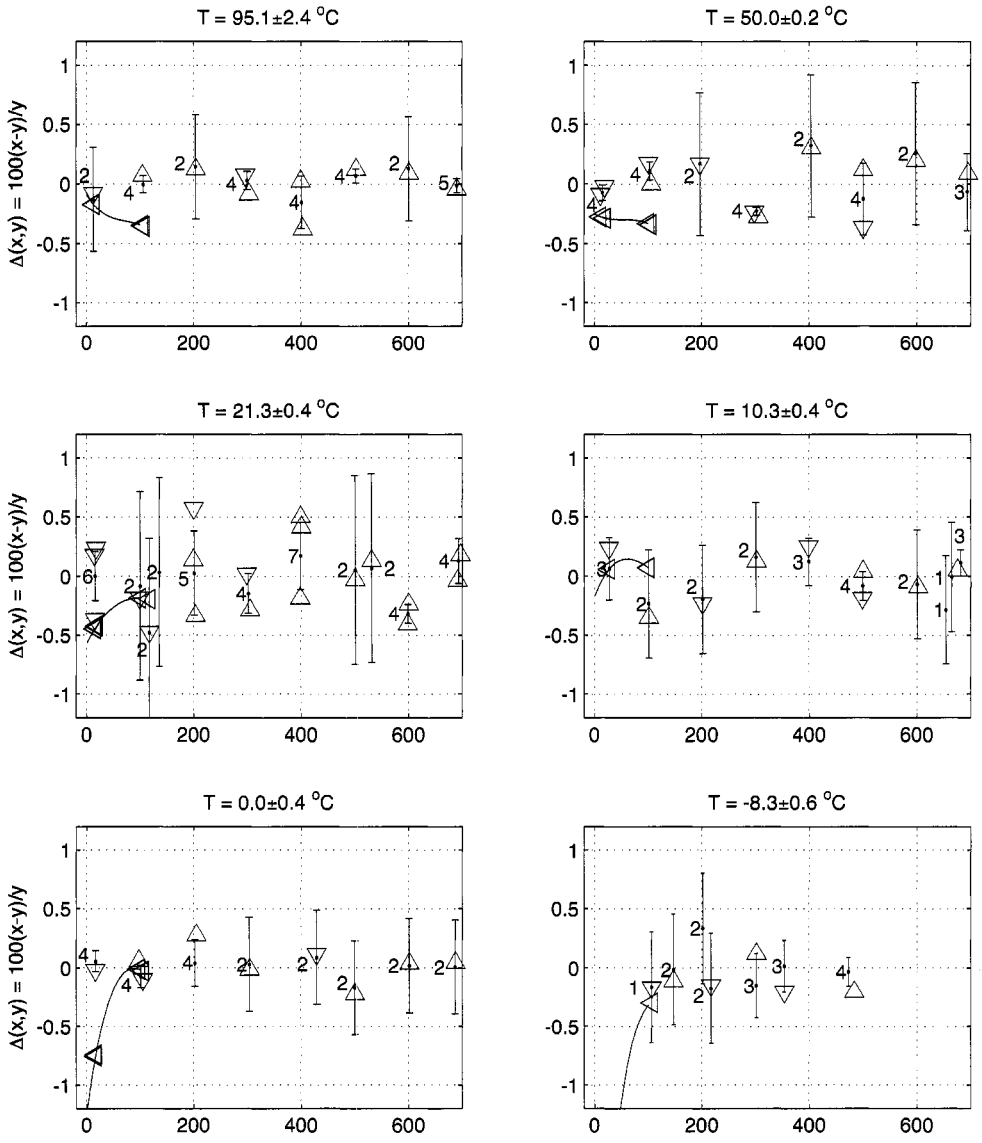

Figure 6.3: Residuals of velocity measurements (x), along isotherms, with polynomial fits (y) in pressure for 0.0800 m $MgSO_4$. The number of points in a given bin is displayed next to each error bar. Two standard errors of the fit are shown where more than two data points area available; two standard deviations are shown otherwise. Upward and downward facing triangles indicate individual measurements taken after an increase or decrease in pressure of more than 20 MPa has occurred. Solid lines: Chen et al. [1978]. Leftward pointing triangles indicate comparison between actual data points.

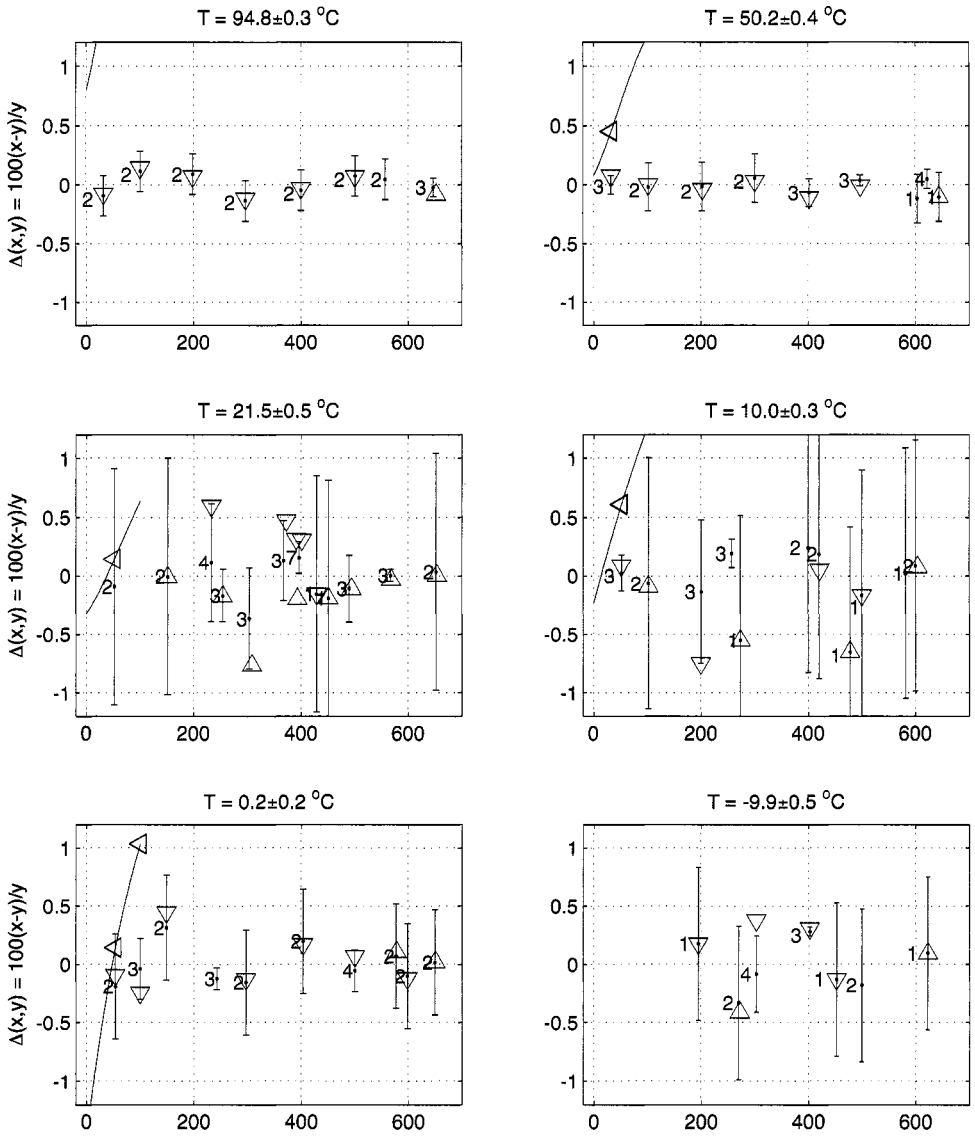

Figure 6.4: Residuals of velocity measurements (x), along isotherms, with polynomial fits (y) in pressure for 0.5103 m $MgSO_4$. The number of points in a given bin is displayed next to each error bar. Two standard errors of the fit are shown where more than two data points area available; two standard deviations are shown otherwise. Upward and downward facing triangles indicate individual measurements taken after an increase or decrease in pressure of more than 20 MPa has occurred. Solid lines: Chen et al. [1978]. Leftward pointing triangles indicate comparison between actual data points.

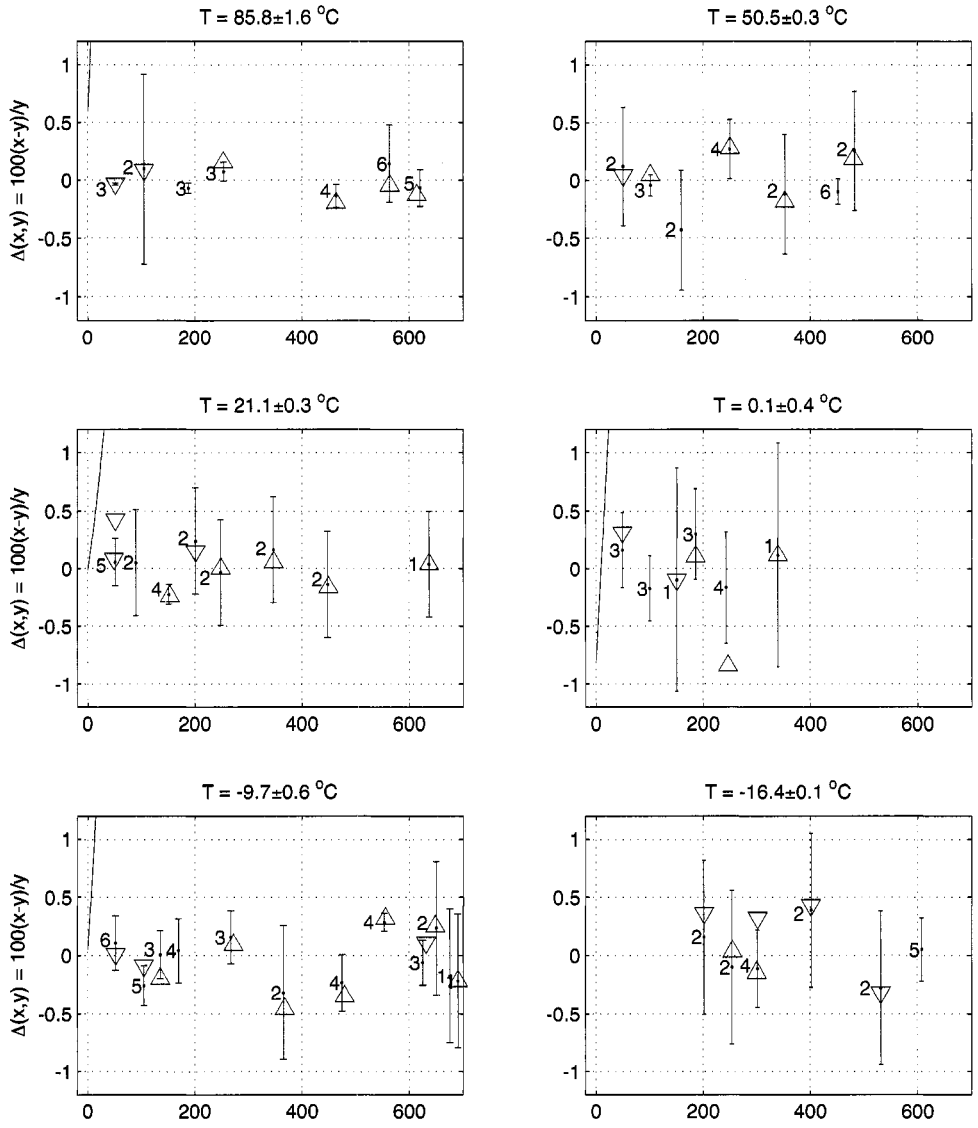

Figure 6.5: Residuals of velocity measurements (x), along isotherms, with polynomial fits (y) in pressure for 0.9965 m $MgSO_4$. The number of points in a given bin is displayed next to each error bar. Two standard errors of the fit are shown where more than two data points area available; two standard deviations are shown otherwise. Upward and downward facing triangles indicate individual measurements taken after an increase or decrease in pressure of more than 20 MPa has occurred. Solid lines: Chen et al. [1978]. Leftward pointing triangles indicate comparison between actual data points.

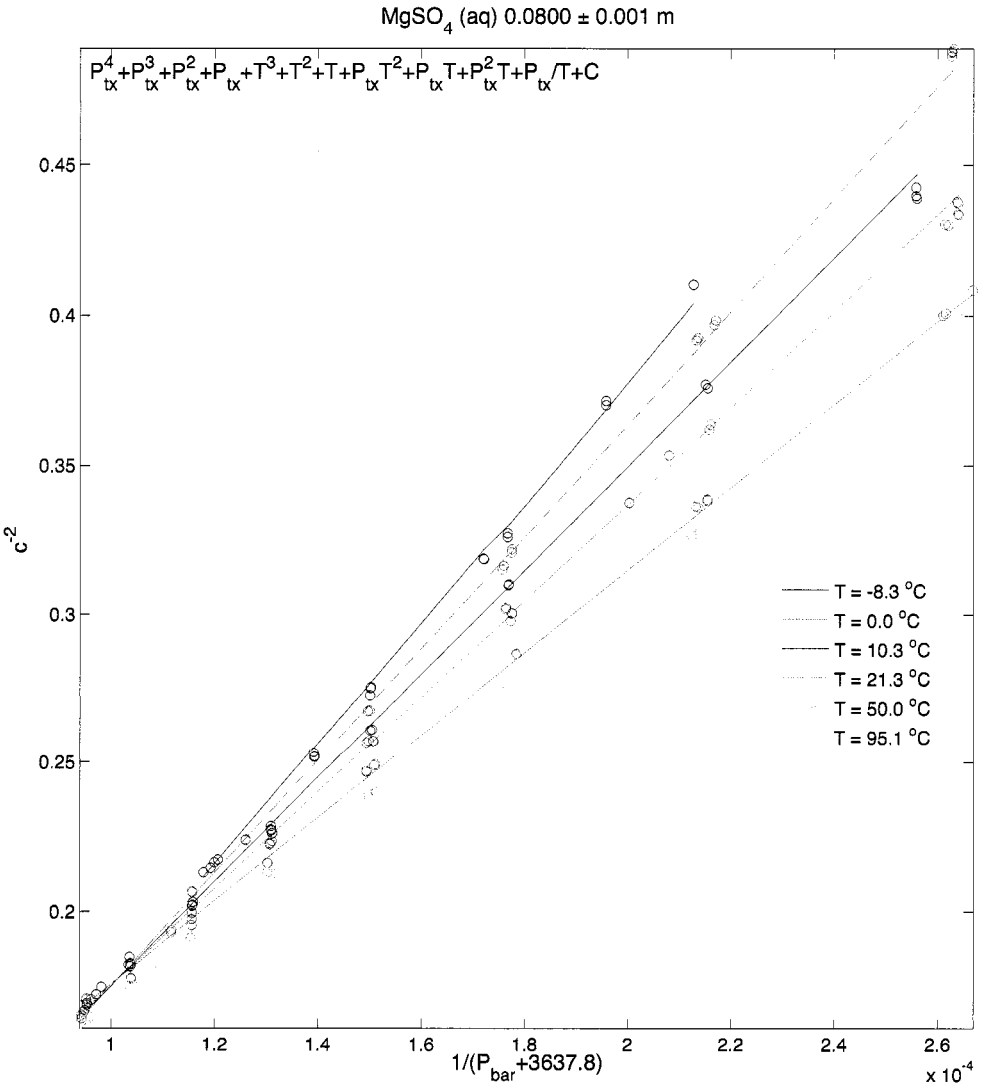

Figure 6.6: Fits to inverse velocity squared (y-axis) vs the inverse of velocity, $P_{tx} = 1/(P+b)$, for 0.0800 m $MgSO_4$ (aq). Velocity measurements at selected temperatures of measurement (median value $\pm$ ~ 1 ^{o}C) are plotted as open circles. Temperature increases moving downward. An optimum functional fit and transform (b) are chosen for each concentration.

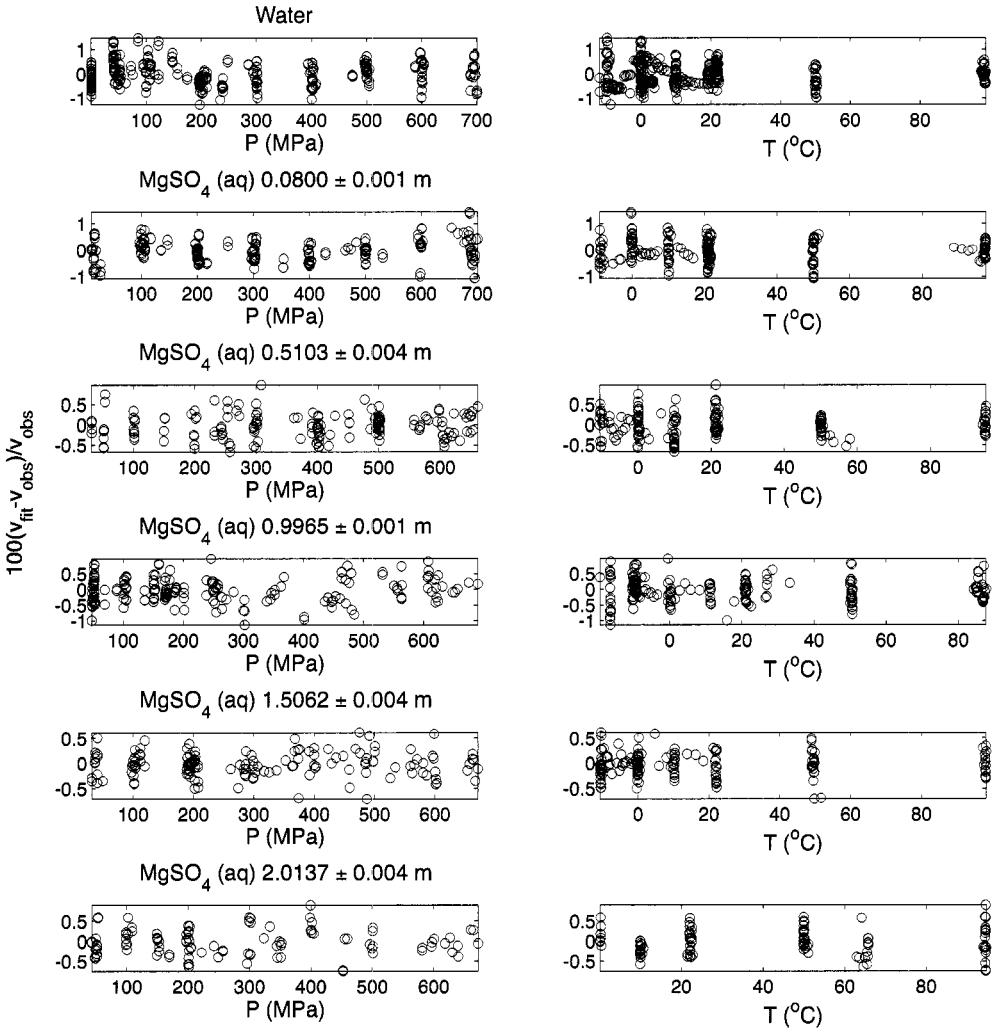

Figure 6.7: Residuals of velocity surfaces used to calculate density. Concentration increases downward by row. For each concentration, the difference between the fit and individual observations is plotted in percent as a function of pressure in the left column and temperature in the right. The error in the fit to individual points is within two standard deviations (see Fig. 6.8) for all except one measurement.

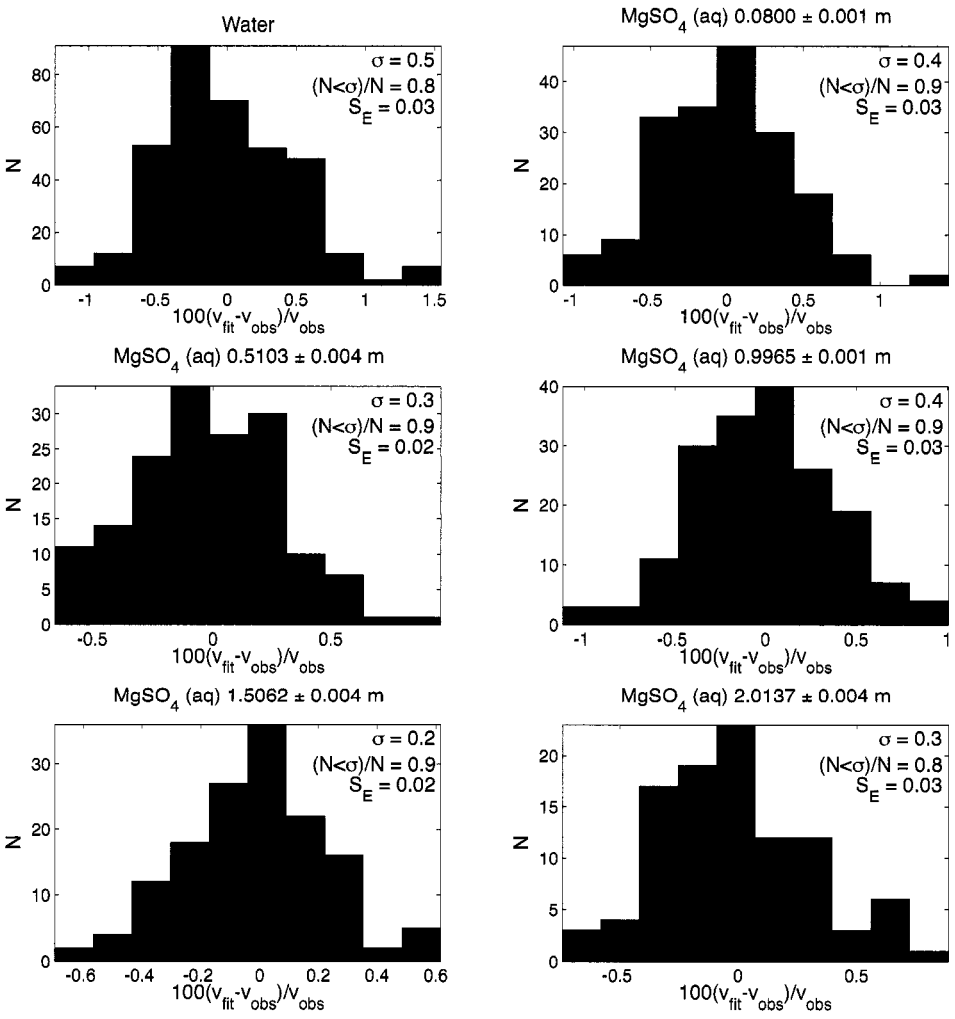

Figure 6.8: Distribution of residuals of velocity surfaces used to calculate density. For each concentration, the standard deviation of the overall fit, σ, is displayed in the upper right corner along with the standard error, S_E. Distributions are gaussian, with standard errors roughly a tenth of the measurement error for all concentrations.

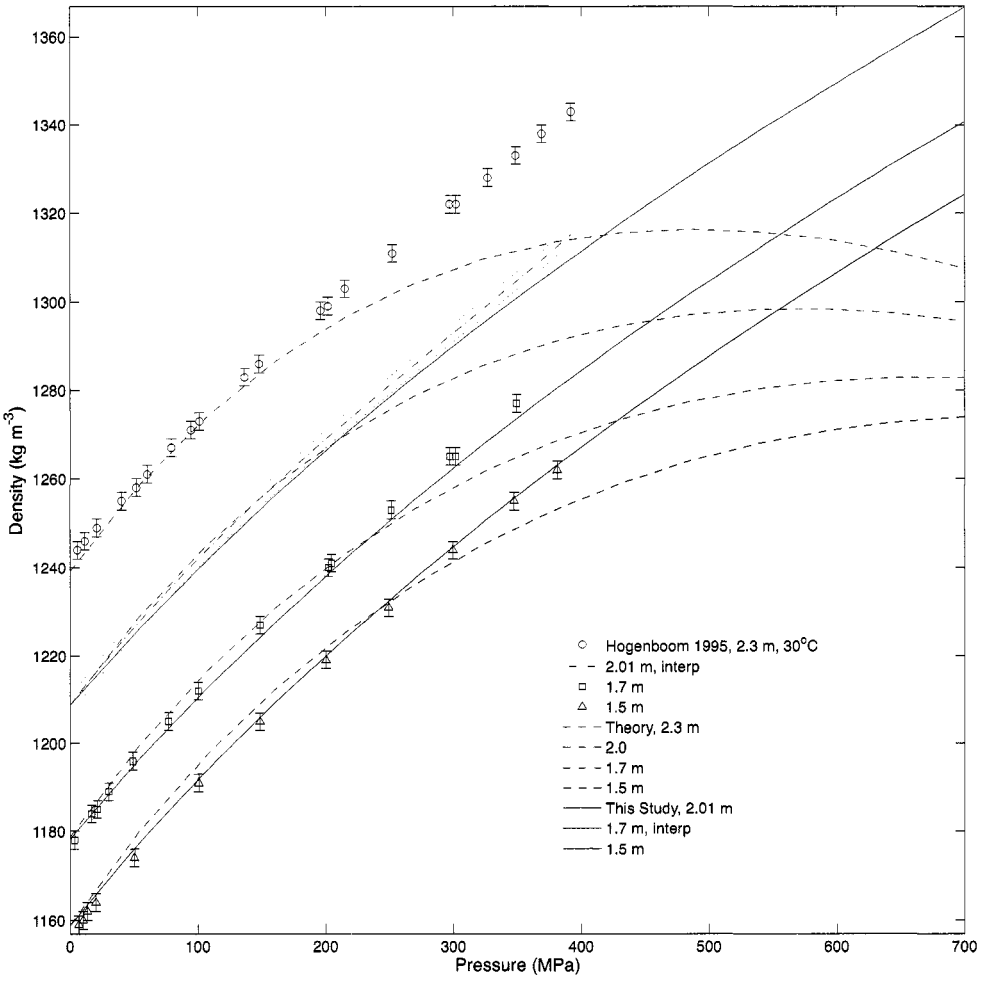

Figure 6.9: Densities of aqueous $MgSO_4$ (aq) at 30 °C versus pressure to 400 MPa for 1.5, 1.7, 2.01 and 2.3 mol per kg of H_2O. Symbols are digitized from the graphical representation of data in Hogenboom et al. [1995]. Error bars are based on the the cited authors' assessment of their results. Dashed lines are densities calculated using parameters from Marion et al. [2005]. Solid lines are densities calculated from the present sound velocity measurements. For 2.01 m measurements of the present study, the dot-dashed line was computed for comparison by interpolation of the data displayed for 1.7 and 2.3 m. Estimated error bounds for the 2.01 m line are denoted by light-toned dashed lines.

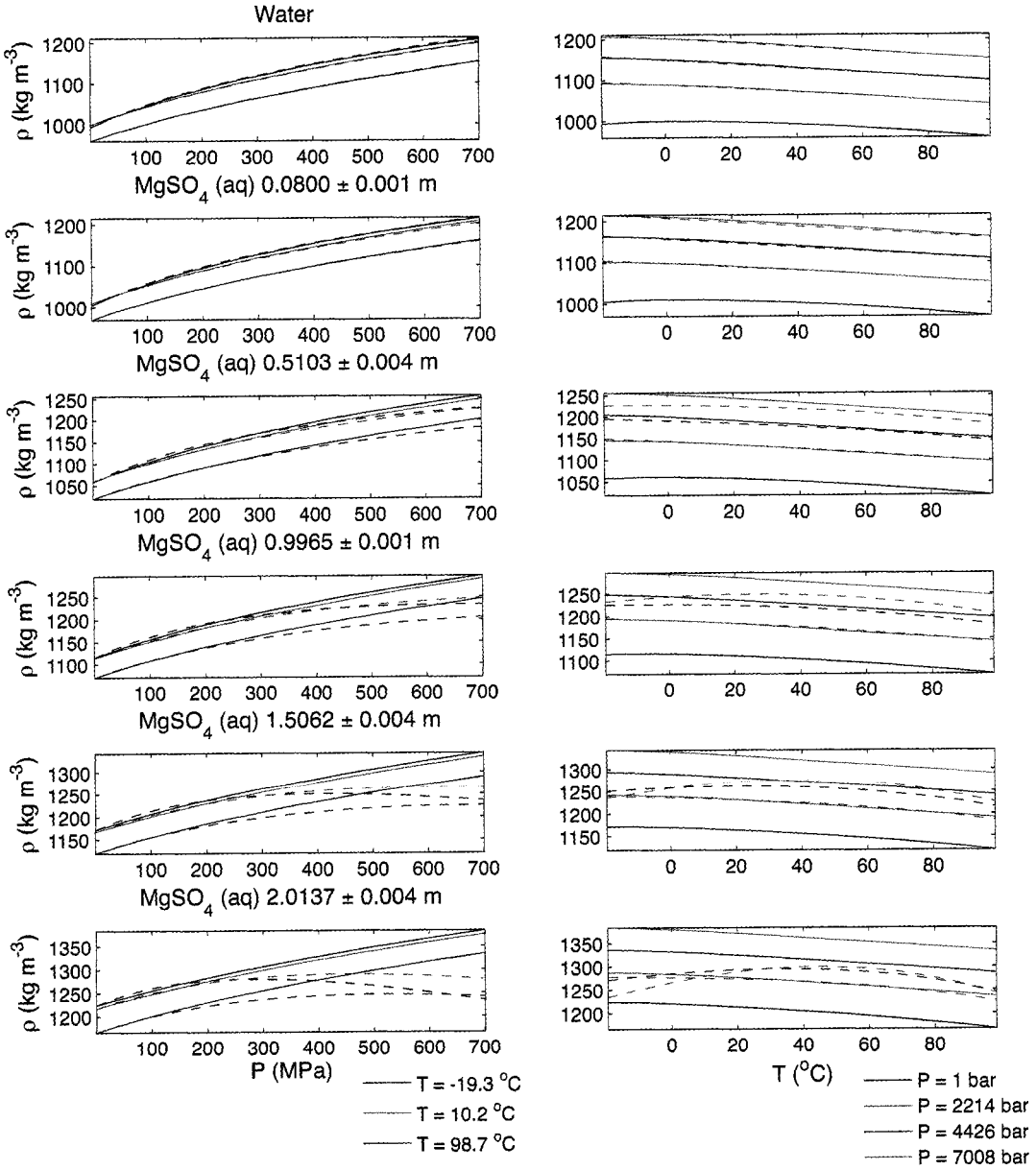

Figure 6.10: Densities in aqueous $MgSO_4$ (aq) to 700 MPa from -18 to 96 °C from measured sound velocities. Densities are plotted on the vertical axes (in kg m^{-3}) as a function of pressure (in MPa) on the horizontal axis of the left pane, and as a function of temperature (in °C) on the horizontal axis of the right pane. Predicted values from Marion et al. [2005] are plotted (dotted lines) for comparison.

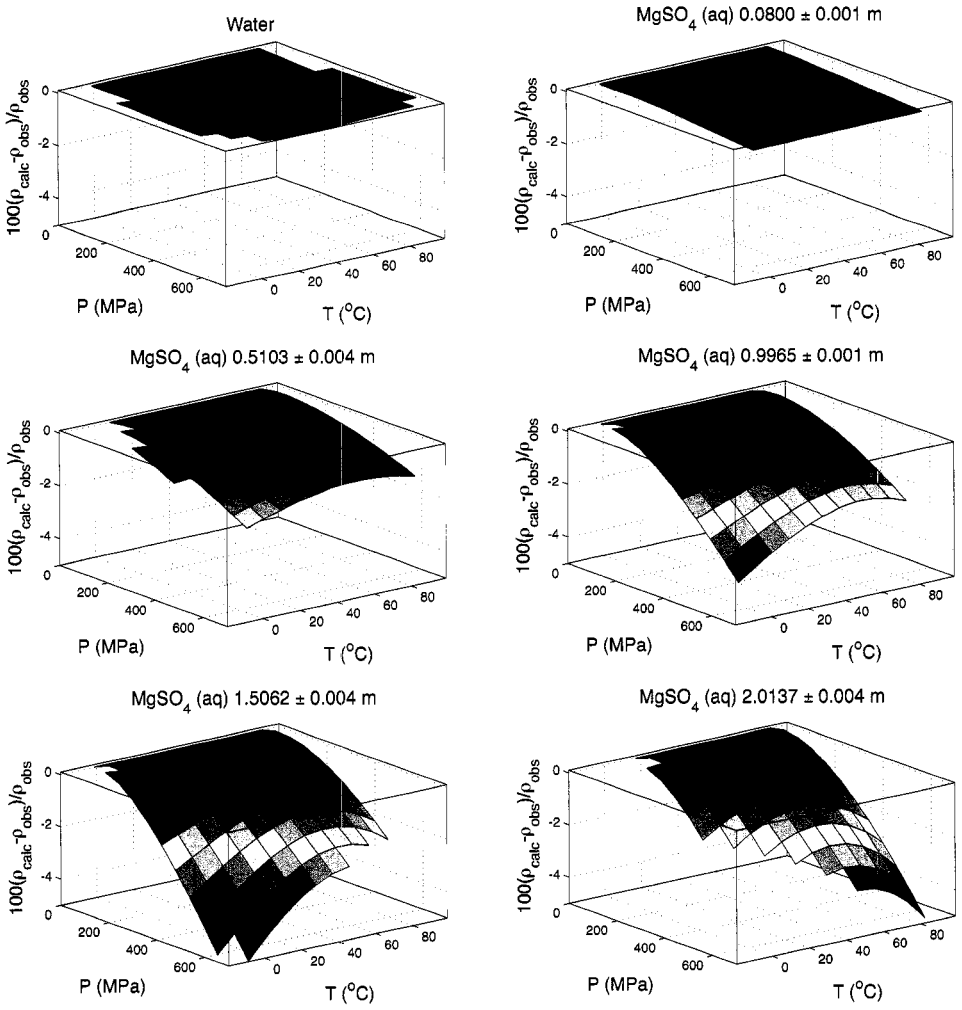

Figure 6.11: Comparison of densities with predictions from Marion et al. [2005]. For each concentration, the difference is plotted on the vertical axis, as a percentage of our data, versus pressure and temperature on the horizontal axes. Each surface spans only the range of P and T where measurements were made.

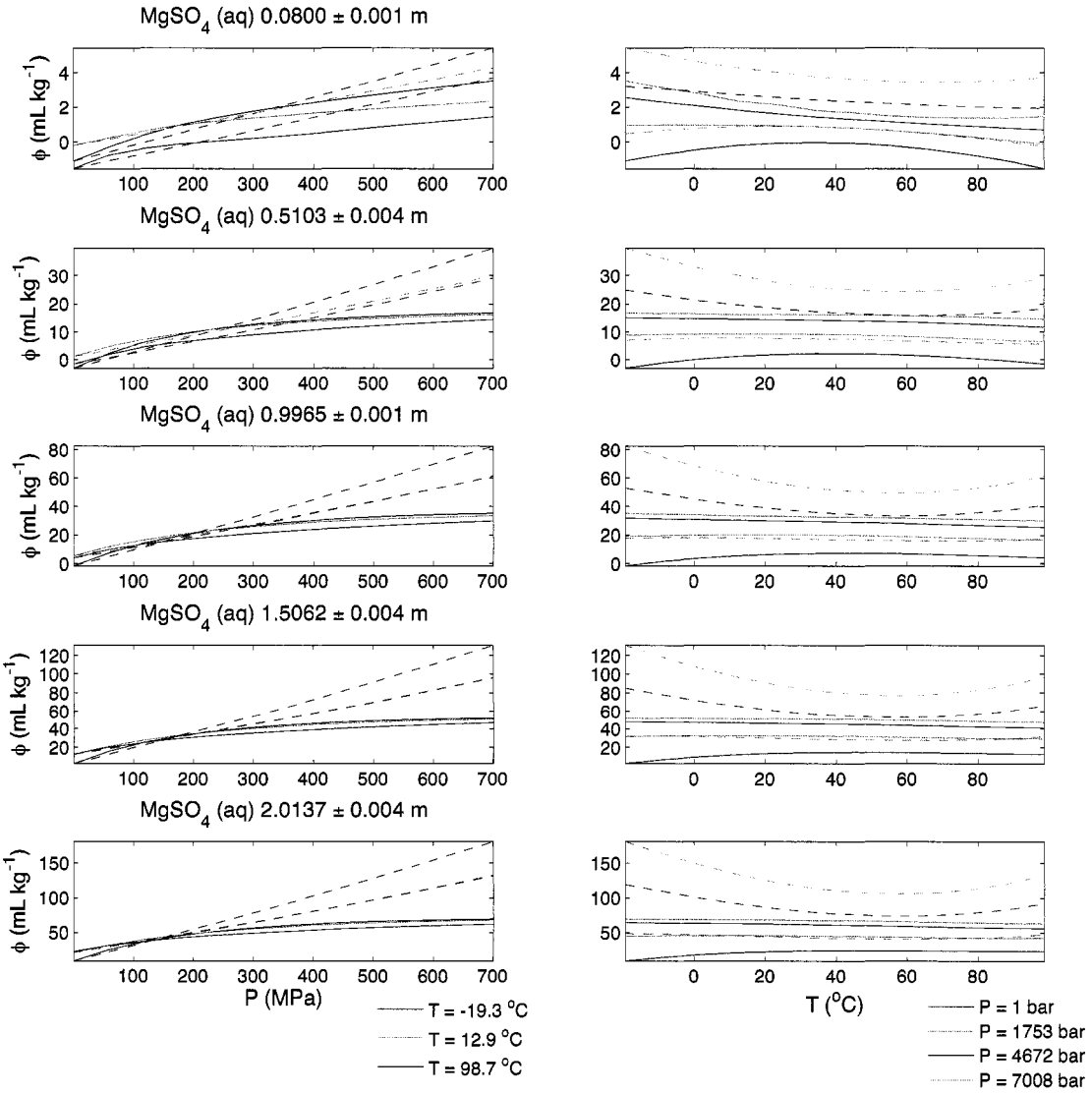

Figure 6.12: Comparison of calculated apparent molal volumes with predictions from Marion et al. [2005]. Values inferred from the present study are displayed as solid lines, with theoretical predictions [Marion et al., 2005] for comparison as dashed lines. Solution concentration increases downward.

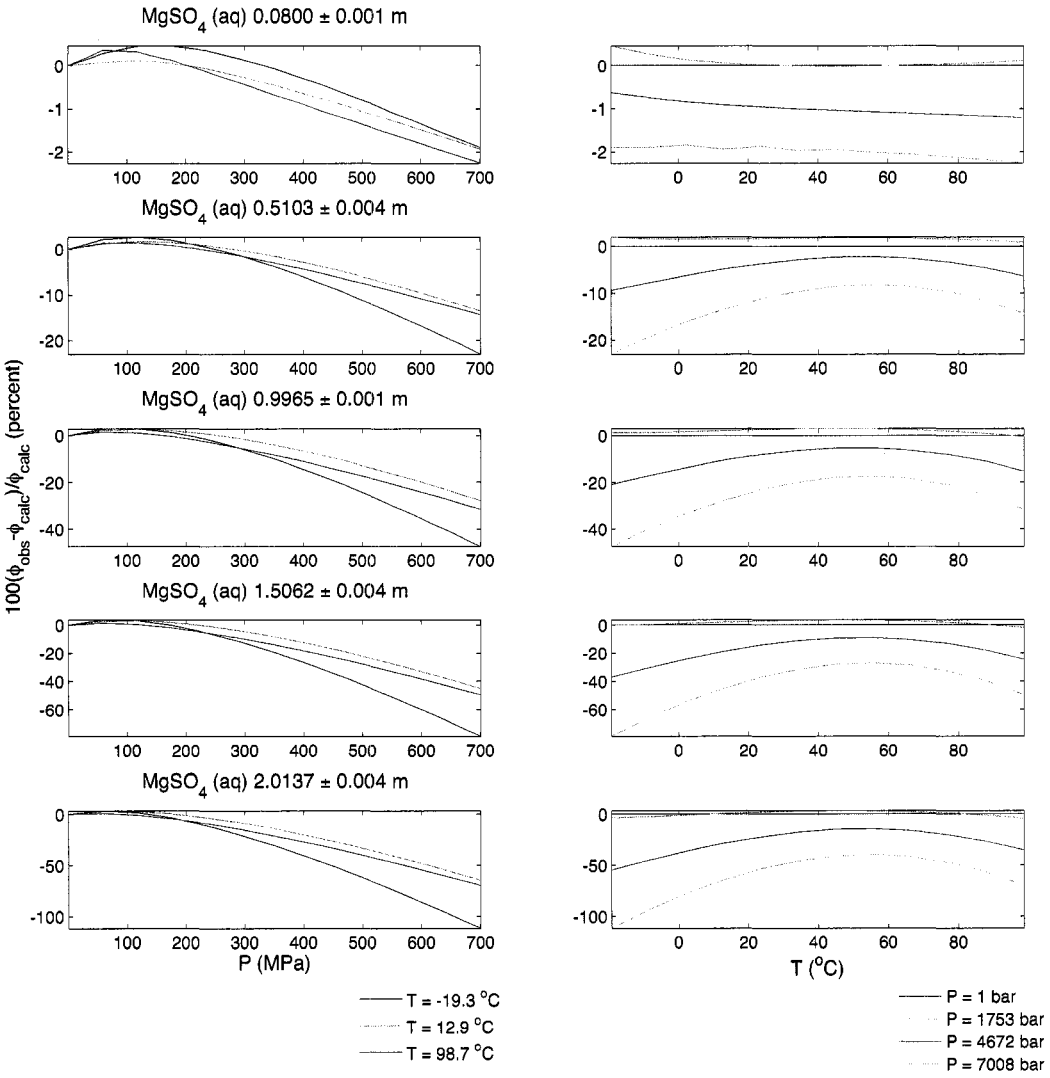

Figure 6.13: Residuals of apparent molal volumes with predictions from Marion et al. [2005]. Residals are plotted against pressure in the left column, and against temperature in the right column. Solution concentration increases downward.

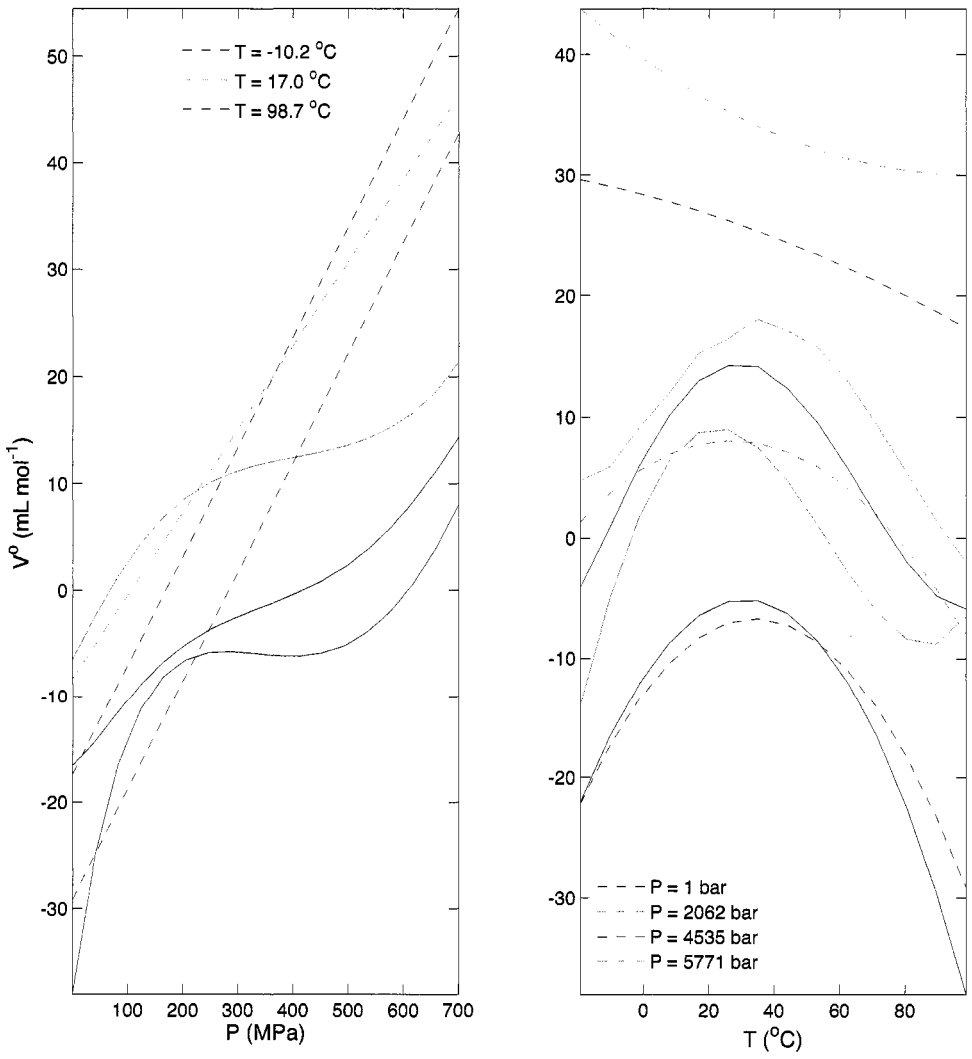

Figure 6.14: Partial molal volumes at infinite dilution, V^o, at selected pressures (right) and temperatures (left) covering the range over which velocity measurements were made. The left pane plots V^o as a function of pressure and the right pane as a function of temperature.

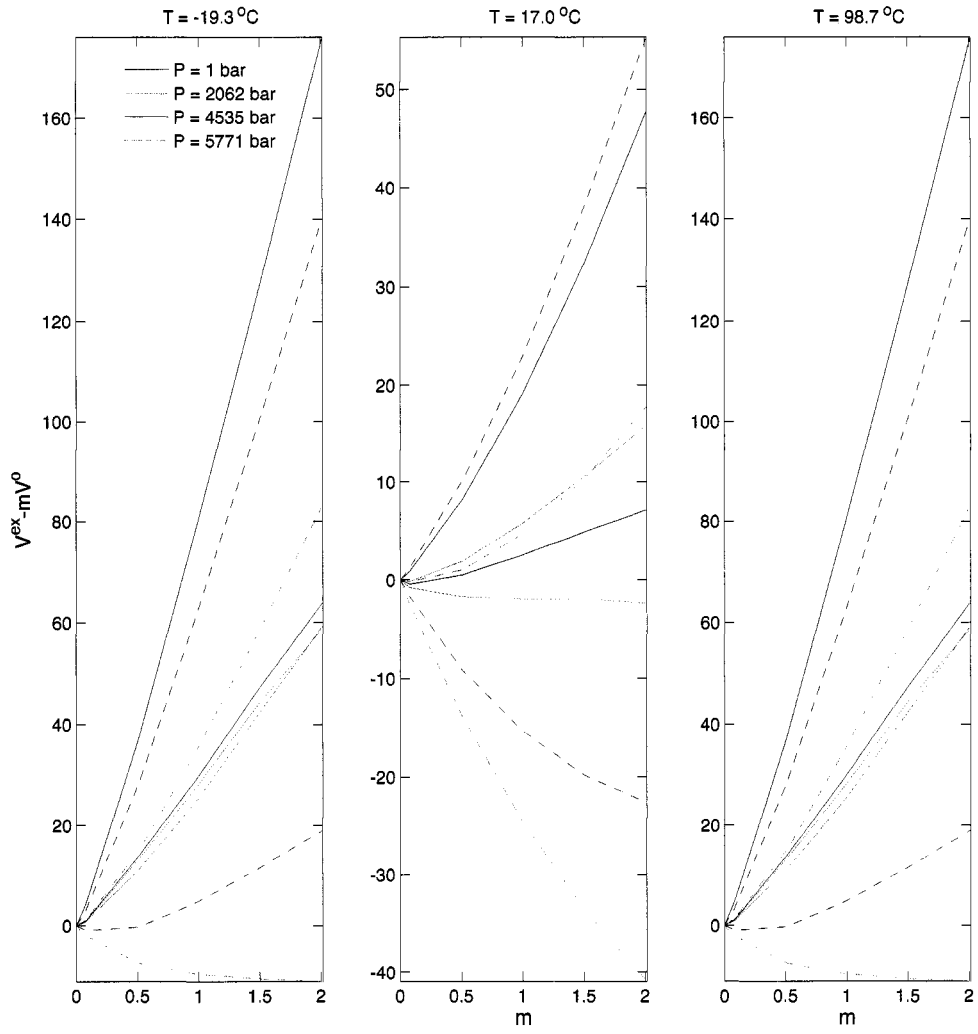

Figure 6.15: Comparison of the contribution to the apparent molal volume from excess volumes and partial molal volumes at infinite dilution. The difference is plotted as a function of concentration at selected pressures. Each pane shows the comparison for a different temperature in the range of our measurements. Dashed lines denote predictions from Marion et al. [2005].

Chapter 7

CONCLUSION: A DEEPER UNDERSTANDING OF THE PROSPECTS FOR LIFE IN OCEAN PLANETS

The preceding chapters directly address the scientific questions raised in the introduction. Chapter 2 gives the first quantitative estimates of fluid percolation depths in extraterrestrial lithospheres. Greater fluid penetration depths in smaller objects, which have slighter increases in pressure and temperature with increasing depth (see, e.g., Fig. 7.1), mean order-of-magnitude increase in the volume for potential fluid rock interaction. These results indicate that small ocean planets are potentially much more habitable than previously thought.

Chapter 3 demonstrates a mechanism for isolating a deep seafloor from the near-surface environment based on pressure's influence on the density of aqueous magnesium sulfate. The prospect for stratification in an otherwise well-mixed europan ocean suggests possibilities for diverse trophic systems at different depths — such as exist in Earth's — and for increased storage of radiogenic heat from the moon's interior, which would relate to resurfacing of Europa's icy lithosphere that occurred within the last 80 Myr [Zahnle et al., 2003].

The densities produced by the buoyancy calculation in Chapter 3 are based on extrapolation of previously measured volumetric properties above 100 MPa. These are found to be in fair agreement with densities inferred from measurements of sound velocity in Chapter 6. The concepts they motivate can be considered qualitatively sound. However, the deviation between actual and predicted densities will become important as constraints ocean depth and composition become available, in which case predictions of the depth of neutral buoyancy and other pressure gradient dependent

properties will help in distinguishing viable scenarios.

Improved inversion of existing or future moment of inertia and magnetometer measurements may reveal large-scale structure in the subsurfaces of icy satellites [Anderson et al., 2003]. As our understanding of icy satellite interiors moves beyond simple nested-sphere approximation (a larger version of the oft-disdained "spherical cow"), improved understanding of aqueous chemistry will be vital in understanding these alien environments.

For example, if detailed mapping of Europa's surface by a future exploration mission reveals chaos features that are verifiably caused by subsurface destabilization and are telling of the salt composition of the waters directly beneath, detailed knowledge of pressure's effect on sulfate chemistry will help to constrain the depth and temperature at which the fluids can have formed. Latitudinal variation in the composition of surface deposits might be combined with observations of their frequency or size to give a picture of the material and heat flux through the ocean.

7.1 The Propects for Life in Europa and Elsewhere as Revealed by the Present Contribution

In light of the present work, the prospects for life in small ocean planets are significantly improved. Primordial anhydrous mantle may serve as a "redox capacitor" in ocean planets, releasing hydrogen by progressive serpentinization as the planets cool. Heat energy from serpentinization supplements radiogenic and tidal heating, reducing kinetic limitations to biological activity so that, in the presence of a source of oxidants, conditions better favor the development of the as-yet-undefined chemistry necessary for the development of simple organisms.

However, it remains impossible to confirm the habitability of known ocean planets (Earth being the exception). The scenario for stratification in Europa's ocean introduced in Chapter 3 serves as a caution that an oxidation-reduction cycle driven by interactions between Europa's serpentinizing seafloor and its radiolytically processed

ice shell may be limited despite the ocean's high Rayleigh number.

New measurements of apparent and partial molal volumes in aqueous magnesium sulfate under europan seafloor conditions confirm and extend the few previous measurements [Hogenboom et al., 1995], revealing important discrepancies between predicted and actual solution properties. This new information provides a means for more accurate predictions of ocean and subseafloor chemistry.

Revisiting the discussion of material presented in Chapters 2 and 3, we see that the these measurements apply to a broad range of planetary conditions. Models of pressure's effect on aqueous chemistry based on Pitzer's virial coefficients should be considered adequate for calculations of magnesium sulfate chemistry under europan ocean and subseafloor conditions (e.g., the calculations in Chapter 3), with the understanding that phenomena dependent on gradients in solution properties with pressure may yield incorrect numerical results. Such models will benefit from a recalculation of compressibility coefficients based on the present and future measurements.

7.2 Future Work

Addressing the question of life's emergence and persistence elsewhere in the Universe ultimately requires direct detection — or, at least, inference from observation of the proper chemical signatures. As discussed above, interpretation of future observations and, in the more immediate future, further constraints on habitability will benefit from additional measurements comparable to those presented here. In this final section, we motivate future measurements using impulsive stimulated scattering with some modifications to the Icy Satellite Ocean Simulator.

7.2.1 Extended Simulations of Ocean Chemistry

The present work increases the confidence with which one may explore the chemistry of europan ocean composed primarily of magnesium sulfate. A more complete treatment of the most abundant electrolytes has applications beneath Earth's oceans

and extraterrestrial oceans. A proper template for future work exists in the work of Millero and coworkers [Chen et al., 1978, Millero, 1983], cited previously, who measured densities in NaCl, KCl, $MgCl_2$ and Na_2SO_4 to 100 MPa between 0 and 50°C. ISIS can be used for measurements in the these and other aqueous solutions in the same manner as has been described here for $MgSO_4$.

Because the potentially corrosive samples treated in ISIS are separated from the steel of the pressure system, ISIS allows for detailed measurements in highly concentrated aqueous solutions for which such data are lacking. Impulsive stimulated scattering offers a means checking previous sound velocity measurements in water and other solvents [e.g. Abramson et al., 1999]. Studies in ternary mixtures will allow further refinement of excess volumes. All of these research directions will be useful for understanding the principles underlying the chemistry of electrolyte solutions.

7.2.2 Some Like it Cold

As discussed in Chapter 2, recent discoveries of Kuiper Belt Objects larger than Pluto, some with orbiting companions, suggests the possibility that a vast number of potential astrobiological targets exist beyond the orbit of Jupiter, where deep subsurface oceans are expected to contain some amount of ammonia (NH_3). The melting point of pure ammonia is -90 °C, and aqueous mixtures of the substance can have eutectic points far below those of electrolyte systems such as the one examined here. The phase diagram for the water-ammonia system has been described in recent years from direct observation [Leliwa-Kopystynski et al., 2002, 0-0.23 M to 300 MPa at 200-273 K]; [Mousis et al., 2002, 25 Wt % to 1 GPa at 273-175 K]; [Hogenboom et al., 1997], but few measurements of density exist at high pressures for aqueous ammonia. The equation of state reported by Croft et al. [1988] from 0-100 Wt % to 1 GPa is based on measurements in pure NH_3 to 500 MPa [Haar and Gallagher, 1978]. The behavior of intermediate compositions comes from one source [Sourirajan and Kennedy, 1963], who published measurements to only 140 MPa. Bulk moduli

inferred by Croft et al (1988) differ in extrapolation from those of the end members by a few percent, suggesting that a study in our lab would yield improvements in the equation of state for aqueous ammonia. Density data at elevated pressures are limited to a single binary-phase study [Sourirajan and Kennedy, 1963] to 140 MPa, far below pressures in Titan's ocean (Fig. 7.1).

As it is currently set up, ISIS can examine ammonia and ammonium sulfate compositions thought to occur in Titan other kronian satellites [Croft et al., 1988]. With improved thermal isolation and control, ISIS can be used to examine near-cryogenic solutions under pressure. Such measurements would help in understanding the role of ammonia in deep hydrothermal environments and ecosystems.

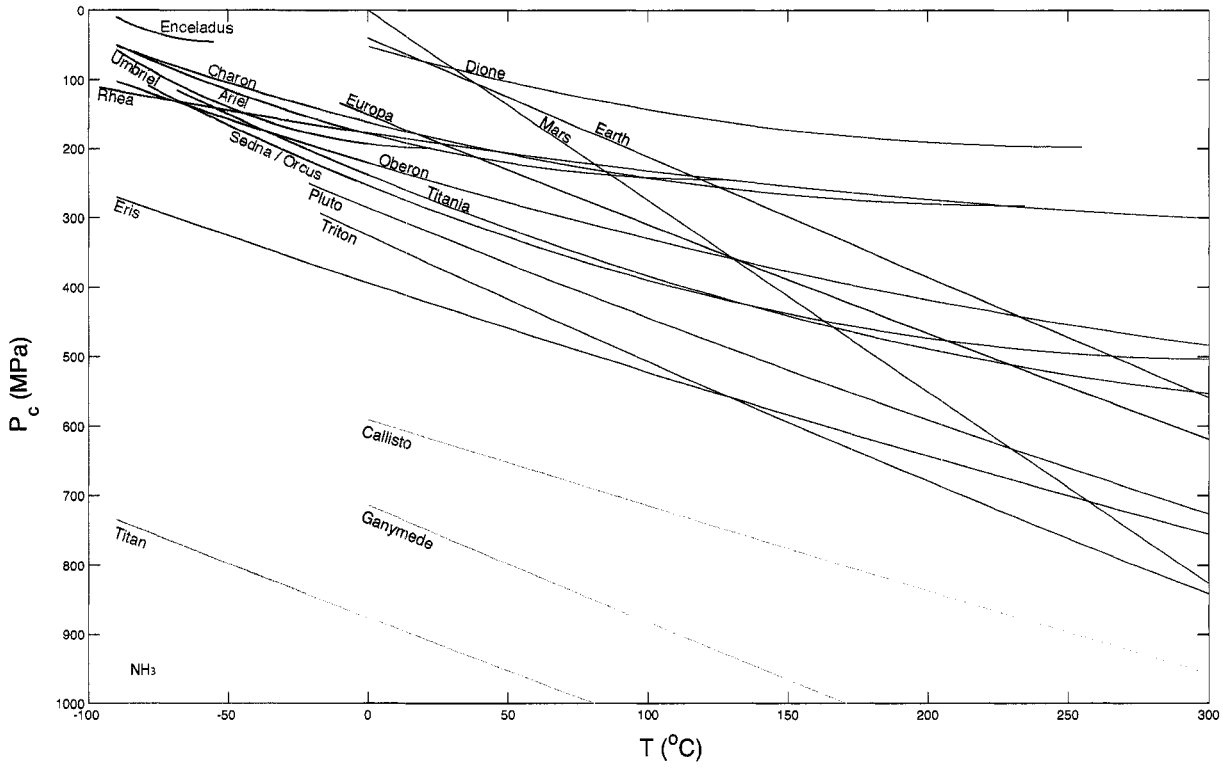

Figure 7.1: Extended pressure-temperature profiles for objects of interest in the study of aqueous solutions. The y-axis shows the range of pressure obtainable in the current configuration of the Icy Satellite Interior Simulator. The domain of temperatures displayed on the x-axis extends above and below the range currently obtainable, where future measurements should be made. Stability region for selected materials and some of their respective phases are indicated.

BIBLIOGRAPHY

I. M. Abdulagatov, N. D. Azizov, and A. B. Zeinalova. Viscosities, densities, apparent and partial molar volumes of concentrated aqueous $MgSO_4$ solutions at high temperatures and high pressures. *Physics And Chemistry Of Liquids*, 45(2):127–148, 2007.

T.A. Abrajano, N.C. Sturchio, B. M. Kennedy, K. Muehlenbachs, and J. K. Bohlke. Geochemistry of reduced gas related to serpentinization of Zambales Ophiolite, Philippines. *Applied Geochemistry*, 5:625–630, 1990.

E. H. Abramson, J. M. Brown, and L. J. Slutsky. Applications of impulsive stimulated scattering in the earth and planetary sciences. *Annual Review of Physical Chemistry*, 50:279–313, 1999.

E.H. Abramson, J.M. Brown, L.J. Slutsky, and S. Wiryana. Measuring speed of sound and thermal diffusivity in the diamond-anvil cell. *International Journal of Thermophysics*, 22:405 – 414, 2001.

D. E. Allen and W. E. Seyfried. Compositional controls on vent fluids from ultramatic-hosted hydrothermal systems at mid-ocean ridges: An experimental study at 400 degrees C, 500 bars. *Geochimica et Cosmochimica Acta*, 67(8):1531–1542, 2003.

D. E. Allen and W. E. Seyfried. Serpentinization and heat generation: Constraints from Lost City and Rainbow hydrothermal systems. *Geochimica et Cosmochimica Acta*, 68(6):1347–1354, 2004.

F. S. Anderson, A. F. C. Haldemann, N. T. Bridges, M. P. Golombek, T. J. Parker,

and G. Neumann. Analysis of mola data for the mars exploration rover landing sites. *Journal of Geophysical Research-Planets*, 108(E12):8084, 2003.

J. D. Anderson and G. Schubert. Saturn's satellite Rhea is a homogeneous mix of rock and ice. *Geophysical Research Letters*, 34(2):L02202, January 2007.

J. D. Anderson, E. L. Lau, W. L. Sjogren, G. Schubert, and W. B. Moore. Gravitational evidence for an undifferentiated Callisto. *Nature*, 387(6630):264–266, 1997.

J.D. Anderson, G. Schubert, R.A. Jacobson, E.L. Lau, W.B. Moore, and W.L. Sjogren. Europa's differentiated internal structure: inferences from four Galileo encounters. *Science*, 281(5385):2019 – 2022, 1998.

Roger N. Anderson, Mark D. Zoback, Stephen H. Hickman, and Robin L. Newmark. Permeability versus depth in the upper oceanic crust: In situ measurements in DSDP hole 504B, Eastern Equatorial Pacific. *Journal of Geophysical Research*, 90 B5:3659–3669, 1985.

P. Anschutz, J. S. Turner, and G. Blanc. The development of layering, fluxes through double-diffusive interfaces, and location of hydrothermal sources of brines in the atlantis ii deep: Red sea. *Journal of Geophysical Research-Oceans*, 103(C12):27809–27819, 1998.

K. Ariga, H. Yuki, J. Kikuchi, O. Dannemuller, A. M. Albrecht-Gary, Y. Nakatani, and G. Ourisson. Monolayer studies of single-chain polyprenyl phosphates. *Langmuir*, 21(10):4578–4583, May 2005.

B. K. Atkinson. Subcritical crack-growth in geological-materials. *Journal of Geophysical Research*, 89(NB6):4077–4114, 1984.

Philipp Baaske, Franz M. Weinert, Stefan Duhr, Kono H. Lemke, Michael J. Russell, and Dieter Braun. From the cover: Extreme accumulation of nucleotides in simu-

lated hydrothermal pore systems. *Proceedings of the National Academy of Sciences*, 104(9346-9351), 2007.

V. R. Baker, J. M. Dohm, A. G. Fairen, T. P. A. Ferre, J. C. Ferris, H. Miyamoto, and D. Schulze-Makuch. Extraterrestrial hydrogeology. *Hydrogeology Journal*, 13 (1):51–68, 2005.

Amy C. Barr and William B. McKinnon. Convection in enceladus' ice shell: Conditions for initiation. *Geophysical Research Letters*, doi:10.1029/2006GL028799: L09202, 2007.

K. Becker. Seeding the oceans with observations. *Oceanus*, 42(1):2–5, 2000.

K. Becker, R. P. Von Herzen, T. J. G. Francis, R. N. Anderson, J. Honnorez, A. C. Adamson, J. C. Alt, R. Emmermann, P. D. Kempton, H. Kinoshita, C. Laverne, M. J. Mottl, and R. L. Newmark. Insitu electrical-resistivity and bulk porosity of the oceanic-crust Costa-Rica rift. *Nature*, 300(5893):594–598, 1982.

M. E. Berndt, D. E. Allen, and W. E. Seyfried. Reduction of CO_2 during serpentinization of olivine at 300 degrees C and 500 bar. *Geology*, 24(4):351–354, 1996.

G. Blanc and P. Anchutz. New stratification in the hydrothermal brine system of the Atlantis-II Deep, Red Sea. *Geology*, 23(6):543–546, 1995.

M. A. Bouhifd, D. Andrault, G. Fiquet, and P. Richet. Thermal expansion of forsterite up to the melting point. *Geophysical Research Letters*, 23(10):1143–1146, 1996.

D. J. Bradley and K. S. Pitzer. Thermodynamics of electrolytes. 12. dielectric properties of water and debye-hueckel parameters to 350. degree. c and 1 kbar. *The Journal of Physical Chemistry*, 83:1599–1603, 1979.

M. D. Brasier, O.R. Green, A.P. Jephcoat, A.K. Kleppe, M.J. Van Kranendonk, J.F.

Lindsay, A. Steele, and N.V. Grassineau. Questioning the evidence for Earth's oldest fossils. *Nature*, 416:76–81, 2002.

M. E. Brown, C. Trujillo, and D. Rabinowitz. Discovery of a candidate inner oort cloud planetoid. *Astrophysical Journal*, 617(1):645–649, dec 2004.

M. E. Brown, A. H. Bouchez, D. Rabinowitz, R. Sari, C. A. Trujillo, M. van Dam, R. Campbell, J. Chin, S. Hartman, E. Johansson, R. Lafon, D. Le Mignant, P. Stomski, D. Summers, and P. Wizinowich. Keck observatory laser guide star adaptive optics discovery and characterization of a satellite to the large kuiper belt object 2003 el61. *Astrophysical Journal*, 632(1):L45–L48, oct 2005.

J. P. Canales, R. S. Detrick, J. Lin, J. A. Collins, and D. R. Toomey. Crustal and upper mantle seismic structure beneath the rift mountains and across a nontransform offset at the Mid-Atlantic Ridge (35 degrees N). *Journal of Geophysical Research-Solid Earth*, 105(B2):2699–2719, 2000.

M. H. Carr. *Water on Mars*. Oxford University Press, 1996.

J. L. Charlou, Y. Fouquet, H. Bougault, J. P. Donval, J. Etoubleau, P. Jean-Baptiste, A. Dapoigny, P. Appriou, and P. A. Rona. Intense CH_4 plumes generated by serpentinization of ultramafic rocks at the intersection of the 15 degrees 20 ' N fracture zone and the Mid-Atlantic Ridge. *Geochimica et Cosmochimica Acta*, 62 (13):2323–2333, 1998.

J. L. Charlou, J. P. Donval, Y. Fouquet, P. Jean-Baptiste, and N. Holm. Geochemistry of high H_2 and CH_4 vent fluids issuing from ultramafic rocks at the Rainbow hydrothermal field (36 degrees 14 ' N, MAR). *Chemical Geology*, 191(4):345–359, 2002.

C. T. Chen, R. A. Fine, and F. J. Millero. Equation of state of pure water determined from sound speeds. *Journal of Chemical Physics*, 66(5):2142–2144, 1977.

C. T. Chen, L. S. Chen, and F. J. Millero. Speed of sound in NaCl, $MgCl_2$, Na_2SO_4, and $MgSO_4$ aqueous-solutions as functions of concentration, temperature, and pressure. *Journal of the Acoustic Society of America*, 63(6):1795–1800, 1978.

G. Chen, B. M. Znosko, X. Q. Jiao, and D. H. Turner. Factors affecting thermodynamic stabilities of rna 3x3 internal loops. *Biochemistry*, 43(40):12865–12876, October 2004.

I. A. Chen, K. Salehi-Ashtiani, and J. W. Szostak. RNA catalysis in model protocell vesicles. *Journal of the American Chemical Society*, 127(38):13213–13219, September 2005.

C. F. Chyba, D. G. Jankowski, and P. D. Nicholson. Tidal evolution in the Neptune-Triton system. *Astronomy and Astrophysics*, 219:L23–L26, 1989.

G. D. Cody, R. J. Bellows, D. J. Goldfarb, H. A. Wolf, and G. V. Storch. A novel non-intrusive probe of particle motion and gas generation in the feed injection zone of the feed riser of a fluidized bed catalytic cracking unit. *Powder Technology*, 110 (1-2):128–142, May 2000.

G.C. Collins, J.W. Head III, R.T. Pappalardo, and N.A. Spaun. Evaluation of models for the formation of chaotic terrain on Europa. *Journal of Geophysical Research*, 105 E1:1709–1716, 2000.

S. K. Croft, J. I. Lunine, and J. Kargel. Equation of state of ammonia water liquid: Derivation and planetological applications. *Icarus*, 73(2):279–293, 1988.

T. J. Crone and W. S. D. Wilcock. Modeling the effects of tidal loading on mid-ocean ridge hydrothermal systems. *Geochemistry Geophysics Geosystems*, 6:Q07001, 2005.

C. de Bergh, B. L. Lutz, T. Owen, and J.-P. Maillard. Monodeuterated methane in the outer solar system. IV - Its detection and abundance on Neptune. , 355: 661–666, June 1990. doi: 10.1086/168799.

D. Deamer, J. P. Dworkin, S. A. Sandford, M. P. Bernstein, and L. J. Allamandola. The first cell membranes. *Astrobiology*, 2(4):371–381, 2002.

V.A. DelGrosso and C.W. Mader. Speed of sound in pure water. *Journal of the Acoustical Society of America*, 52:1442, 1972.

Audrey C. Delsanti and David C. Jewitt. *Solar System Update*, chapter The Solar System beyond the Planets, pages 267–294. Springer-Praxis, 2006.

B. deMartin, G. Hirth, and B. Evans. *Mid-Ocean Ridges: Hydrothermal Interactions Between the Lithosphere and Oceans, Geophysical Monograph Series 148*, chapter Experimental Constraints on Thermal Cracking of Peridotite at Oceanic Spreading Centers, pages 167–185. American Geophysical Union, 2004.

Steven D'Hondt, Bo Barker Jørgensen, D. Jay Miller, Anja Batzke, Ruth Blake, Barry A. Cragg, Heribert Cypionka, Gerald R. Dickens, Timothy Ferdelman, Kai-Uwe Hinrichs, Nils G. Holm, Richard Mitterer, Arthur Spivack, Guizhi Wang, Barbara Bekins, Bert Engelen, Kathryn Ford, Glen Gettemy, Scott D. Rutherford, Henrik Sass, C. Gregory Skilbeck, Ivano W. Aiello, Gilles Guèrin, Christopher H. House, Fumio Inagaki, Patrick Meister, Thomas Naehr, Sachiko Niitsuma, R. John Parkes, Axel Schippers, David C. Smith, Andreas Teske, Juergen Wiegel, Christian Naranjo Padilla, and Juana Luz Solis Acosta. Distributions of microbial activities in deep subseafloor sediments. *Science*, 306(5705):2216–2221, 2004.

E. Douville, J. L. Charlou, E. H. Oelkers, P. Bienvenu, C. F. J. Colon, J. P. Donval, Y. Fouquet, D. Prieur, and P. Appriou. The Rainbow vent fluids (36 degrees 14' N, MAR): the influence of ultramafic rocks and phase separation on trace metal content in Mid-Atlantic Ridge hydrothermal fluids. *Chemical Geology*, 184(1-2): 37–48, 2002.

A. M. Dziewonski and D. L. Anderson. Preliminary reference Earth model. *Physics of the Earth and Planetary Interiors*, 25(4):297–356, 1981.

A.G. Evans and D.R. Clarke. *Thermal Stress in Severe Environments*, chapter Residual Stresses and Microcracking Induced by Thermal Contraction Inhomogeneity, pages 629–648. Plenum Press, New York, 1980.

H. J. S. Fernando. Oceanographic implications of laboratory experiments on diffusive interfaces. *Journal of Physical Oceanography*, 19(11):1707–1715, 1989.

P. H. Figueredo and R. Greeley. Resurfacing history of Europa from pole-to-pole geological mapping. *Icarus*, 167(2):287–312, 2004.

A. T. Fisher. Permeability within basaltic oceanic crust. *Reviews of Geophysics*, 36 (2):143–182, 1998.

A. T. Fisher and K. Becker. Channelized fluid flow in oceanic crust reconciles heatflow and permeability data. *Nature*, 403(6765):71–74, 2000.

M. R. Fisk and S. J. Giovannoni. Sources of nutrients and energy for a deep biosphere on Mars. *Journal of Geophysical Research-Planets*, 104(E5):11805–11815, 1999.

V. Formisano, S. Atreya, T. Encrenaz, N. Ignatiev, and M. Giuranna. Detection of methane in the atmosphere of Mars. *Science*, 306(5702):1758–1761, 2004.

J. T. Fredrich and T. F. Wong. Micromechanics of thermally induced cracking in 3 crustal rocks. *Journal of Geophysical Research-Solid Earth*, 91(B12):2743–2764, 1986.

K. Fujii and R. Masui. Accurate measurements of the sound-velocity in pure water by combining a coherent phase-detection technique and a variable path-length interferometer. *Journal Of The Acoustical Society Of America*, 93(1):276–282, January 1993.

R. Furuuchi, E. I. Imai, H. Honda, K. Hatori, and K. Matsuno. Evolving lipid vesicles in prebiotic hydrothermal environments. *Origins of Life and Evolution of the Biosphere*, 35(4):333–343, August 2005.

R.E. Gagnon, H. Kiefte, Clouter M.J., and E. Whalley. Pressure dependence of the elastic constants of ice ih to 2.8 kbar by Brillouin spectroscopy. *Journal of Physical Chemistry*, 89(8):4522–4528, 1988.

T. Gold. The deep, hot biosphere. *Proceedings of the National Academy of Sciences of the United States of America*, 89(13):6045–6049, 1992.

J. C. Goodman, G. C. Collins, J. Marshall, and R. T. Pierrehumbert. Hydrothermal plume dynamics on Europa: Implications for chaos formation. *Journal of Geophysical Research-Planets*, 109(E3):E03008, doi:10.1029/2003JE002073, 2004.

L. Haar and J.S. Gallagher. Thermodynamic properties of ammonia. *Journal of Physical and Chemical Reference Data*, 7:635–792, 1978.

R. M. Hazen, N. Boctor, J. A. Brandes, G. D. Cody, R. J. Hemley, A. Sharma, and H. S. Yoder. High pressure and the origin of life. *Journal of Physics-Condensed Matter*, 14(44):11489–11494, November 2002.

G. Hirth and D. L. Kohlstedt. Experimental constraints on the dynamics of the partially molten upper-mantle .2. Deformation in the dislocation creep regime. *Journal of Geophysical Research-Solid Earth*, 100(B8):15441–15449, 1995.

R. A. Hoare. Problems of heat transfer in Lake Vanda a density stratified antarctic lake. *Nature*, 210(5038):787–&, 1966.

A.M. Hofmeister. Mantle values of thermal conductivity and the geotherm from phonon lifetimes. *Science*, 283:1699–1706, 1999.

D. L. Hogenboom, J. S. Kargel, J. P. Ganasan, and L. Lee. Magnesium sulfate-water to 400 MPa using a novel piezometer: Densities, phase equilibria, and planetological implications. *Icarus*, 115(2):258–277, June 1995. URL http://www.Sciencedirect.com/Science/article/B6WGF-45NJJ40-14/2/5f176b700065df4efb2e1eba3abd3224.

D. L. Hogenboom, J. S. Kargel, G. J. Consolmagno, T. C. Holden, L. Lee, and M. Buyyounouski. The ammonia-water system and the chemical differentiation of icy satellites. *Icarus*, 128(1):171–180, 1997.

Gerald Holton, M. Paul Hagelberg, Samuel Kao, and Jr. Walter H. Johnson. Ultrasonic-velocity measurements in water at pressures to 10 000 kg/cm^2. *The Journal of the Acoustical Society of America*, 43(1):102–107, 1968.

H. Hussmann, F. Sohl, and T. Spohn. Subsurface oceans and deep interiors of medium-sized outer planet satellites and large trans-neptunian objects,. *Icarus*, 185:258–273, 2006.

Hauke Hussmann and Tilman Spohn. Thermal-orbital evolution of Io and Europa. *Icarus*, 171(2):391–410, October 2004. URL http://www.Sciencedirect.com/Science/article/B6WGF-4CYWKGX-1/2/c07e17c5fd3dd29cb06a8af1b7f8e586.

C. E. Jacob. On the flow of water in an elastic artesian aquifer. *Eos Trans. AGU*, 21: 574–586, 1940.

B. M. Jakosky and E. L. Shock. The biological potential of Mars, the early Earth, and Europa. *Journal of Geophysical Research-Planets*, 103(E8):19359–19364, August 1998.

D.R. Janecky and W.E. Seyfried. Hydrothermal serpentinization of peridotite within the oceanic-crust - experimental investigations of mineralogy and major element chemistry. *Geochimica et Cosmochimica Acta*, 50(7):1357–1378, 1986.

J. S. Kargel, S. K. Croft, J. I. Lunine, and J. S. Lewis. Rheological properties of ammonia-water liquids and crystal-liquid slurries: Planetological applications. *Icarus*, 89(1):93–112, January 1991. URL `http://www.Sciencedirect.com/Science/article/B6WGF-4731DBC-PH/2/095524e86f5d56ba14d05e89867f687a`.

Jeffrey S. Kargel. The volcanic and tectonic history of Enceladus. *Icarus*, 119:385–404, 1996.

Jeffrey S. Kargel, Jonathan Z. Kaye, James W. Head, III, Giles M. Marion, Roger Sassen, James K. Crowley, Olga Prieto Ballesteros, Steven A. Grant, and David L. Hogenboom. Europa's crust and ocean: Origin, composition, and the prospects for life. *Icarus*, 148(1):226–265, November 2000.

D. E. Kelley, H. J. S. Fernando, A. E. Gargett, J. Tanny, and E. Ozsoy. The diffusive regime of double-diffusive convection. *Progress in Oceanography*, 56(3-4):461–481, 2003.

D. S. Kelley and G. L. Fruh-Green. Volatile lines of descent in submarine plutonic environments: Insights from stable isotope and fluid inclusion analyses. *Geochimica et Cosmochimica Actaa*, 65(19):3325–3346, 2001.

D. S. Kelley, J. A. Karson, G. L. Fruh-Green, D. R. Yoerger, T. M. Shank, D. A. Butterfield, J. M. Hayes, M. O. Schrenk, E. J. Olson, G. Proskurowski, M. Jakuba, A. Bradley, B. Larson, K. Ludwig, D. Glickson, K. Buckman, A. S. Bradley, W. J. Brazelton, K. Roe, M. J. Elend, A. Delacour, S. M. Bernasconi, M. D. Lilley, J. A. Baross, R. T. Summons, and S. P. Sylva. A serpentinite-hosted ecosystem: The Lost City hydrothermal field. *Science*, 307(5714):1428–1434, 2005.

R. A. Kerr. Planetary science: Cassini catches mysterious hot spot on icy-cold Enceladus. *Science*, 309(5736):859–860, 2005.

V. A. Krasnopolsky. A sensitive search for SO_2 in the martian atmosphere: Implications for seepage and origin of methane. *Icarus*, 178(2):487–492, November 2005.

B. S. Krumgalz, A. Starinsky, and K. S. Pitzer. Ion-interaction approach: Pressure effect on the solubility of some minerals in submarine brines and seawater. *JOURNAL OF SOLUTION CHEMISTRY*, 28(6):667–692, 1999.

A. Leger, F. Selsis, C. Sotin, T. Guillot, D. Despois, D. Mawet, M. Ollivier, A. Labeque, C. Valette, and F. Brachet. A new family of planets? "Ocean-Planets". *Icarus*, 169(2):499–504, June 2004.

Jacek Leliwa-Kopystynski, Minoru Maruyama, and Toshio Nakajima. The water-ammonia phase diagram up to 300 MPa: Application to icy satellites. *Icarus*, 159: 518–528, 2002.

Lindsey S. Link, Bruce M. Jakosky, and Geoffrey D. Thyne. Biological potential of low-temperature aqueous environments on Mars. *International Journal of Astrobiology*, 4:155–164, 2005.

Jere H. Lipps and Sarah Rieboldt. Habitats and taphonomy of Europa. *Icarus*, 177 (2):515–527, October 2005.

C. R. B. Lister. Penetration of water into hot rock. *Geophysical Journal of the Royal Astronomical Society*, 39(3):465–509, 1974.

Robert P. Lowell and Myesha DuBose. Hydrothermal systems on Europa. *Geophysical Research Letters*, 32(5):L05202, doi:10.1029/2005GL022375, 2005. ISSN 0094-8276. URL `http://dx.doi.org/10.1029/2005GL022375`.

W. Berry Lyons, Kathleen A. Welch, Glen Snyder, John Olesik, Elizabeth Y. Graham, Giles M. Marion, and Robert J. Poreda. Halogen geochemistry of the McMurdo

dry valleys lakes, Antarctica: Clues to the origin of solutes and lake evolution. *Geochimica et Cosmochimica Acta*, 69(2):305–323, January 2005.

Giles M. Marion, Jeffrey S. Kargel, David C. Catling, and Scott D. Jakubowski. Effects of pressure on aqueous chemical equilibria at subzero temperatures with applications to Europa. *Geochimica et Cosmochimica Acta*, 69(2):259–274, January 2005.

B. Martin and W. S. Fyfe. Some experimental and theoretical observations on kinetics of hydration reactions with particular reference to serpentinization. *Chemical Geology*, 6(3):185–&, 1970.

J.T. Martin and R.P. Lowell. Precipitation of quartz during high-temperature, fracture controlled hydrothermal upflow at ocean ridges: Equilibrium versus linear kinetics. *Journal of Geophysical Research-Solid Earth*, 105(B1):869–882, 2000.

T. M. McCollom and J. S. Seewald. A reassessment of the potential for reduction of dissolved CO_2 to hydrocarbons during serpentinization of olivine. *Geochemica et Cosmochimica Acta*, 65(21):3769–3778, 2001.

T. M. McCollom and E. L. Shock. Geochemical constraints on chemolithoautotrophic metabolism by microorganisms in seafloor hydrothermal systems. *Geochimica et Cosmochimica Acta*, 61(20):4375–4391, 1997.

T. M. McCollom and E. L. Shock. Fluid-rock interactions in the lower oceanic crust: Thermodynamic models of hydrothermal alteration. *Journal of Geophysical Research-Solid Earth*, 103(B1):547–575, 1998.

T. M. McCollom, G. Ritter, and B. R. T. Simoneit. Lipid synthesis under hydrothermal conditions by Fischer-Tropsch-type reactions. *Origins of Life and Evolution of the Biosphere*, 29(2):153–166, 1999.

T. B. McCord and C. Sotin. Ceres: Evolution and current state. *Journal of Geophysical Research-Planets*, 110(E5):E05009, 2005.

W. B. McKinnon and M. E. Zolensky. Sulfate content of Europa's ocean and shell: Evolutionary considerations and some geological and astrobiological implications. *Astrobiology*, 3(4):879–897, 2003.

H. J. Melosh, A. G. Ekholm, A. P. Showman, and R. D. Lorenz. The temperature of Europa's subsurface water ocean. *Icarus*, 168(2):498–502, 2004.

W. J. Merryfield. Origin of thermohaline staircases. *Journal of Physical Oceanography*, 30(5):1046–1068, 2000.

F. J. Millero. The thermodynamics of seawater .2. thermochemical properties. *Ocean Science and Engineering*, 8(1):1–40, 1983.

P. A. Monnard, C. L. Apel, A. Kanavarioti, and D. W. Deamer. Influence of ionic inorganic solutes on self-assembly and polymerization processes related to early forms of life: Implications for a prebiotic aqueous medium. *Astrobiology*, 2(2): 139–152, 2002.

D. R. Montgomery and A. Gillespie. Formation of martian outflow channels by catastrophic dewatering of evaporite deposits. *GEOLOGY*, 33(8):625–628, Aug 2005. ISSN 0091-7613.

J.B. Moody. Serpentinization - review. *Lithos*, 9(2):125–138, 1976.

W. B. Moore and G. Schubert. The tidal response of Europa. *Icarus*, 147(1):317–319, 2000.

M. A. Motin. Temperature and concentration dependence of apparent molar volumes and viscosities of NaCl, NH_4Cl, $CuCl_2$, $CuSO_4$, and MgSO4 in pure water and water + urea mixtures. *Journal of Chemical and Engineering Data*, 49:94–98, 2004.

O. Mousis, J. Pargamin, O. Grasset, and C. Sotin. Experiments in the NH_3-H_2O system in the [0,1 GPa] pressure range - implications for the deep liquid layer of large icy satellites. *Geophysical Research Letters*, 29(24):2192, 2002.

Carl D. Murray and Stanley F. Dermott. *Solar System Dynamics.* Cambridge University Press, 1998.

C. Neal and G. Stanger. Hydrogen generation from mantle source rocks in Oman. *Earth and Planetary Science Letters*, 66:315–320, 1983.

K. H. Nealson. Hydrogen and energy flow as "sensed" by molecular genetics. *Proceedings of the National Academy of Sciences of the United States of America*, 102 (11):3889–3890, 2005.

H.W. Nesbitt and O.P. Bricker. Low-temperature alteration processes affecting ultramafic bodies. *Geochimica Et Cosmochimica Acta*, 42(4):403–409, 1978.

David P. O'Brien, Paul Geissler, and Richard Greenberg. A melt-through model for chaos formation on Europa. *Icarus*, 156(152-161), 2002.

Dennis O'Hanley. Solution to the volume problem in serpentinization. *Geology*, 20: 705–708, 1992.

Chris H. Okubo and Alfred S. McEwen. Fracture-controlled paleo-fluid flow in candor chasma, Mars. *Science*, 315:983–985, 2007.

C. Oze and M. Sharma. Have olivine, will gas: Serpentinization and the abiogenic production of methane on Mars. *Geophysical Research Letters*, 32(10):L10203, 2005.

E. Ozsoy and U. Unluata. Oceanography of the Black Sea: a review of some recent results. *Earth Science Reviews*, 42(4):231–272, 1997.

N.R. Pace. A molecular view of microbial diversity and the biosphere. *Science*, 276: 734–740, 1997.

M. S. Paterson. Effect of pressure on young's modulus and the glass transition in rubbers. *Journal of Applied Physics*, 35:176–179, 1964.

K. Pedersen. Exploration of deep intraterrestrial microbial life: current perspectives. *FEMS Microbiology Letters*, 185(1):9–16, 2000.

K. Pedersen, S. Ekendahl, E. L. Tullborg, H. Furnes, I. G. Thorseth, and O. Tumyr. Evidence of ancient life at 207 m depth in a granitic aquifer. *Geology*, 25(9):827–830, 1997.

Y. J. Pendleton and L. J. Allamandola. The organic refractory material in the diffuse interstellar medium: Mid-infrared spectroscopic constraints. *Astrophysical Journal Supplement Series*, 138(1):75–98, January 2002.

Ramesh C. Phutela and Kenneth S. Pitzer. Densities and apparent molar volumes of aqueous magnesium sulfate and sodium sulfate to 473 K and 100 bar. *Journal of Chemical and Engineering Data*, 31:320–327, 1986.

Kenneth S. Pitzer. Thermodytriarnics of electrolytes. I . theoretical basis and general equation. *The Journal of Physical Chemistry*, 77:268–277, 1973.

M. Podolak, R.T. Reynolds, and R. Young. POST Voyager comparisons of the interiors of Uranus and Neptune. *Geophysical Research Letters*, 17:1737–1740, September 1990.

C. C. Porco, P. Helfenstein, P. C. Thomas Thomas, A. P. Ingersoll, J. Wisdom, R. West, G. Neukum, T. Denk, R. Wagner, T. Roatsch, E. Kieffer, S. Turtle, A. McEwen, T. V. Johnson, J. Rathbun, J. Veverka, D. Wilson, J. Perry, J. Spitale, A. Brahic, J. A. Burns, A. D. DelGenio, L. Dones, C. D. Murray, and S. Squyres. Cassini observes the active south pole of Enceladus. *Science*, 311:1393–1401, 2006.

L. M. Prockter, F. Nimmo, and R. Pappalardo. A shear heating origin for ridges on triton. *Geophysical Research Letters*, 32(L14202):doi:10.1029/2005GL022832, 2005.

D. L. Rabinowitz, K. Barkume, M. E. Brown, H. Roe, M. Schwartz, S. Tourtellotte, and C. Trujillo. Photometric observations constraining the size, shape, and albedo of 2003 EL61, a rapidly rotating, Pluto-sized object in the Kuiper Belt. *Astrophysical Journal*, 639(2):1238–1251, mar 2006.

S.N. Raymond, A.M. Mandel, and S. Sigurdsson. Exotic earths: Forming habitable worlds with giant planet formation. *Science*, 313:1413–1416, 2006.

A. L. Reysenbach and E. Shock. Merging genomes with geochemistry in hydrothermal ecosystems. *Science*, 296(5570):1077–1082, 2002.

M. T. Rosing. 13C-depleted carbon microparticles in > 3700-Ma sea-floor sedimentary rocks from west Greenland. *Science*, 283:74–76, 1999.

M. N. Ross and G. Schubert. Viscoelastic models of tidal heating in Enceladus. *Icarus*, 78:90–101, 1989.

Javier Ruiz and Alberto G. Fairen. Seas under ice: Stability of liquid-water oceans within icy worlds. *Earth, Moon and Planets*, 97:79–90, 2005.

Patrick S. Russell and James W. Head, III. The martian hydrologic system: Multiple recharge centers at large volcanic provinces and the contribution of snowmelt to outflow channel activity. *Planetary And Space Science*, 55:315–332, 2007.

M. G. Sacerdote and J. W. Szostak. Semipermeable lipid bilayers exhibit diastereoselectivity favoring ribose. *Proceedings of the National Academy of Sciences of the United States of America*, 102(17):6004–6008, April 2005.

T. Schroeder, B. John, and B.R. Frost. Geologic implications of seawater circulation through peridotite exposed at slow-spreading mid-ocean ridges. *Geology*, 30(4): 367–370, 2002.

G. Schubert, T. Spohn, and R. Reynolds. *Satellites*, chapter Thermal histories, compositions and internal structures of the moons of the Solar System, pages 224–292. Univ. of Arizona Press, 1986.

Mitch Schulte, David Blake, Tori Hoehler, and Thomas McCollom. Serpentinization and its implications for life on the early Earth and Mars. *Astrobiology*, 6:364–376, 2006.

J.G Sclater, C. Jaupart, and D. Galson. The heat flow through oceanic and continental crust and the heat loss of the Earth. *Rev. Geophys. Space Phys*, 18:269–311, 1980.

M. Segatz, Spohn T., Ross M.N., and Schubert G. Tidal dissipation, surface heat flow and figures of viscoelastic models of Io. *Icarus*, 75:187–206, 1988.

W.E. Seyfried and W.E. Dibble. Seawater-peridotite interaction at 300-degrees-C and 500-bars - implications for the origin of oceanic serpentites. *Geochimica et Cosmochimica Acta*, 44(2):309–321, 1980.

E. L. Shock. Quenching, mixing, reaction progress, and the hydrothermal support of the biosphere. *Geochimica et Cosmochimica Acta*, 68(11):A259–A259, 2004.

M.C. Sinha and R.L. Evans. *Mid-Ocean Ridges: Hydrothermal Interactions Between the Lithosphere and Oceans*, chapter Geophysical Constraints Upon the Thermal Regime of the Ocean Crust. AGU Press, Washington DC, 2004.

A.R. Skelton, R. WhitMarsh, F. Arghe, P. Crill, and H. Koyi. Constraining the rate and extent of mantle serpentinization from seismic and petrological data: implications for chemosynthesis and tectonic processes. *Geofluids*, 5(3):153–164, 2005.

N.H. Sleep, A. Meibom, Th. Fridriksson, R.G. Coleman, and D.K. Bird. H_2-rich fluids from serpentinization: Geochemical and biotic implications. *PNAS*, 101: 12818–12823, 2004.

S. Sourirajan and G.C. Kennedy. Specific volumes of liquid ammonia-water mixtures in the temperature range 0^o to 25^o and pressure range 100 to 1400 bars. *J. Geophys. Res.*, 68:4149–4155, 1963.

J. R. Spencer, J. C. Pearl, M. Segura, F. M. Flasar, A. Mamoutkine, P. Romani, B. J. Buratti, A. R. Hendrix, L. J. Spilker, and R. M. C. Lopes. Cassini encounters Enceladus: Background and the discovery of a south polar hot spot. *Science*, 311: 1401 – 1405, 2006.

T. Spohn and G. Schubert. Oceans in the icy galilean satellites of Jupiter? *Icarus*, 161(2):456–467, 2003.

S. W. Squyres, R. E. Arvidson, J. F. Bell, J. Bruckner, N. A. Cabrol, W. Calvin, M. H. Carr, P. R. Christensen, B. C. Clark, L. Crumpler, D. J. Des Marais, C. d'Uston, T. Economou, J. Farmer, W. Farrand, W. Folkner, M. Golombek, S. Gorevan, J. A. Grant, R. Greeley, J. Grotzinger, L. Haskin, K. E. Herkenhoff, S. Hviid, J. Johnson, G. Klingelhofer, A. Knoll, G. Landis, M. Lemmon, R. Li, M. B. Madsen, M. C. Malin, S. M. McLennan, H. Y. McSween, D. W. Ming, J. Moersch, R. V. Morris, T. Parker, J. W. Rice, L. Richter, R. Rieder, M. Sims, M. Smith, P. Smith, L. A. Soderblom, R. Sullivan, H. Wanke, T. Wdowiak, M. Wolff, and A. Yen. The Spirit Rover's Athena science investigation at Gusev Crater, Mars. *Science*, 305(5685): 794–799, 2004.

C.A. Stein, S. Stein, and A. Pelayo. *Seafloor Hydrothermal Systems, Geophysical Monograph Series, Vol. 91*, chapter Heat flow and hydrothermal circulation, pages 425–445. AGU, 1995.

David J. Stevenson. Planetary magnetic fields. *Earth and Planetary Science Letters*, 208:1–11, 2003.

J. W. Szostak, D. P. Bartel, and P. L. Luisi. Synthesizing life. *Nature*, 409(6818): 387–390, January 2001.

R. E. Thomson and J. R. Delaney. Evidence for a weakly stratified europan ocean sustained by seafloor heat flux. *Journal of Geophysical Research-Planets*, 106(E6): 12355–12365, 2001.

G. Tobie, O. Grasset, J. I. Lunine, A. Mocquet, and C. Sotin. Titan's internal structure inferred from a coupled thermal-orbital model. *Icarus*, 175(2):496–502, 2005a.

G. Tobie, A. Mocquet, and C. Sotin. Tidal dissipation within large icy satellites: Applications to Europa and Titan. *Icarus*, 177(2):534–549, October 2005b.

J. T. Trevors. The subsurface origin of microbial life on the Earth. *Research in Microbiology*, 153(8):487–491, 2002.

D. L. Turcotte and G. Schubert. *Geodynamics: Applications of Continuum Physics to Geological Problems.* Wiley, New York, 1982.

J. S. Turner and ChenC. F. Layer generation in double-diffusive systems. *Bulletin of the American Physical Society*, 18(11):1467–1467, 1973.

G. Van der Kamp and J. E. Gale. Theory of Earth tide and barometric effects in porous formations with compressible grains. *Water Resources Research*, 19(2):538–544, 1983.

M. Van Kranendonk. Volcanic degassing, hydrothermal circulation and the flourishing of life on Earth: A review of the evidence from c. 3490-3240 Ma rocks of the Pilbara Supergroup, Pilbara Craton, Western Australia. *Earth Science Review*, 74:197–240, 2006.

S Vance, J Harnmeijer, J Kimura, H Hussmann, B deMartin, and J. M. Brown. Hydrothermal systems in small ocean planets. *Astrobiology*, in press, 2007.

Steve Vance and J.M. Brown. Layering and double-diffusion style convection in europa's ocean. *Icarus*, 177(2):506–514, 2005.

Gregory T. Ventura, Fabien Kenig, Christopher M. Reddy, Juergen Schieber, Glenn S. Frysinger, Robert K. Nelson, Etienne Dinel, Richard B. Gaines, and Philippe Schaeffer. Molecular evidence of late archean archaea and the presence of a subsurface hydrothermal biosphere. *Proceedings of the National Academy of Sciences*, 104 (14260-14265), 2007.

Philippe Vergne. New high-pressure viscosity measurements on di(2-ethylhexyl) sebecate and comparisons with previous data. *High Temperatures-High Pressures*, 22: 613–621, 1990.

W. Wagner and A. Pruss. The IAPWS formulation 1995 for the thermodynamic properties of ordinary water substance for general and scientific use. *Journal of Physical and Chemical Reference Data*, 31(2):387–535, 2002.

Kelin Wang and Earl E. Davis. Theory for the propagation of tidally induced pore pressure variations in layered subseafloor formations. *Journal of Geophysical Research*, 101 B5:11483–11495, 1996.

Kelin Wang, Garth van der Kamp, and Earl E. Davis. Limits of tidal energy disspation by fluid flow in subsea formations. *Geophysical Journal International*, 139:763–768, 1999.

W.W. Wegner and W.G. Ernst. Experimentally determined hydration and dehydration reaction rates in the system MgO-SiO_2-H_2O. *American Journal of Science*, 283-A:151–180, 1983.

B. P. Weiss and A. P. Ingersoll. Cold spots in the martian polar regions: Evidence of carbon dioxide depletion? *Icarus*, 144(2):432–435, 2000.

L. R. Wetzel and E. L. Shock. Distinguishing ultramafic- from basalt-hosted submarine hydrothermal systems by comparing calculated vent fluid compositions. *Journal of Geophysical Research-Solid Earth*, 105(B4):8319–8340, 2000.

William B. Whitman, David C. Coleman, and William J. Wiebe. Prokaryotes: The unseen majority. *Proceedings of the National Academy of Sciences*, 95:6578–6583, 1998.

W. D. Wilson. Speed of sound in distilled water as a function of temperature and pressure. *Journal Of The Acoustical Society Of America*, 31(8):1067–1072, 1959.

Surya Wiryana. *Physical Properties of Aqueous Solutions Under High Pressures and Temperatures*. PhD thesis, University of Washington, 1998.

R.A. Wogelius and J.V. Walther. Olivine dissolution kinetics at near-surface conditions. *Chemical Geology*, 97(1-2):101–112, 1992.

K. Zahnle, P. Schenk, H. Levison, and L. Dones. Cratering rates in the outer solar system. *Icarus*, 163(2):263–289, 2003.

C. Zimmer, K. K. Khurana, and M. G. Kivelson. Subsurface oceans on Europa and Callisto: Constraints from Galileo magnetometer observations. *Icarus*, 147(2):329–347, 2000.

R.W. Zimmerman, W.H. Somerton, and M.S. King. Compressibility of porous rocks. *Journal of Geophysical Research*, 91:12765–12777, 1986.

Appendix A

MEASUREMENT OF INDEPENDENT PARAMETERS

A.0.3 Assessing Precisions Needed for the ISS Experiment

In any measurement of state variables, independent thermodynamic variables need to be known to a precision better than that of the property being measured. For the present purpose, pressure, temperature and salinity are needed to better than the 0.1% error in velocity afforded by good ISS measurements.

The absolute error in a property X is related to the velocity (v) as $\Delta X = \Delta v(\delta X/\delta v)$. For pressure and temperature, the required precision is measured from the absolute error using the IAPWS95 equation of state for pure water. For all pressures and temperatures of interest, the error in velocity is less than the 0.7 MPa error for the Omega strain gauge or the 0.1 K error for the Omega thermocouple and reader (see Figures A.2 and A.1). The error in concentration equivalent to a 0.1 % error in velocity is estimated using solute properties from Marion et al. [2005].

A.0.4 Calibration of the Instruments

The Heise pressure gauge was found to lag the reading of the Omega transducer. A number of correlative measurements were made with the two gauges connected in parallel by a short (~10 cm) piece of high pressure tubing. The unit was returned to the factory, where a new Bourdon tube was fitted to the gauge calibrated against the factory dead-weight standard. This corrected the problem. Cross-calibration of the Bourdon tube gauge with the strain gauge insures accurate measurement of pressure to within 1.4 MPa. This is close to the 0.7 MPa equivalent to a 0.1 % error in velocity.

Figure A.3 shows the results of tests for hysteresis prior to replacement of the de-

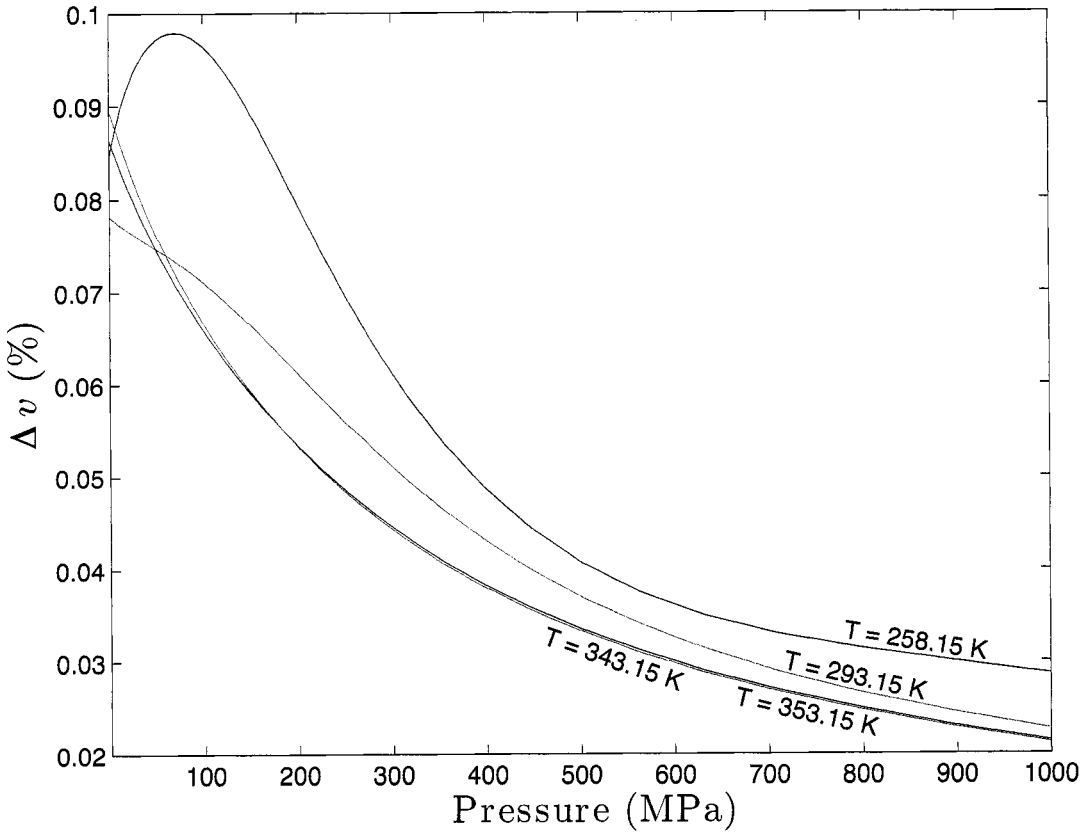

Figure A.1: Error in H_2O sound velocity equivalent to a 0.7 MPa error in pressure. Velocities are calculated from the IAPWS95 equation of state at the pressures and temperatures of interest for the present set of experiments ($P = 0.1 - 1000$ MPa; $T = 250 - 360$ K).

fective Bourdon tube. Similar tests after replacement showed no noticeable hysteresis within the 0.7 MPa error precision of the gauge.

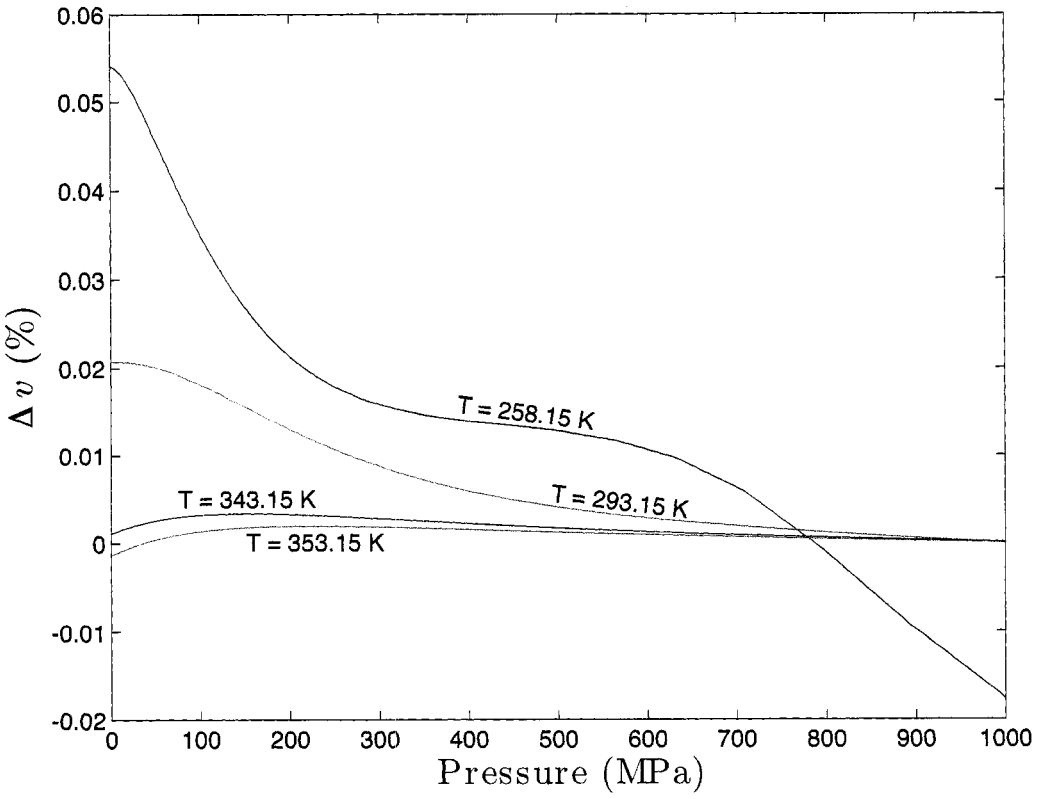

Figure A.2: Error in H_2O sound velocity equivalent to a 0.1 °C error in temperature. Velocities are calculated from the IAPWS95 equation of state at the pressures and temperatures of interest for the present set of experiments ($P = 0.1 - 700MPa; T = 250 - 360K$). We are interested in temperatures as low as 240 K, but the equation of state appears to become unstable below $T = 250$K.

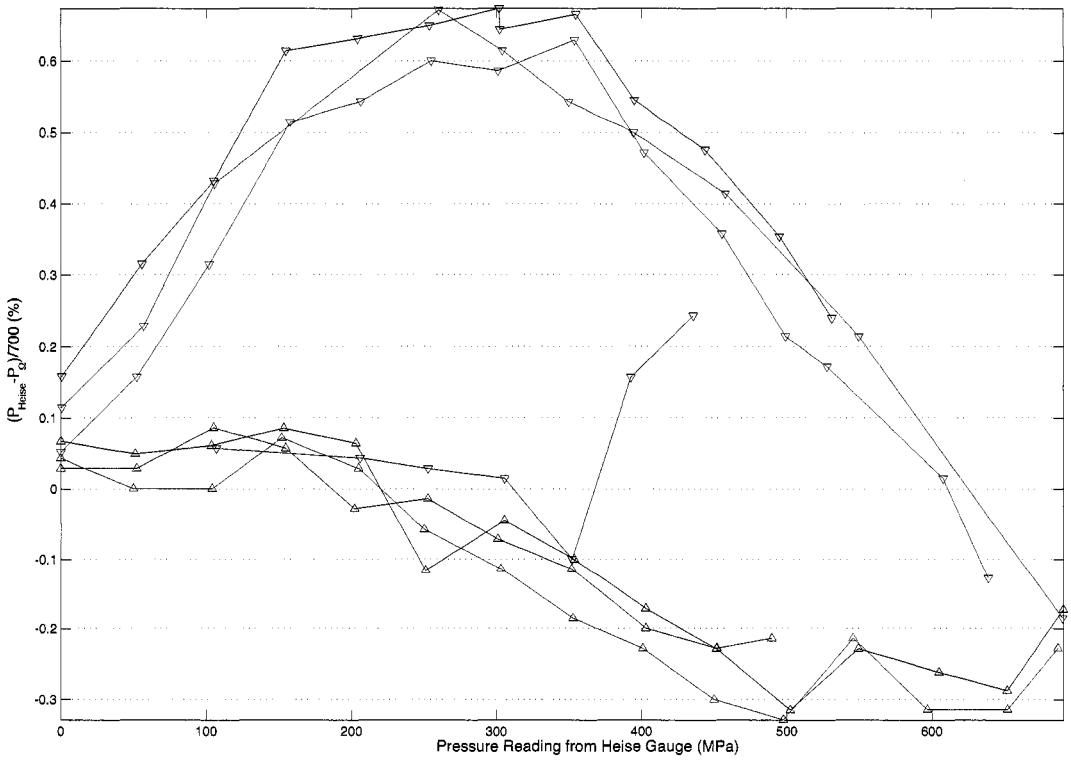

Figure A.3: Calibration of the Omega pressure transducer with the Heise CM model Bourdon tube gauge. Percent deviation is shown on the y-axis as a function of Heise gauge reading, in MPa. Repeated measurements show a clear hysteresis with maximum width much greater than the 0.1% ratings of the gauges.

Appendix B

ISS VELOCITY DATA

Water

P (MPa)	T (^{o}C)	f (GHz)	v ($\frac{km}{s}$)	ρ ($\frac{kg}{m^3}$)	file	date (ISO 8601)
T = -9.7 ^{o}C						
853	-9.7	0.3692	1.503	1040	214	20070916T225100
853	-9.7	0.3697	1.505	1040	215	20070916T225600
1219	-9.4	0.3861	1.572	1055	217	20070916T231000
1221	-9.6	0.3853	1.569	1055	216	20070916T230700
1477	-9.5	0.3980	1.620	1065	211	20070916T223700
1478	-9.3	0.3997	1.628	1065	209	20070916T223100
1478	-9.4	0.3995	1.627	1065	210	20070916T223400
1962	-9.4	0.4222	1.719	1082	25	20070807T221200
1978	-9.8	0.4249	1.730	1083	22	20070807T214000
2032	-9.4	0.4247	1.729	1085	219	20070916T232400
2033	-9.3	0.4251	1.731	1085	218	20070916T232100
2345	-10.1	0.4410	1.796	1095	233	20070917T003100
2401	-10.1	0.4410	1.796	1097	234	20070917T003700
3004	-9.5	0.4652	1.894	1115	222	20070916T234100
3006	-9.5	0.4655	1.895	1116	221	20070916T233700
3008	-9.5	0.4652	1.894	1116	220	20070916T233400
4071	-9.6	0.5051	2.057	1144	225	20070916T235400
4074	-9.5	0.5053	2.058	1144	224	20070916T235100
4081	-9.5	0.5051	2.057	1144	223	20070916T234800
4973	-9.8	0.5333	2.172	1165	229	20070917T001000
4975	-9.8	0.5329	2.170	1165	228	20070917T000500
4978	-9.8	0.5336	2.173	1165	227	20070917T000200

Continued on next page

Table B.1: Water

– continued from previous page

P (MPa)	T (^{o}C)	f (GHz)	v ($\frac{km}{s}$)	ρ ($\frac{kg}{m^3}$)	file	date (ISO 8601)
4986	-9.6	0.5342	2.175	1165	226	20070916T235900
5970	-9.9	0.5647	2.300	1186	232	20070917T002200
5973	-9.9	0.5647	2.299	1186	231	20070917T001900
5982	-9.8	0.5651	2.301	1186	230	20070917T001600
T = -9.3 to -0.3 ^{o}C						
1	0.4	0.3431	1.398	1000	96	20071001T212100
1	0.5	0.3429	1.398	1000	97	20071001T212300
1	0.8	0.3422	1.395	1000	99	20071001T212900
1	-1.1	0.3420	1.394	1000	100	20071001T213300
1470	-8.9	0.3988	1.624	1065	206	20070916T222200
1477	-9.0	0.3997	1.628	1065	207	20070916T222500
1478	-9.2	0.3998	1.628	1065	208	20070916T222800
1972	-8.7	0.4279	1.742	1083	23	20070807T214800
2016	-3.1	0.4324	1.761	1083	15	20070807T203800
2376	-7.8	0.4415	1.798	1096	200	20070916T220000
2381	-7.9	0.4418	1.799	1096	201	20070916T220300
2382	-8.1	0.4419	1.799	1096	202	20070916T220600
2382	-8.3	0.4420	1.800	1096	203	20070916T221000
2382	-8.4	0.4414	1.797	1096	204	20070916T221300
2382	-8.5	0.4412	1.797	1096	205	20070916T221500
4023	-5.5	0.5068	2.063	1142	191	20070916T212600
4024	-7.4	0.5058	2.060	1142	199	20070916T215100
4025	-7.2	0.5058	2.060	1142	198	20070916T214800
4026	-6.6	0.5059	2.060	1142	196	20070916T214300
4026	-6.9	0.5059	2.060	1142	197	20070916T214600
4027	-6.7	0.5059	2.060	1142	195	20070916T214000
4028	-5.9	0.5063	2.062	1142	192	20070916T212900
4028	-6.2	0.5065	2.062	1142	193	20070916T213400
4028	-6.4	0.5060	2.060	1142	194	20070916T213700

Continued on next page

Table B.1: Water

– continued from previous page

P (MPa)	T (^{o}C)	f (GHz)	v ($\frac{km}{s}$)	ρ ($\frac{kg}{m^3}$)	file	date (ISO 8601)
4741	-2.9	0.5308	2.161	1158	185	20070916T210700
4745	-4.9	0.5302	2.159	1158	190	20070916T212100
4746	-4.6	0.5302	2.159	1158	189	20070916T211800
4747	-3.2	0.5309	2.162	1158	186	20070916T211000
4747	-4.2	0.5306	2.161	1158	188	20070916T211500
4748	-3.7	0.5307	2.161	1158	187	20070916T211300
5989	-2.0	0.5693	2.318	1184	184	20070916T210200
5990	-1.5	0.5695	2.319	1184	183	20070916T210000
5992	-1.0	0.5697	2.320	1183	182	20070916T205700
5994	0.5	0.5700	2.321	1183	181	20070916T205400
$T = 0.2$ ^{o}C						
1	0.7	0.3461	1.411	1000	71	20071001T194800
1	0.6	0.3471	1.415	1000	72	20071001T195100
1	0.6	0.3469	1.414	1000	73	20071001T195300
1	0.6	0.3464	1.412	1000	74	20071001T195600
1	0.6	0.3467	1.413	1000	75	20071001T195900
1	0.5	0.3460	1.410	1000	76	20071001T200200
1	0.5	0.3467	1.413	1000	77	20071001T200400
1	0.4	0.3467	1.413	1000	78	20071001T200700
1	0.4	0.3465	1.412	1000	79	20071001T201000
1	0.3	0.3465	1.412	1000	80	20071001T201500
1	0.2	0.3466	1.413	1000	82	20071001T202100
1	0.2	0.3463	1.411	1000	83	20071001T202300
1	0.0	0.3448	1.405	1000	85	20071001T203100
1	0.1	0.3435	1.400	1000	86	20071001T203400
1	0.0	0.3471	1.415	1000	87	20071001T205600
1	0.0	0.3467	1.413	1000	90	20071001T210400
1	0.0	0.3430	1.398	1000	91	20071001T210700
1	0.0	0.3434	1.400	1000	92	20071001T211000

Continued on next page

Table B.1: Water

– continued from previous page

P (MPa)	T (^{o}C)	f (GHz)	v ($\frac{km}{s}$)	ρ ($\frac{kg}{m^3}$)	file	date (ISO 8601)
1	0.0	0.3478	1.418	1000	93	20071001T211200
1	0.2	0.3468	1.413	1000	94	20071001T211500
1	0.2	0.3465	1.412	1000	95	20071001T211800
400	0.0	0.3593	1.463	1019	160	20070916T191200
401	0.3	0.3606	1.468	1019	158	20070916T185500
401	0.1	0.3583	1.459	1019	159	20070916T190000
402	0.2	0.3585	1.460	1019	157	20070916T182800
403	0.0	0.3605	1.468	1019	156	20070916T182500
404	0.3	0.3588	1.461	1019	154	20070916T181900
404	0.0	0.3588	1.461	1019	155	20070916T182200
405	0.7	0.3617	1.473	1019	153	20070916T181600
945	0.4	0.3862	1.572	1043	40	20070805T164200
945	0.8	0.3867	1.573	1043	53	20070805T163500
946	0.1	0.3865	1.573	1043	41	20070805T164500
1026	0.1	0.3887	1.583	1046	163	20070916T193000
1026	0.0	0.3880	1.580	1046	164	20070916T193300
1029	0.1	0.3869	1.575	1046	162	20070916T192200
1035	0.1	0.3881	1.580	1046	161	20070916T191900
2026	0.1	0.4334	1.764	1083	42	20070805T165100
2027	0.2	0.4357	1.773	1083	43	20070805T165400
2028	0.8	0.4358	1.773	1083	44	20070805T165800
2036	0.1	0.4325	1.761	1083	14	20070807T202800
2080	0.0	0.4347	1.770	1085	167	20070916T194500
2084	0.0	0.4352	1.772	1085	166	20070916T194200
2094	0.0	0.4355	1.773	1085	165	20070916T193900
3012	0.2	0.4716	1.920	1113	170	20070916T195700
3013	0.1	0.4719	1.922	1113	169	20070916T195400
3020	0.8	0.4760	1.937	1113	48	20070805T172200
3020	0.0	0.4721	1.922	1113	168	20070916T195200

Continued on next page

Table B.1: Water

– continued from previous page

P (MPa)	T (^{o}C)	f (GHz)	v ($\frac{km}{s}$)	ρ ($\frac{kg}{m^3}$)	file	date (ISO 8601)
3021	0.8	0.4754	1.934	1113	47	20070805T171800
3969	0.8	0.5058	2.058	1138	50	20070805T174000
4012	0.0	0.5079	2.068	1139	174	20070916T201400
4013	0.0	0.5076	2.067	1139	173	20070916T201000
4015	0.0	0.5078	2.068	1140	172	20070916T200700
4019	0.1	0.5086	2.071	1140	171	20070916T200400
5009	0.0	0.5400	2.199	1163	177	20070916T202500
5011	0.0	0.5401	2.199	1163	176	20070916T202300
5016	0.1	0.5404	2.200	1163	175	20070916T202000
5998	0.0	0.5701	2.322	1183	180	20070916T204000
5999	0.0	0.5700	2.321	1183	179	20070916T203700
6002	0.0	0.5701	2.321	1183	178	20070916T203500
$T = 0.8$ to 9.4 ^{o}C						
1	3.6	0.3489	1.422	1000	48	20071001T183900
1	3.5	0.3488	1.422	1000	49	20071001T184200
1	3.4	0.3489	1.422	1000	50	20071001T183600
1	3.6	0.3487	1.421	1000	51	20071001T185000
1	3.6	0.3487	1.421	1000	52	20071001T185300
1	3.4	0.3486	1.421	1000	53	20071001T185600
1	3.3	0.3484	1.420	1000	54	20071001T185800
1	3.1	0.3484	1.420	1000	55	20071001T190100
1	2.9	0.3483	1.420	1000	56	20071001T190400
1	2.7	0.3482	1.419	1000	57	20071001T190800
1	2.6	0.3481	1.419	1000	58	20071001T191100
1	2.6	0.3480	1.418	1000	59	20071001T191400
1	2.4	0.3479	1.418	1000	60	20071001T191700
1	2.2	0.3477	1.417	1000	61	20071001T191900
1	2.1	0.3476	1.417	1000	62	20071001T192200
1	2.1	0.3475	1.416	1000	63	20071001T192500

Continued on next page

Table B.1: Water

– continued from previous page

P (MPa)	T (^{o}C)	f (GHz)	v ($\frac{km}{s}$)	ρ ($\frac{kg}{m^3}$)	file	date (ISO 8601)
1	1.8	0.3474	1.416	1000	64	20071001T192800
1	1.5	0.3472	1.415	1000	65	20071001T193000
1	1.4	0.3471	1.415	1000	66	20071001T193300
1	1.3	0.3462	1.411	1000	67	20071001T193600
1	1.1	0.3469	1.414	1000	68	20071001T193900
1	1.0	0.3468	1.414	1000	69	20071001T194100
1	0.9	0.3463	1.411	1000	70	20071001T194400
405	1.4	0.3622	1.475	1019	151	20070916T181100
405	1.0	0.3618	1.473	1019	152	20070916T181400
406	1.6	0.3622	1.475	1019	150	20070916T180800
407	2.3	0.3636	1.480	1019	148	20070916T180200
407	1.9	0.3633	1.479	1019	149	20070916T180500
408	2.7	0.3635	1.480	1019	147	20070916T175900
409	3.5	0.3656	1.489	1019	145	20070916T175300
409	3.1	0.3656	1.489	1019	146	20070916T175600
410	4.5	0.3659	1.490	1019	143	20070916T174800
410	4.0	0.3652	1.487	1019	144	20070916T175100
411	4.8	0.3667	1.493	1019	142	20070916T174500
412	5.1	0.3671	1.495	1019	141	20070916T174200
413	5.4	0.3660	1.490	1019	140	20070916T174000
414	6.0	0.3683	1.499	1019	139	20070916T173600
415	6.5	0.3684	1.500	1019	138	20070916T173200
416	7.2	0.3694	1.504	1019	137	20070916T172900
417	7.8	0.3701	1.507	1019	136	20070916T172600
3998	3.8	0.5114	2.082	1138	117	20070916T152800
$T = 9.9$ ^{o}C						
1	9.5	0.3543	1.441	1000	9	20070930T170100
1	9.5	0.3543	1.441	1000	10	20070930T170400
1	9.5	0.3543	1.441	1000	11	20070930T170700

Continued on next page

Table B.1: Water

– continued from previous page

P (MPa)	T (°C)	f (GHz)	v ($\frac{km}{s}$)	ρ ($\frac{kg}{m^3}$)	file	date (ISO 8601)
1	9.7	0.3543	1.441	1000	12	20070930T171700
1	9.7	0.3544	1.441	1000	13	20070930T171900
1	9.8	0.3545	1.441	1000	14	20070930T172200
1	9.9	0.3544	1.441	1000	15	20070930T172500
1	9.9	0.3544	1.441	1000	16	20070930T172700
1	10.0	0.3545	1.442	1000	17	20070930T173100
1	9.9	0.3546	1.442	1000	18	20070930T173400
422	10.1	0.3720	1.515	1019	134	20070916T170100
422	10.0	0.3723	1.516	1019	135	20070916T170700
423	10.1	0.3723	1.516	1019	133	20070916T165900
992	10.1	0.3978	1.618	1043	34	20070805T150900
992	10.1	0.3976	1.617	1043	35	20070805T151500
992	10.0	0.3975	1.616	1043	36	20070805T151900
995	10.0	0.4011	1.631	1043	37	20070805T155800
1060	10.0	0.4003	1.630	1045	129	20070916T163500
1069	10.0	0.3995	1.627	1046	130	20070916T163800
1071	10.0	0.3995	1.627	1046	131	20070916T164100
1072	10.0	0.4000	1.629	1046	132	20070916T164400
1971	9.5	0.4392	1.788	1078	109	20070916T130800
1972	9.6	0.4397	1.790	1078	107	20070916T125500
1972	9.6	0.4380	1.784	1078	108	20070916T125800
1972	9.4	0.4386	1.786	1078	110	20070916T131200
1973	10.5	0.4391	1.788	1078	105	20070916T124200
1973	10.3	0.4385	1.785	1078	106	20070916T124400
2096	10.0	0.4449	1.811	1082	13	20070807T200300
3004	10.2	0.4788	1.949	1109	112	20070916T132300
3006	10.1	0.4783	1.948	1109	111	20070916T132000
3998	10.0	0.5113	2.082	1135	118	20070916T153100
3999	9.9	0.5113	2.082	1135	119	20070916T153500

Continued on next page

Table B.1: Water

– continued from previous page

P (MPa)	T (^{o}C)	f (GHz)	v ($\frac{km}{s}$)	ρ ($\frac{kg}{m^3}$)	file	date (ISO 8601)
4002	10.3	0.5152	2.098	1135	114	20070916T135200
4003	10.4	0.5176	2.108	1135	113	20070916T134900
5016	10.1	0.5450	2.219	1159	122	20070916T155200
5019	10.0	0.5449	2.219	1159	121	20070916T154900
5025	10.0	0.5451	2.219	1159	120	20070916T154700
6034	10.1	0.5737	2.336	1180	125	20070916T160600
6036	10.1	0.5740	2.337	1180	124	20070916T160300
6043	10.1	0.5743	2.339	1180	123	20070916T155900
6948	10.0	0.5978	2.434	1197	128	20070916T162000
6952	10.1	0.5976	2.433	1197	127	20070916T161700
6963	9.9	0.5979	2.434	1197	126	20070916T161400
T = 10.5 to 21.4 ^{o}C						
482	19.0	0.3843	1.563	1020	27	20070805T124600
482	19.1	0.3844	1.563	1020	28	20070805T124900
486	19.2	0.3845	1.564	1020	46	20070805T131900
500	20.1	0.3838	1.563	1020	8	20070807T150800
512	20.7	0.3843	1.565	1021	7	20070807T150100
513	19.4	0.3871	1.567	1021	3	20070715T145900
514	19.5	0.3875	1.562	1021	2	20070706T151700
514	19.4	0.3858	1.562	1021	4	20070715T150800
516	19.5	0.3865	1.558	1021	3	20070706T155000
520	20.7	0.3874	1.578	1021	6	20070807T145900
522	19.5	0.3891	1.575	1021	2	20070703T192000
524	19.5	0.3879	1.570	1021	3	20070703T203200
524	19.5	0.3861	1.563	1021	4	20070703T205800
524	19.5	0.3838	1.553	1021	5	20070703T213800
531	19.5	0.3884	1.568	1022	10	20070704T010400
531	19.5	0.3890	1.570	1022	11	20070704T012300
626	21.2	0.3919	1.595	1025	2	20070807T105600

Continued on next page

Table B.1: Water

– continued from previous page

P (MPa)	T (°C)	f (GHz)	v ($\frac{km}{s}$)	ρ ($\frac{kg}{m^3}$)	file	date (ISO 8601)
754	19.2	0.3958	1.606	1031	17	20070706T223900
1084	19.7	0.4112	1.657	1043	5	20070706T163000
1085	19.7	0.4114	1.658	1044	4	20070706T162100
1150	19.5	0.4149	1.675	1046	12	20070704T014100
1221	19.1	0.4163	1.689	1049	15	20070706T220600
1222	19.1	0.4156	1.686	1049	16	20070706T222000
1567	19.6	0.4289	1.740	1061	8	20070706T202600
1568	19.4	0.4300	1.744	1061	9	20070706T203800
1743	19.4	0.4379	1.776	1067	14	20070706T215100
1744	19.2	0.4373	1.774	1067	13	20070706T214200
1974	11.3	0.4392	1.788	1077	103	20070916T123500
1974	11.0	0.4401	1.792	1078	104	20070916T123800
1975	11.7	0.4403	1.793	1077	102	20070916T123100
1976	12.0	0.4409	1.795	1077	101	20070916T122800
1977	12.7	0.4419	1.799	1077	99	20070916T122200
1977	12.5	0.4407	1.795	1077	100	20070916T122500
1978	13.6	0.4420	1.800	1077	97	20070916T121700
1978	13.0	0.4414	1.797	1077	98	20070916T122000
1980	14.2	0.4425	1.802	1077	96	20070916T121400
1982	14.9	0.4438	1.807	1076	95	20070916T121100
1984	15.7	0.4439	1.807	1076	94	20070916T120900
1985	16.7	0.4447	1.811	1076	93	20070916T120600
1988	18.0	0.4457	1.815	1075	92	20070916T120300
1991	19.2	0.4466	1.818	1075	91	20070916T120000
1994	20.1	0.4473	1.821	1075	90	20070916T115700
2002	20.9	0.4480	1.824	1075	89	20070916T115400
2098	19.1	0.4503	1.826	1079	10	20070706T205400
2099	19.4	0.4514	1.831	1078	11	20070706T210200
$T = 21.9$ °C						

Continued on next page

Table B.1: Water

– continued from previous page

P (MPa)	T (^{o}C)	f (GHz)	v ($\frac{km}{s}$)	ρ ($\frac{kg}{m^3}$)	file	date (ISO 8601)
449	22.0	0.3806	1.549	1018	27	20070915T153100
449	22.1	0.3803	1.548	1018	28	20070915T153400
722	21.6	0.3945	1.604	1029	268	20070917T222000
723	21.6	0.3939	1.602	1029	269	20070917T222300
1058	22.0	0.4079	1.660	1042	25	20070915T150800
1060	22.2	0.4081	1.661	1042	26	20070915T151100
2047	22.0	0.4488	1.826	1076	23	20070915T145800
2054	22.1	0.4489	1.827	1076	24	20070915T150100
2481	21.6	0.4629	1.882	1089	242	20070917T172700
2481	21.6	0.4633	1.884	1089	243	20070917T173000
2856	21.7	0.4775	1.942	1100	266	20070917T215400
2856	21.6	0.4773	1.941	1100	267	20070917T215800
2971	22.1	0.4835	1.969	1103	6	20070915T115400
3004	21.5	0.4819	1.959	1104	245	20070917T190000
3009	22.1	0.4841	1.970	1104	21	20070915T144800
3010	21.4	0.4819	1.960	1104	244	20070917T185600
3017	22.1	0.4848	1.973	1104	22	20070915T145100
4013	22.3	0.5192	2.114	1130	8	20070915T121900
4016	21.6	0.5164	2.100	1130	246	20070917T192300
4016	21.5	0.5162	2.099	1130	247	20070917T192600
4025	21.7	0.5174	2.104	1130	263	20070917T212700
4026	21.6	0.5185	2.108	1130	264	20070917T213100
4027	22.0	0.5198	2.117	1130	7	20070915T121100
4027	21.5	0.5179	2.106	1131	265	20070917T213500
4985	21.5	0.5474	2.226	1153	249	20070917T194200
4986	21.4	0.5481	2.229	1153	248	20070917T193800
5000	22.2	0.5494	2.237	1153	10	20070915T123200
5002	21.6	0.5453	2.217	1153	259	20070917T210500
5005	21.7	0.5470	2.224	1153	260	20070917T210800

Continued on next page

Table B.1: Water

– continued from previous page

P (MPa)	T (^{o}C)	f (GHz)	v ($\frac{km}{s}$)	ρ ($\frac{kg}{m^3}$)	file	date (ISO 8601)
5006	21.5	0.5464	2.222	1153	261	20070917T211200
5006	21.6	0.5470	2.224	1153	262	20070917T211600
5007	22.1	0.5499	2.239	1153	9	20070915T122900
5880	21.5	0.5724	2.327	1171	257	20070917T205500
5887	21.7	0.5730	2.330	1171	258	20070917T205800
6012	22.3	0.5794	2.359	1174	11	20070915T124200
6014	21.6	0.5767	2.345	1174	251	20070917T195200
6020	21.7	0.5765	2.344	1174	250	20070917T194900
6884	21.8	0.6046	2.459	1191	270	20070917T223700
6932	21.5	0.5999	2.439	1192	256	20070917T204900
6933	21.5	0.6026	2.450	1192	255	20070917T204600
6934	21.6	0.6004	2.441	1192	254	20070917T204300
6952	22.1	0.6019	2.449	1192	20	20070915T143700
6961	21.6	0.6005	2.442	1192	253	20070917T200600
6968	21.6	0.6009	2.444	1192	252	20070917T200300
6975	22.0	0.6025	2.452	1192	19	20070915T143000
T = 22.3 to 49.8 ^{o}C						
1	49.4	0.3784	1.538	988	25	20070930T212500
6004	22.4	0.5785	2.356	1173	12	20070915T124400
T = 50.1 ^{o}C						
1	50.0	0.3780	1.537	988	27	20070930T223500
1	50.0	0.3781	1.537	988	28	20070930T223800
1	50.0	0.3781	1.537	988	29	20070930T224000
481	50.0	0.4011	1.632	1008	30	20070915T162400
483	50.3	0.4016	1.634	1008	29	20070915T162100
998	50.3	0.4249	1.729	1027	32	20070915T163700
1000	50.4	0.4251	1.730	1027	31	20070915T163400
1985	50.2	0.4624	1.882	1060	34	20070915T164600
1996	50.3	0.4630	1.884	1061	33	20070915T164200

Continued on next page

Table B.1: Water

– continued from previous page

P (MPa)	T (^{o}C)	f (GHz)	v ($\frac{km}{s}$)	ρ ($\frac{kg}{m^3}$)	file	date (ISO 8601)
3005	50.2	0.4951	2.014	1090	45	20070915T182000
3005	50.2	0.4951	2.014	1090	46	20070915T182200
3006	50.3	0.4952	2.014	1090	44	20070915T181600
4037	50.0	0.5271	2.144	1116	48	20070915T184000
4039	50.0	0.5271	2.144	1116	47	20070915T183700
5044	50.1	0.5580	2.269	1139	53	20070915T192400
5045	49.8	0.5586	2.272	1139	52	20070915T191600
5047	49.9	0.5575	2.267	1139	51	20070915T191000
5050	49.9	0.5549	2.257	1139	50	20070915T185800
5996	50.3	0.5846	2.378	1159	56	20070915T195000
5999	50.2	0.5846	2.378	1159	55	20070915T194400
6002	50.1	0.5830	2.371	1159	54	20070915T193800
7000	50.1	0.6054	2.462	1179	59	20070915T201000
7003	50.1	0.6046	2.459	1179	58	20070915T200600
7008	50.1	0.6052	2.461	1179	57	20070915T200200
T = 50.4 to 97.6 ^{o}C						
1	97.4	0.3801	1.545	960	33	20070930T232400
1	97.4	0.3802	1.546	960	34	20070930T232700
T = 98.2 ^{o}C						
1	98.4	0.3803	1.546	959	30	20070930T231600
1	98.6	0.3801	1.545	959	31	20070930T231900
1	97.8	0.3801	1.545	960	32	20070930T232200
1	97.7	0.3801	1.545	960	35	20070930T233000
1	98.0	0.3801	1.545	960	36	20070930T233300
1	98.3	0.3801	1.545	960	37	20070930T233500
1	98.4	0.3801	1.545	959	38	20070930T233800
430	98.4	0.4016	1.633	979	81	20070915T232800
436	98.5	0.4015	1.633	979	82	20070915T233100
1058	98.3	0.4283	1.742	1003	84	20070915T234000

Continued on next page

Table B.1: Water

– continued from previous page

P (MPa)	T (^{o}C)	f (GHz)	v ($\frac{km}{s}$)	ρ ($\frac{kg}{m^3}$)	file	date (ISO 8601)
1062	98.4	0.4285	1.743	1003	83	20070915T233800
2001	98.7	0.4667	1.898	1035	79	20070915T231800
2002	98.7	0.4665	1.897	1035	80	20070915T232100
2942	98.5	0.4984	2.027	1062	77	20070915T230500
2949	98.5	0.4982	2.026	1062	78	20070915T230800
3937	98.4	0.5284	2.149	1087	75	20070915T225500
3944	98.4	0.5284	2.149	1087	76	20070915T225800
4963	98.2	0.5573	2.266	1111	73	20070915T224700
4964	98.3	0.5566	2.263	1111	74	20070915T224900
6008	97.7	0.5829	2.370	1133	67	20070915T220700
6009	97.9	0.5853	2.380	1133	68	20070915T221300
6009	98.7	0.5856	2.381	1132	69	20070915T222400
6009	98.6	0.5855	2.381	1132	70	20070915T222700
6009	98.4	0.5868	2.386	1132	71	20070915T223100
6009	98.5	0.5879	2.391	1132	72	20070915T223500
6884	98.0	0.6056	2.463	1150	66	20070915T215100
6885	98.0	0.6051	2.461	1150	65	20070915T214600
6886	97.9	0.6055	2.462	1150	63	20070915T213700
6886	98.0	0.6056	2.463	1150	64	20070915T214000

$MgSO_4$ (aq) 0.0800 ± 0.001 m

P (MPa)	T (^{o}C)	f (GHz)	v ($\frac{km}{s}$)	ρ ($\frac{kg}{m^3}$)	V^o ($\frac{mL}{mol}$)	V^{ex} (mL)	file	date (ISO 8601)
T = -8.3 ^{o}C								
1061	-8.8	0.3826	1.561	1058	-6.1	0.6	99	20071007T010800
1468	-8.1	0.4020	1.641	1074	-1.8	0.6	101	20071007T012300

Continued on next page

Table B.2: $MgSO_4$ (aq) 0.0800 ± 0.001 m
– continued from previous page

P (MPa)	T (^{o}C)	f (GHz)	v ($\frac{km}{s}$)	ρ ($\frac{kg}{m^3}$)	V^o ($\frac{mL}{mol}$)	V^{ex} (mL)	file	date (ISO 8601)
1468	-8.1	0.4028	1.644	1074	-1.8	0.6	102	20071007T012600
2019	-7.7	0.4291	1.751	1094	3.8	0.6	84	20071006T231800
2019	-7.8	0.4283	1.748	1094	3.8	0.6	85	20071006T232100
2170	-8.9	0.4341	1.772	1099	5.1	0.6	96	20071007T004000
2173	-8.9	0.4340	1.771	1099	5.1	0.6	97	20071007T004300
3015	-8.4	0.4669	1.905	1125	13.7	0.6	88	20071006T235300
3020	-8.4	0.4670	1.906	1125	13.7	0.6	87	20071006T234800
3023	-8.4	0.4690	1.914	1125	13.7	0.6	86	20071006T234500
3535	-8.8	0.4881	1.992	1139	18.9	0.6	95	20071007T003200
3540	-8.8	0.4883	1.993	1139	18.9	0.6	94	20071007T002900
3545	-8.8	0.4869	1.987	1140	18.0	0.6	93	20071007T002500
4647	-8.7	0.5257	2.145	1167	30.1	0.6	92	20071007T001400
4694	-8.6	0.5268	2.150	1168	30.5	0.6	91	20071007T001100
4745	-8.6	0.5290	2.159	1169	31.1	0.6	90	20071007T000800
4843	-8.7	0.5309	2.167	1171	32.0	0.6	89	20071007T000500
T = -7.7 to -0.3 ^{o}C								
2027	-5.2	0.4313	1.760	1093	4.4	0.6	83	20071006T223800
2032	-3.5	0.4323	1.764	1093	4.8	0.5	82	20071006T222300
2034	-3.1	0.4327	1.766	1093	4.9	0.5	81	20071006T222000
T = 0.0 ^{o}C								
162	0.0	0.3504	1.430	1018	-11.6	0.6	73	20071006T212700
167	0.1	0.3507	1.431	1018	-11.6	0.6	76	20071006T213700
168	0.0	0.3508	1.432	1018	-11.6	0.6	74	20071006T213000
168	0.1	0.3513	1.434	1018	-11.5	0.6	75	20071006T213300
968	0.1	0.3882	1.584	1054	-4.2	0.5	78	20071006T214900
974	0.1	0.3890	1.588	1054	-4.2	0.5	77	20071006T214600
1042	0.2	0.3911	1.596	1056	-3.5	0.5	60	20071006T200800
1048	0.3	0.3915	1.598	1057	-3.5	0.5	59	20071006T200500
1993	0.2	0.4318	1.762	1091	5.1	0.5	56	20071006T194500

Continued on next page

Table B.2: $MgSO_4$ (aq) 0.0800 ± 0.001 m
– continued from previous page

P (MPa)	T (°C)	f (GHz)	v ($\frac{km}{s}$)	ρ ($\frac{kg}{m^3}$)	V^o ($\frac{mL}{mol}$)	V^{ex} (mL)	file	date (ISO 8601)
1994	0.4	0.4326	1.766	1091	5.2	0.5	55	20071006T194100
2044	0.3	0.4356	1.778	1093	5.5	0.5	80	20071006T220000
2051	0.0	0.4364	1.781	1093	5.6	0.5	79	20071006T215600
3026	0.2	0.4736	1.933	1123	14.5	0.5	62	20071006T201700
3042	0.0	0.4737	1.933	1123	14.7	0.5	61	20071006T201400
4292	0.1	0.5180	2.114	1155	26.1	0.5	69	20071006T205700
4292	0.0	0.5176	2.113	1155	26.1	0.5	70	20071006T210000
5000	0.3	0.5393	2.201	1171	32.6	0.5	64	20071006T202900
5005	0.3	0.5389	2.200	1172	32.7	0.5	63	20071006T202600
6011	0.0	0.5696	2.325	1192	41.8	0.6	72	20071006T211100
6015	0.1	0.5699	2.326	1192	41.9	0.6	71	20071006T210800
6862	0.2	0.5926	2.419	1208	49.7	0.6	66	20071006T204200
6872	0.2	0.5933	2.422	1208	49.8	0.6	65	20071006T203900
T = 0.4 to 9.9 °C								
1995	0.8	0.4331	1.768	1091	5.2	0.5	54	20071006T193800
1997	1.8	0.4336	1.770	1091	5.4	0.5	53	20071006T192800
1998	2.4	0.4352	1.776	1090	5.5	0.5	52	20071006T192500
1999	2.9	0.4352	1.776	1090	5.6	0.5	51	20071006T192100
2002	4.0	0.4361	1.780	1090	5.8	0.5	49	20071006T191400
2002	3.6	0.4358	1.779	1090	5.7	0.5	50	20071006T191700
2004	4.8	0.4370	1.783	1090	5.9	0.5	48	20071006T191000
2005	5.2	0.4370	1.784	1090	6.0	0.5	47	20071006T190700
2007	6.2	0.4381	1.788	1090	6.2	0.5	46	20071006T190500
2009	7.1	0.4382	1.789	1089	6.3	0.5	45	20071006T190200
T = 10.3 °C								
268	10.1	0.3699	1.510	1022	-7.7	0.5	24	20071006T170400
270	10.2	0.3695	1.508	1022	-7.7	0.5	25	20071006T170700
270	10.1	0.3683	1.503	1022	-7.7	0.5	26	20071006T170900
1001	10.0	0.3997	1.631	1053	-1.7	0.5	28	20071006T171900

Continued on next page

Table B.2: $MgSO_4$ (aq) 0.0800 ± 0.001 m
– continued from previous page

P (MPa)	T (^{o}C)	f (GHz)	v ($\frac{km}{s}$)	ρ ($\frac{kg}{m^3}$)	V^o ($\frac{mL}{mol}$)	V^{ex} (mL)	file	date (ISO 8601)
1010	10.1	0.3991	1.629	1053	-1.6	0.5	27	20071006T171600
2012	10.1	0.4399	1.795	1088	6.7	0.5	42	20071006T184000
2014	10.2	0.4402	1.797	1088	6.7	0.5	43	20071006T184200
3007	10.1	0.4794	1.957	1118	14.9	0.5	30	20071006T172800
3022	10.1	0.4796	1.957	1119	15.0	0.5	29	20071006T172500
3993	10.1	0.5141	2.098	1144	23.1	0.5	21	20071006T164500
3998	10.2	0.5126	2.092	1144	23.1	0.5	22	20071006T164700
3999	10.3	0.5139	2.098	1144	23.1	0.5	23	20071006T165200
4990	10.0	0.5436	2.219	1167	31.3	0.5	41	20071006T182900
4991	10.0	0.5437	2.219	1167	31.4	0.5	40	20071006T182600
4997	10.0	0.5449	2.224	1167	31.4	0.5	32	20071006T174000
5005	10.1	0.5453	2.225	1167	31.5	0.5	31	20071006T173700
5995	10.0	0.5731	2.339	1188	39.7	0.5	34	20071006T175100
6029	10.0	0.5737	2.342	1188	39.9	0.5	33	20071006T174800
6545	9.9	0.5859	2.391	1198	44.2	0.5	37	20071006T180700
6652	9.9	0.5902	2.409	1200	45.1	0.5	36	20071006T180300
6760	10.0	0.5931	2.421	1202	45.0	0.5	35	20071006T180000
6846	10.4	0.5953	2.429	1203	46.6	0.5	20	20071006T163600
6850	10.7	0.5962	2.433	1203	46.6	0.5	19	20071006T163300
T = 10.7 to 20.9 ^{o}C								
995	20.6	0.4056	1.650	1049	0.3	0.5	19	20071005T113700
1002	20.7	0.4052	1.648	1049	0.2	0.5	18	20071005T113400
2549	20.7	0.4670	1.899	1101	11.6	0.4	12	20071005T103200
2549	20.6	0.4678	1.903	1101	11.6	0.4	13	20071005T103600
2976	20.8	0.4841	1.969	1113	14.8	0.4	25	20071005T143600
3021	20.8	0.4852	1.974	1114	15.2	0.4	24	20071005T123700
3025	20.7	0.4852	1.974	1114	15.2	0.4	23	20071005T123400
6875	12.6	0.5993	2.446	1203	46.3	0.5	18	20071006T161500
6880	13.5	0.5996	2.447	1203	46.1	0.5	17	20071006T161200

Continued on next page

Table B.2: $MgSO_4$ (aq) 0.0800 ± 0.001 m
– continued from previous page

P (MPa)	T (^{o}C)	f (GHz)	v ($\frac{km}{s}$)	ρ ($\frac{kg}{m^3}$)	V^o ($\frac{mL}{mol}$)	V^{ex} (mL)	file	date (ISO 8601)
6891	14.4	0.6010	2.453	1203	45.0	0.5	16	20071006T160800
6899	15.5	0.6014	2.455	1202	45.8	0.5	15	20071006T160600
6906	16.9	0.6022	2.458	1202	45.5	0.5	14	20071006T160300
T = 21.3 ^{o}C								
148	20.9	0.3741	1.519	1014	-6.7	0.5	4	20071004T111200
150	21.0	0.3740	1.518	1014	-6.6	0.5	5	20071004T111500
150	20.9	0.3718	1.512	1014	-6.6	0.5	17	20071005T112500
152	20.9	0.3715	1.511	1014	-6.6	0.5	16	20071005T112200
177	20.9	0.3749	1.525	1015	-6.4	0.5	38	20071005T154800
186	20.9	0.3748	1.524	1016	-6.4	0.5	39	20071005T155100
991	20.9	0.4077	1.658	1049	0.3	0.5	36	20071005T154000
995	20.9	0.4087	1.662	1049	0.2	0.5	37	20071005T154200
1168	21.0	0.4136	1.682	1055	1.1	0.5	14	20071005T110600
1168	21.0	0.4136	1.682	1055	1.1	0.5	15	20071005T110900
1353	21.0	0.4240	1.721	1062	2.5	0.5	2	20071004T110200
1353	21.0	0.4239	1.721	1062	2.5	0.5	3	20071004T110500
1990	21.0	0.4493	1.824	1083	7.3	0.4	7	20071004T112800
1994	21.0	0.4494	1.825	1084	7.4	0.4	6	20071004T112600
2002	21.7	0.4490	1.832	1083	7.4	0.4	5	20071006T145600
2029	21.6	0.4472	1.819	1084	7.6	0.4	21	20071005T115400
2030	21.6	0.4475	1.820	1084	7.7	0.4	20	20071005T114800
2993	20.9	0.4846	1.971	1113	14.9	0.4	34	20071005T152800
2998	21.0	0.4846	1.971	1113	14.0	0.4	35	20071005T153100
3035	21.0	0.4854	1.971	1114	15.3	0.4	9	20071004T113800
3053	21.0	0.4861	1.974	1115	15.4	0.4	8	20071004T113500
3978	21.2	0.5171	2.104	1138	22.4	0.4	27	20071005T144500
3986	21.0	0.5170	2.103	1139	22.5	0.4	26	20071005T144200
3988	21.4	0.5183	2.116	1138	22.5	0.4	9	20071006T151800
3994	21.5	0.5145	2.100	1139	22.5	0.4	8	20071006T151100

Continued on next page

Table B.2: $MgSO_4$ (aq) 0.0800 ± 0.001 m
– continued from previous page

P (MPa)	T (°C)	f (GHz)	v ($\frac{km}{s}$)	ρ ($\frac{kg}{m^3}$)	V^o ($\frac{mL}{mol}$)	V^{ex} (mL)	file	date (ISO 8601)
3999	21.5	0.5191	2.119	1139	22.5	0.4	7	20071006T150700
4010	21.4	0.5190	2.121	1139	22.6	0.4	46	20071005T175700
4012	21.2	0.5185	2.119	1139	22.7	0.4	45	20071005T175400
5006	21.0	0.5505	2.239	1162	30.2	0.4	29	20071005T145700
5012	20.9	0.5498	2.236	1162	30.3	0.4	28	20071005T145400
5310	21.5	0.5567	2.272	1168	32.5	0.4	11	20071006T152900
5316	21.5	0.5576	2.276	1169	32.5	0.4	10	20071006T152600
5981	21.2	0.5728	2.341	1182	37.6	0.4	48	20071005T180900
5985	21.2	0.5726	2.340	1182	37.6	0.4	47	20071005T180600
5993	21.1	0.5763	2.344	1183	37.7	0.4	31	20071005T150900
6002	21.1	0.5768	2.346	1183	37.8	0.4	30	20071005T150500
6888	21.0	0.6015	2.447	1200	44.5	0.4	33	20071005T151900
6909	21.0	0.6018	2.448	1200	44.7	0.4	32	20071005T151600
6953	21.3	0.6033	2.462	1201	44.9	0.4	13	20071006T154500
6965	21.4	0.6024	2.459	1201	44.0	0.4	12	20071006T154200
T = 21.7 to 49.8 °C								
2002	21.8	0.4486	1.831	1083	7.4	0.4	4	20071006T145200
2027	22.0	0.4477	1.821	1084	7.6	0.4	22	20071005T122100
6904	49.7	0.5992	2.449	1186	40.4	0.3	52	20071005T190700
T = 50.0 °C								
108	50.1	0.3830	1.565	1002	-7.4	0.5	75	20071005T211200
110	50.0	0.3829	1.565	1002	-7.4	0.5	76	20071005T211500
185	50.1	0.3866	1.580	1005	-6.9	0.5	59	20071005T194600
192	50.0	0.3869	1.581	1006	-6.8	0.5	60	20071005T194900
1002	50.0	0.4207	1.719	1037	-1.1	0.4	73	20071005T210200
1002	50.0	0.4205	1.718	1037	-1.1	0.4	74	20071005T210500
1041	50.0	0.4221	1.725	1039	0.8	0.4	62	20071005T195700
1052	50.0	0.4219	1.724	1039	0.8	0.4	61	20071005T195400
1963	50.0	0.4569	1.867	1069	5.6	0.4	57	20071005T193600

Continued on next page

Table B.2: $MgSO_4$ (aq) 0.0800 ± 0.001 m
– continued from previous page

P (MPa)	T (°C)	f (GHz)	v ($\frac{km}{s}$)	ρ ($\frac{kg}{m^3}$)	V^o ($\frac{mL}{mol}$)	V^{ex} (mL)	file	date (ISO 8601)
1969	50.2	0.4571	1.868	1069	5.7	0.4	58	20071005T193900
2981	50.2	0.4901	2.003	1098	12.8	0.3	55	20071005T192800
2988	50.3	0.4905	2.004	1098	12.8	0.3	56	20071005T193100
3054	50.1	0.4926	2.013	1100	13.3	0.3	64	20071005T200800
3056	50.2	0.4923	2.012	1100	13.3	0.3	63	20071005T200500
4033	50.1	0.5262	2.151	1125	20.2	0.3	66	20071005T201700
4040	50.1	0.5262	2.151	1125	20.2	0.3	65	20071005T201400
5007	49.8	0.5507	2.251	1147	27.1	0.3	53	20071005T191800
5007	50.1	0.5535	2.262	1147	27.0	0.3	68	20071005T202700
5010	49.9	0.5506	2.250	1147	27.1	0.3	54	20071005T192100
5012	50.1	0.5535	2.262	1147	27.1	0.3	67	20071005T202400
5982	50.1	0.5806	2.373	1168	33.9	0.3	70	20071005T203800
5988	50.1	0.5801	2.371	1168	33.9	0.3	69	20071005T203500
6917	49.9	0.5998	2.451	1186	40.5	0.3	51	20071005T190400
6953	50.1	0.6037	2.467	1186	40.7	0.3	72	20071005T204800
6960	50.1	0.6037	2.467	1187	40.8	0.3	71	20071005T204600
T = 50.3 to 92.7 °C								
1062	88.7	0.4282	1.750	1019	-13.0	0.6	77	20071005T214500
1066	90.9	0.4284	1.751	1018	-14.1	0.6	78	20071005T214800
5947	51.0	0.5715	2.336	1166	33.5	0.3	50	20071005T185600
5949	51.5	0.5708	2.333	1166	33.5	0.3	49	20071005T185300
T = 95.1 °C								
129	97.2	0.3863	1.579	977	-26.9	0.8	99	20071005T234400
134	97.3	0.3861	1.578	977	-26.9	0.8	100	20071005T234700
1034	97.3	0.4273	1.746	1013	-17.8	0.7	102	20071005T235500
1042	97.3	0.4279	1.749	1013	-17.7	0.7	101	20071005T235300
1068	92.7	0.4285	1.751	1017	-15.0	0.6	79	20071005T215100
1070	93.8	0.4281	1.750	1016	-15.6	0.6	80	20071005T215400
2033	96.2	0.4674	1.910	1047	-7.2	0.6	82	20071005T220500

Continued on next page

Table B.2: $MgSO_4$ (aq) 0.0800 ± 0.001 m
– continued from previous page

P (MPa)	T (°C)	f (GHz)	v ($\frac{km}{s}$)	ρ ($\frac{kg}{m^3}$)	V^o ($\frac{mL}{mol}$)	V^{ex} (mL)	file	date (ISO 8601)
2039	95.8	0.4674	1.910	1047	-7.0	0.6	81	20071005T220200
2970	97.4	0.4996	2.042	1073	1.7	0.5	97	20071005T233600
2975	97.4	0.4996	2.042	1073	1.8	0.5	98	20071005T233900
3027	96.8	0.5015	2.049	1075	2.5	0.5	84	20071005T221300
3038	96.8	0.5010	2.048	1075	2.6	0.5	83	20071005T221100
3995	97.2	0.5310	2.170	1099	12.1	0.4	86	20071005T222300
4000	97.2	0.5310	2.170	1099	12.2	0.4	85	20071005T222000
4030	97.4	0.5302	2.167	1100	12.4	0.4	104	20071006T000700
4038	97.4	0.5300	2.166	1100	12.5	0.4	103	20071006T000400
5017	97.3	0.5591	2.285	1122	22.4	0.4	89	20071005T225700
5017	97.4	0.5590	2.284	1122	22.4	0.4	90	20071005T230100
5020	97.3	0.5596	2.287	1122	22.4	0.4	88	20071005T223700
5026	97.4	0.5599	2.288	1122	22.5	0.4	87	20071005T223400
5998	97.3	0.5849	2.390	1142	32.3	0.3	92	20071005T231000
6008	97.3	0.5846	2.389	1143	32.4	0.3	91	20071005T230800
6773	97.5	0.6032	2.465	1157	40.2	0.3	95	20071005T232400
6819	97.5	0.6039	2.468	1158	40.6	0.3	94	20071005T232100
6898	97.5	0.6054	2.474	1160	41.4	0.3	93	20071005T231800
6980	97.3	0.6072	2.482	1161	42.2	0.3	106	20071006T001800
7006	97.4	0.6078	2.484	1162	42.5	0.3	105	20071006T001400

$MgSO_4$ (aq) 0.5103 ± 0.004 m

P (MPa)	T (°C)	f (GHz)	v ($\frac{km}{s}$)	ρ ($\frac{kg}{m^3}$)	V^o ($\frac{mL}{mol}$)	V^{ex} (mL)	file	date (ISO 8601)
T = -9.9 °C								
1947	-10.3	0.4366	1.777	1137	2.5	7.1	90	20070902T031800

Continued on next page

Table B.3: $MgSO_4$ (aq) 0.5103 ± 0.004 m

– continued from previous page

P (MPa)	T (^{o}C)	f (GHz)	v ($\frac{km}{s}$)	ρ ($\frac{kg}{m^3}$)	V^o ($\frac{mL}{mol}$)	V^{ex} (mL)	file	date (ISO 8601)
2686	-10.3	0.4640	1.889	1160	10.1	7.1	92	20070902T035200
2720	-10.3	0.4646	1.891	1161	10.4	7.1	91	20070902T034400
3025	-10.4	0.4763	1.939	1169	13.6	7.2	89	20070902T030600
3026	-10.5	0.4778	1.945	1169	13.5	7.2	88	20070902T025800
3033	-10.5	0.4773	1.943	1169	13.6	7.2	87	20070902T023800
3035	-10.3	0.4802	1.955	1169	13.7	7.2	98	20070902T023500
4025	-10.2	0.5159	2.096	1195	23.8	7.3	82	20070902T015300
4026	-10.2	0.5159	2.096	1195	23.8	7.3	83	20070902T015600
4027	-9.9	0.5155	2.094	1195	23.8	7.3	84	20070902T015900
4525	-9.4	0.5285	2.151	1206	28.9	7.4	99	20070902T043600
4996	-9.8	0.5440	2.210	1216	33.7	7.6	81	20070902T014700
4999	-9.6	0.5438	2.209	1216	33.7	7.6	80	20070902T014400
6227	-9.9	0.5779	2.352	1241	46.3	8.2	93	20070902T040000
T = -9.4 to -0.0 ^{o}C								
2968	0.2	0.4848	1.976	1165	14.0	6.1	46	20070901T222300
3005	0.1	0.4863	1.982	1165	14.4	6.1	45	20070901T221900
4528	-6.6	0.5320	2.166	1205	28.7	7.0	100	20070902T044200
4528	-7.9	0.5294	2.155	1205	28.8	7.2	101	20070902T043900
5007	-7.8	0.5445	2.212	1216	33.6	7.3	79	20070902T012900
5009	-7.3	0.5465	2.220	1216	33.6	7.3	78	20070902T012700
5012	-6.7	0.5468	2.221	1216	33.5	7.2	77	20070902T012300
5014	-6.1	0.5488	2.229	1215	33.5	7.1	76	20070902T012000
5016	-5.5	0.5484	2.228	1215	33.4	7.1	75	20070902T011500
5020	-4.6	0.5465	2.220	1215	33.3	6.9	74	20070902T010800
5022	-4.2	0.5485	2.229	1215	33.3	6.9	73	20070902T010500
5024	-3.5	0.5486	2.229	1215	33.2	6.8	72	20070902T010300
5026	-2.8	0.5478	2.226	1215	33.2	6.7	71	20070902T010000
5029	-2.0	0.5484	2.228	1214	33.1	6.6	70	20070902T005700
T = 0.2 ^{o}C								

Continued on next page

Table B.3: $MgSO_4$ (aq) 0.5103 ± 0.004 m
– continued from previous page

P (MPa)	T (^{o}C)	f (GHz)	v ($\frac{km}{s}$)	ρ ($\frac{kg}{m^3}$)	V^o ($\frac{mL}{mol}$)	V^{ex} (mL)	file	date (ISO 8601)
538	0.0	0.3849	1.566	1084	-8.2	6.5	41	20070901T213700
540	0.0	0.3842	1.564	1085	-8.2	6.5	42	20070901T214000
1002	0.0	0.4068	1.655	1103	-3.0	6.4	40	20070901T212900
1003	0.0	0.4079	1.660	1103	-3.9	6.4	39	20070901T212400
1004	0.0	0.4062	1.653	1103	-3.9	6.4	38	20070901T212100
1497	0.5	0.4302	1.751	1120	0.7	6.2	36	20070901T210100
1498	0.5	0.4291	1.746	1120	0.7	6.2	37	20070901T210400
2432	0.4	0.4647	1.891	1149	9.2	6.1	35	20070901T205400
2437	0.3	0.4646	1.891	1150	9.2	6.1	34	20070901T205000
2440	0.2	0.4655	1.895	1150	9.2	6.1	33	20070901T204700
2974	0.1	0.4847	1.969	1165	14.1	6.1	65	20070902T001300
2976	0.1	0.4850	1.971	1165	14.1	6.1	64	20070902T001000
4039	0.0	0.5210	2.117	1191	23.8	6.2	62	20070902T000100
4039	0.1	0.5212	2.118	1191	23.8	6.2	63	20070902T000400
5005	0.0	0.5484	2.228	1213	32.6	6.4	61	20070901T235300
5006	0.0	0.5488	2.230	1213	32.6	6.4	60	20070901T235000
5007	0.0	0.5468	2.222	1213	32.7	6.4	59	20070901T234700
5008	0.0	0.5490	2.230	1213	32.7	6.4	58	20070901T234500
5770	0.0	0.5701	2.316	1229	39.6	6.6	57	20070901T232700
5783	0.0	0.5709	2.319	1229	39.8	6.6	56	20070901T232400
5987	0.1	0.5754	2.338	1233	41.6	6.7	69	20070902T003800
5988	0.1	0.5752	2.337	1233	41.6	6.7	68	20070902T003500
6494	0.2	0.5899	2.397	1242	46.2	6.9	66	20070902T002300
6509	0.2	0.5904	2.398	1243	46.3	6.9	67	20070902T002000
T = 0.5 to 9.7 ^{o}C								
2454	2.0	0.4671	1.901	1149	9.5	5.9	30	20070901T203800
2463	3.0	0.4688	1.908	1149	9.7	5.9	32	20070901T203500
4049	9.4	0.5244	2.135	1188	23.6	5.3	6	20070901T164600
4057	9.4	0.5237	2.133	1188	23.6	5.3	5	20070901T164200

Continued on next page

Table B.3: $MgSO_4$ (aq) 0.5103 ± 0.004 m
– continued from previous page

P (MPa)	T (^{o}C)	f (GHz)	v ($\frac{km}{s}$)	ρ ($\frac{kg}{m^3}$)	V^o ($\frac{mL}{mol}$)	V^{ex} (mL)	file	date (ISO 8601)
6112	8.2	0.5833	2.377	1232	40.0	5.8	104	20070902T051200
6400	6.3	0.5868	2.391	1238	43.9	6.2	103	20070902T050800
T = 10.0 ^{o}C								
513	9.9	0.3953	1.610	1081	-5.7	5.9	17	20070901T190000
516	9.9	0.3945	1.607	1082	-5.7	5.9	18	20070901T190200
518	9.9	0.3956	1.612	1082	-5.7	5.9	19	20070901T190600
1016	9.9	0.4165	1.697	1101	-1.6	5.7	21	20070901T191600
1017	9.9	0.4163	1.696	1101	-1.6	5.7	20	20070901T191300
1996	9.9	0.4562	1.858	1133	6.5	5.4	16	20070901T185300
1998	9.9	0.4567	1.860	1133	6.6	5.4	15	20070901T184900
2000	9.8	0.4524	1.843	1133	6.6	5.4	14	20070901T184100
2565	9.9	0.4768	1.942	1150	11.3	5.3	26	20070901T200200
2578	9.9	0.4783	1.948	1150	11.4	5.3	25	20070901T195900
2584	9.9	0.4778	1.946	1150	11.4	5.3	24	20070901T195600
2730	9.9	0.4794	1.953	1154	12.6	5.3	22	20070901T192900
3989	10.0	0.5240	2.135	1186	23.1	5.2	13	20070901T175200
3995	9.8	0.5242	2.135	1186	23.1	5.2	9	20070901T174900
4187	9.8	0.5304	2.161	1191	24.7	5.2	11	20070901T183000
4210	9.8	0.5297	2.158	1191	24.9	5.2	10	20070901T182600
4774	10.3	0.5419	2.208	1204	29.5	5.3	12	20070901T175800
5000	10.3	0.5507	2.244	1209	31.4	5.3	110	20070902T053700
5813	10.2	0.5732	2.336	1225	38.1	5.5	109	20070902T052900
5955	10.3	0.5773	2.352	1228	39.3	5.6	106	20070902T052100
6040	9.8	0.5794	2.361	1230	40.1	5.6	108	20070902T051800
T = 10.3 to 21.0 ^{o}C								
4955	10.5	0.5494	2.239	1208	30.0	5.3	111	20070902T054000
4957	10.4	0.5515	2.247	1208	31.0	5.3	112	20070902T054600
T = 21.5 ^{o}C								
520	21.2	0.4017	1.636	1078	-3.8	5.4	4	20070831T143000

Continued on next page

Table B.3: $MgSO_4$ (aq) 0.5103 ± 0.004 m
– continued from previous page

P (MPa)	T (°C)	f (GHz)	v ($\frac{km}{s}$)	ρ ($\frac{kg}{m^3}$)	V^o ($\frac{mL}{mol}$)	V^{ex} (mL)	file	date (ISO 8601)
520	21.0	0.4015	1.635	1078	-3.8	5.5	5	20070831T143300
1513	21.0	0.4415	1.798	1113	3.7	4.0	6	20070831T144300
1513	21.0	0.4416	1.798	1113	3.7	4.0	7	20070831T144600
2326	21.2	0.4698	1.913	1138	9.9	4.7	16	20070831T174700
2326	21.3	0.4698	1.914	1138	9.9	4.7	17	20070831T175000
2327	21.5	0.4740	1.931	1138	9.9	4.7	14	20070831T172200
2327	21.5	0.4736	1.929	1138	9.9	4.7	15	20070831T172500
2538	21.1	0.4789	1.951	1144	11.5	4.6	10	20070831T150200
2539	21.1	0.4771	1.943	1144	11.5	4.6	9	20070831T145600
2540	21.1	0.4780	1.947	1144	11.5	4.6	8	20070831T145400
3005	21.3	0.4945	2.014	1157	15.0	4.5	20	20070831T180500
3006	21.3	0.4932	2.009	1157	15.0	4.5	19	20070831T180200
3090	21.3	0.4936	2.011	1159	15.7	4.5	18	20070831T175900
3623	21.3	0.5145	2.096	1172	19.7	4.4	25	20070831T183100
3684	21.3	0.5164	2.103	1174	20.2	4.4	24	20070831T182400
3730	21.3	0.5205	2.120	1175	20.5	4.4	23	20070831T181800
3916	21.4	0.5264	2.140	1179	21.9	4.4	15	20070903T094300
3916	21.3	0.5251	2.135	1179	21.9	4.4	16	20070903T094500
3917	21.3	0.5255	2.137	1179	21.9	4.4	17	20070903T094900
3933	21.4	0.5233	2.131	1180	22.0	4.4	21	20070831T180900
4020	21.6	0.5287	2.153	1181	22.7	4.4	2	20070903T081900
4020	21.6	0.5280	2.150	1181	22.7	4.4	3	20070903T082300
4021	21.7	0.5285	2.152	1181	22.7	4.4	4	20070903T082700
4292	21.5	0.5343	2.176	1188	24.8	4.4	27	20070831T184200
4510	21.8	0.5405	2.201	1193	26.4	4.4	26	20070831T183800
4868	22.0	0.5527	2.250	1200	29.1	4.4	7	20070903T084600
4890	22.0	0.5505	2.242	1201	29.2	4.4	6	20070903T084200
4942	22.0	0.5534	2.253	1202	29.6	4.4	5	20070903T083900
5666	21.7	0.5740	2.337	1217	35.1	4.5	10	20070903T090600

Continued on next page

Table B.3: $MgSO_4$ (aq) 0.5103 ± 0.004 m
– continued from previous page

P (MPa)	T (^{o}C)	f (GHz)	v ($\frac{km}{s}$)	ρ ($\frac{kg}{m^3}$)	V^o ($\frac{mL}{mol}$)	V^{ex} (mL)	file	date (ISO 8601)
5674	21.7	0.5739	2.337	1217	35.2	4.5	9	20070903T090200
5682	21.9	0.5739	2.337	1217	35.2	4.5	8	20070903T085900
6497	21.5	0.5961	2.424	1233	41.4	4.7	19	20070903T101000
6538	21.5	0.5967	2.426	1234	41.7	4.7	18	20070903T100700
T = 50.2 ^{o}C								
323	50.2	0.4075	1.657	1059	-5.9	5.0	39	20070903T125300
327	50.2	0.4073	1.656	1059	-5.9	5.0	40	20070903T125600
328	50.0	0.4073	1.656	1059	-5.8	5.9	41	20070903T130100
1022	50.2	0.4358	1.772	1084	0.0	5.4	37	20070903T124200
1024	50.2	0.4357	1.771	1084	0.0	5.4	38	20070903T124500
2015	50.2	0.4725	1.921	1115	5.0	4.7	36	20070903T123500
2032	50.1	0.4729	1.923	1116	6.1	4.7	35	20070903T123100
3011	49.9	0.5056	2.056	1143	13.0	4.2	33	20070903T121400
3012	49.9	0.5059	2.057	1143	13.0	4.2	34	20070903T121700
4017	50.1	0.5346	2.174	1167	20.1	3.8	32	20070903T115200
4019	50.0	0.5357	2.178	1167	20.1	3.8	31	20070903T114900
4020	50.0	0.5349	2.175	1167	20.1	3.8	30	20070903T114600
4962	50.0	0.5615	2.283	1188	26.7	3.5	29	20070903T113800
4970	50.0	0.5616	2.284	1188	26.8	3.5	28	20070903T112400
4978	50.0	0.5615	2.283	1188	26.8	3.5	27	20070903T112100
6038	50.6	0.5876	2.389	1209	34.2	3.4	26	20070903T111100
6152	50.1	0.5900	2.403	1212	35.1	3.4	47	20070903T134000
6193	50.1	0.5915	2.409	1212	35.4	3.4	46	20070903T133700
6230	50.1	0.5918	2.411	1213	35.6	3.4	45	20070903T133400
6328	50.2	0.5952	2.425	1215	36.3	3.4	44	20070903T132900
6440	50.2	0.5964	2.430	1217	37.1	3.4	43	20070903T132600
T = 50.6 to 94.4 ^{o}C								
6044	51.1	0.5892	2.396	1209	34.2	3.4	25	20070903T110200
6053	52.5	0.5895	2.397	1208	34.1	3.4	24	20070903T105800

Continued on next page

Table B.3: $MgSO_4$ (aq) 0.5103 ± 0.004 m

– continued from previous page

P (MPa)	T (^{o}C)	f (GHz)	v ($\frac{km}{s}$)	ρ ($\frac{kg}{m^3}$)	V^o ($\frac{mL}{mol}$)	V^{ex} (mL)	file	date (ISO 8601)
6064	53.5	0.5909	2.403	1208	34.1	3.4	23	20070903T105400
6074	57.0	0.5921	2.407	1206	33.0	3.5	22	20070903T104800
6079	58.0	0.5912	2.404	1206	33.9	3.5	21	20070903T104500
T = 94.8 ^{o}C								
319	95.0	0.4078	1.659	1035	-23.6	12.0	68	20070903T215900
323	95.0	0.4078	1.659	1035	-23.6	12.0	69	20070903T220200
1010	94.9	0.4380	1.781	1061	-16.8	11.2	66	20070903T215000
1011	95.0	0.4378	1.780	1061	-16.8	11.2	67	20070903T215400
1988	95.1	0.4750	1.932	1092	-7.2	10.1	64	20070903T213900
1992	95.1	0.4754	1.933	1092	-7.2	10.1	65	20070903T214200
2965	95.1	0.5073	2.063	1119	2.4	9.2	62	20070903T213000
2968	95.1	0.5072	2.063	1119	2.4	9.2	63	20070903T213300
4002	95.0	0.5391	2.193	1144	12.6	8.3	60	20070903T212100
4003	95.0	0.5389	2.192	1144	12.7	8.3	61	20070903T212400
5015	95.0	0.5672	2.307	1166	22.6	7.6	58	20070903T211100
5015	95.0	0.5672	2.307	1166	22.6	7.6	59	20070903T211400
5580	94.7	0.5809	2.363	1177	28.2	7.2	53	20070903T204500
5581	94.4	0.5816	2.366	1177	28.2	7.2	52	20070903T204100
6431	95.1	0.6015	2.447	1193	36.6	6.9	57	20070903T210300
6464	95.1	0.6018	2.447	1194	36.9	6.9	56	20070903T210000
6525	95.1	0.6029	2.452	1195	37.5	6.8	55	20070903T205700

$MgSO_4$ (aq) 0.9965 ± 0.001 m

P (MPa)	T (^{o}C)	f (GHz)	v ($\frac{km}{s}$)	ρ ($\frac{kg}{m^3}$)	V^o ($\frac{mL}{mol}$)	V^{ex} (mL)	file	date (ISO 8601)
T = -16.4 ^{o}C								

Continued on next page

Table B.4: $MgSO_4$ (aq) 0.9965 ± 0.001 m

– continued from previous page

P (MPa)	T (^{o}C)	f (GHz)	v ($\frac{km}{s}$)	ρ ($\frac{kg}{m^3}$)	V^o ($\frac{mL}{mol}$)	V^{ex} (mL)	file	date (ISO 8601)
2011	-16.4	0.4582	1.863	1188	1.5	19.4	63	20070826T005200
2018	-16.3	0.4603	1.871	1189	1.6	19.4	62	20070826T004600
2530	-16.3	0.4786	1.946	1203	7.3	19.4	65	20070826T011400
2550	-16.3	0.4807	1.954	1203	7.5	19.4	64	20070826T011000
3005	-16.4	0.4965	2.018	1215	12.5	19.6	67	20070826T013000
3020	-16.4	0.4954	2.014	1216	12.7	19.6	61	20070826T003400
3023	-16.5	0.4972	2.021	1216	12.7	19.7	59	20070826T002200
3025	-16.4	0.4996	2.031	1216	12.7	19.6	58	20070826T001700
4015	-16.5	0.5313	2.160	1239	23.7	20.2	56	20070826T000100
4017	-16.5	0.5309	2.158	1239	23.7	20.2	57	20070826T000400
5319	-16.4	0.5612	2.281	1266	38.1	21.4	54	20070825T234700
5319	-16.4	0.5617	2.283	1266	38.1	21.4	55	20070825T235100
6072	-16.5	0.5841	2.374	1281	46.4	22.4	52	20070825T233100
6076	-16.3	0.5823	2.367	1281	46.4	22.4	51	20070825T232500
6080	-16.3	0.5794	2.355	1281	46.5	22.4	50	20070825T231800
6084	-16.4	0.5821	2.366	1281	46.5	22.4	49	20070825T231400
6085	-16.5	0.5813	2.363	1281	46.6	22.5	48	20070825T231200
T = -9.7 ^{o}C								
522	-9.7	0.3956	1.610	1138	-11.9	18.1	23	20070825T170100
522	-9.8	0.3983	1.621	1138	-11.9	18.1	24	20070825T170700
523	-9.5	0.3967	1.614	1138	-11.8	18.0	22	20070825T165400
524	-9.4	0.3954	1.609	1138	-11.7	17.0	21	20070825T164900
525	-9.2	0.3976	1.618	1138	-11.7	17.0	19	20070825T164300
526	-9.1	0.3958	1.610	1138	-11.6	17.9	18	20070825T164000
1052	-10.1	0.4205	1.715	1157	-6.6	17.9	83	20070815T052900
1053	-10.1	0.4188	1.709	1157	-6.6	17.9	84	20070815T053200
1053	-10.1	0.4190	1.709	1157	-6.6	17.9	85	20070815T053500
1053	-10.1	0.4204	1.715	1157	-6.6	17.9	87	20070815T054100
1053	-10.2	0.4203	1.714	1157	-6.6	17.9	88	20070815T054600

Continued on next page

Table B.4: $MgSO_4$ (aq) 0.9965 ± 0.001 m
– continued from previous page

P (MPa)	T (^{o}C)	f (GHz)	v ($\frac{km}{s}$)	ρ ($\frac{kg}{m^3}$)	V^o ($\frac{mL}{mol}$)	V^{ex} (mL)	file	date (ISO 8601)
1359	-10.3	0.4336	1.769	1168	-3.5	17.8	90	20070815T055800
1359	-10.3	0.4349	1.774	1168	-3.5	17.8	91	20070815T060100
1359	-10.3	0.4349	1.774	1168	-3.5	17.8	92	20070815T060400
1696	-9.9	0.4486	1.830	1178	0.0	17.6	82	20070815T052400
1697	-9.7	0.4461	1.820	1178	0.1	17.6	81	20070815T052100
1700	-9.4	0.4483	1.829	1178	0.2	17.5	80	20070815T051800
1703	-9.2	0.4486	1.830	1178	0.3	17.5	79	20070815T051400
2648	-10.1	0.4835	1.972	1205	9.7	17.7	95	20070815T062000
2651	-10.1	0.4854	1.980	1205	9.8	17.7	94	20070815T061600
2720	-10.1	0.4864	1.984	1207	10.5	17.7	93	20070815T061300
3634	-10.3	0.5157	2.098	1230	19.8	18.0	28	20070825T174600
3681	-10.2	0.5156	2.098	1231	20.3	18.0	27	20070825T174100
4705	-9.8	0.5463	2.223	1253	30.8	18.6	32	20070825T180800
4735	-9.8	0.5447	2.216	1254	31.1	18.6	31	20070825T180400
4764	-10.0	0.5485	2.231	1254	31.4	18.7	30	20070825T180000
4799	-10.3	0.5476	2.228	1255	31.8	18.8	29	20070825T175600
5505	-9.4	0.5689	2.314	1269	38.8	19.2	36	20070825T184200
5509	-9.3	0.5690	2.315	1269	38.9	19.2	35	20070825T183700
5557	-9.2	0.5707	2.322	1270	39.3	19.2	33	20070825T182700
5567	-9.2	0.5713	2.324	1270	39.4	19.2	34	20070825T183200
6189	-9.5	0.5848	2.379	1282	45.8	20.0	41	20070825T193900
6242	-9.5	0.5853	2.381	1283	46.4	20.1	40	20070825T193400
6313	-9.6	0.5891	2.397	1284	47.1	20.2	39	20070825T192900
6482	-9.4	0.5942	2.418	1287	48.8	20.4	37	20070825T185200
6522	-9.7	0.5952	2.422	1288	49.3	20.5	38	20070825T192000
6752	-9.4	0.5987	2.436	1291	51.5	20.8	43	20070825T195900
6902	-9.5	0.6024	2.451	1294	53.1	21.0	42	20070825T195200
T = -9.1 to -0.4 ^{o}C								
523	-6.8	0.3992	1.623	1137	-10.8	17.5	12	20070825T154900

Continued on next page

Table B.4: $MgSO_4$ (aq) 0.9965 ± 0.001 m

– continued from previous page

P (MPa)	T (°C)	f (GHz)	v ($\frac{km}{s}$)	ρ ($\frac{kg}{m^3}$)	V^o ($\frac{mL}{mol}$)	V^{ex} (mL)	file	date (ISO 8601)
1704	-8.2	0.4497	1.835	1178	0.5	17.3	77	20070815T050600
1704	-8.7	0.4493	1.833	1178	0.4	17.4	78	20070815T050900
1707	-7.8	0.4473	1.825	1178	0.7	17.2	76	20070815T050200
1712	-7.1	0.4498	1.835	1178	0.9	16.0	75	20070815T045800
1715	-6.6	0.4500	1.836	1178	1.0	16.9	74	20070815T045500
1720	-5.8	0.4512	1.841	1178	1.3	16.7	73	20070815T045100
1725	-5.1	0.4517	1.843	1178	1.5	16.5	72	20070815T044700
1730	-4.3	0.4530	1.848	1178	1.7	16.3	71	20070815T044400
1733	-3.4	0.4533	1.849	1178	1.0	16.1	70	20070815T044000
T = 0.1 °C								
492	0.5	0.4048	1.652	1135	-8.5	16.1	63	20070815T032800
492	0.2	0.4053	1.653	1135	-8.6	16.1	64	20070815T033200
493	0.3	0.4032	1.645	1135	-8.5	16.1	65	20070815T033500
1008	0.0	0.4271	1.739	1154	-3.9	15.8	51	20070815T020800
1009	0.3	0.4279	1.742	1154	-3.8	15.7	49	20070815T020200
1009	0.1	0.4291	1.747	1154	-3.9	15.7	50	20070815T020400
1507	0.4	0.4486	1.825	1170	0.6	15.6	12	20070816T163400
1859	0.4	0.4600	1.877	1180	3.9	15.3	66	20070815T035000
1859	0.4	0.4627	1.888	1180	3.9	15.3	67	20070815T035200
1859	0.3	0.4601	1.877	1180	3.9	15.3	68	20070815T035700
2386	0.4	0.4800	1.954	1196	8.7	15.3	53	20070815T021900
2390	0.1	0.4781	1.946	1196	8.7	15.2	55	20070815T022700
2465	0.4	0.4771	1.942	1198	9.4	15.3	52	20070815T021600
2485	0.4	0.4815	1.960	1198	9.6	15.3	54	20070815T022300
3395	0.4	0.5133	2.094	1221	17.9	15.1	69	20070815T040800
T = 0.5 to 20.8 °C								
479	15.9	0.4179	1.701	1130	-4.8	13.9	20	20070818T205000
483	17.9	0.4166	1.696	1130	-4.5	13.8	19	20070818T204700
534	11.4	0.4152	1.690	1134	-5.3	14.4	35	20070815T001000

Continued on next page

Table B.4: $MgSO_4$ (aq) 0.9965 ± 0.001 m

– continued from previous page

P (MPa)	T (^{o}C)	f (GHz)	v ($\frac{km}{s}$)	ρ ($\frac{kg}{m^3}$)	V^o ($\frac{mL}{mol}$)	V^{ex} (mL)	file	date (ISO 8601)
534	11.5	0.4153	1.691	1134	-5.3	14.4	36	20070815T001200
534	11.4	0.4149	1.689	1134	-5.3	14.4	37	20070815T001500
1026	11.1	0.4333	1.764	1151	-1.3	13.0	46	20070815T010000
1513	1.5	0.4496	1.829	1170	1.0	15.2	11	20070816T162900
1514	11.2	0.4526	1.843	1166	2.7	13.5	40	20070815T002800
1515	11.3	0.4546	1.851	1166	2.7	13.5	39	20070815T002600
1515	2.8	0.4492	1.828	1169	1.3	14.0	10	20070816T162600
1519	11.3	0.4528	1.843	1167	2.8	13.5	38	20070815T002300
1519	4.3	0.4492	1.828	1169	1.6	14.7	9	20070816T162300
1522	5.8	0.4510	1.835	1169	1.9	14.4	8	20070816T161900
1529	8.3	0.4527	1.842	1168	2.5	13.9	7	20070816T161400
1537	11.5	0.4546	1.850	1167	2.9	13.5	6	20070816T160700
2578	11.0	0.4899	1.995	1197	11.4	12.0	43	20070815T004100
2578	10.9	0.4900	1.995	1197	11.4	13.0	44	20070815T004400
2581	11.2	0.4907	1.998	1197	11.5	12.0	42	20070815T003800
2842	11.1	0.4997	2.035	1203	13.6	12.9	45	20070815T005200
T = 21.1 ^{o}C								
487	21.2	0.4175	1.699	1129	-4.1	13.5	18	20070818T204400
516	21.3	0.4205	1.710	1130	-3.8	13.5	27	20070814T192000
516	21.3	0.4179	1.700	1130	-3.8	13.5	28	20070814T192300
516	21.4	0.4183	1.701	1130	-3.8	13.5	29	20070814T192800
522	21.2	0.4192	1.704	1130	-3.8	13.5	8	20070825T142300
895	21.0	0.4349	1.768	1143	0.0	13.1	4	20070814T152700
898	20.8	0.4347	1.767	1143	0.0	13.1	2	20070814T151400
1511	21.0	0.4573	1.859	1162	3.7	12.4	9	20070814T161800
1511	21.0	0.4565	1.856	1162	3.7	12.4	11	20070814T162400
1511	21.0	0.4564	1.856	1162	3.7	12.4	25	20070814T162100
1537	21.1	0.4576	1.860	1163	3.9	12.4	5	20070814T153500
2013	21.0	0.4763	1.936	1177	7.5	11.0	17	20070814T171600

Continued on next page

Table B.4: $MgSO_4$ (aq) 0.9965 ± 0.001 m

– continued from previous page

P (MPa)	T (°C)	f (GHz)	v ($\frac{km}{s}$)	ρ ($\frac{kg}{m^3}$)	V^o ($\frac{mL}{mol}$)	V^{ex} (mL)	file	date (ISO 8601)
2013	21.0	0.4771	1.940	1177	7.5	11.0	18	20070814T171900
2482	21.0	0.4910	1.996	1190	11.1	11.6	13	20070814T163200
2490	21.0	0.4916	1.999	1190	11.1	11.6	12	20070814T162900
3455	21.0	0.5233	2.128	1214	18.4	11.2	15	20070814T164600
3470	21.0	0.5227	2.125	1214	18.6	11.2	14	20070814T164200
4470	21.2	0.5510	2.240	1237	26.1	10.0	21	20070814T174400
4496	21.2	0.5514	2.242	1237	26.3	10.0	19	20070814T173800
T = 21.4 to 50.1 °C								
491	22.6	0.4203	1.711	1128	-3.9	13.4	17	20070818T203900
498	26.6	0.4213	1.715	1127	-3.4	13.2	16	20070818T203400
505	33.3	0.4227	1.720	1124	-3.2	13.2	15	20070818T202800
509	50.0	0.4280	1.740	1117	-4.6	14.4	6	20070817T104900
520	26.9	0.4223	1.718	1128	-3.2	13.2	4	20070818T180400
521	26.9	0.4194	1.706	1128	-3.2	13.2	2	20070818T175500
521	26.9	0.4209	1.712	1128	-3.2	13.2	3	20070818T175900
694	21.8	0.4258	1.734	1136	-2.4	13.2	3	20070825T115700
695	21.8	0.4278	1.743	1136	-2.4	13.2	2	20070825T114700
1776	27.1	0.4689	1.908	1168	5.9	11.7	5	20070818T181000
1785	28.5	0.4683	1.905	1167	5.0	11.6	6	20070818T181300
T = 50.5 °C								
509	50.3	0.4303	1.749	1117	-4.6	14.5	4	20070817T104300
510	50.1	0.4311	1.752	1117	-4.6	14.4	5	20070817T104600
1018	50.1	0.4488	1.825	1134	-1.0	13.5	7	20070817T105600
1018	50.2	0.4483	1.823	1134	-1.0	13.5	8	20070817T105900
1018	50.3	0.4481	1.822	1134	-1.0	13.5	9	20070817T110200
1597	50.3	0.4670	1.898	1151	3.0	12.5	2	20070817T103000
1598	50.5	0.4672	1.899	1151	3.0	12.5	3	20070817T103300
2501	50.8	0.5009	2.036	1176	9.3	11.2	13	20070817T111900
2502	50.6	0.4995	2.031	1176	9.4	11.2	11	20070817T111300

Continued on next page

Table B.4: $MgSO_4$ (aq) 0.9965 ± 0.001 m

– continued from previous page

P (MPa)	T (^{o}C)	f (GHz)	v ($\frac{km}{s}$)	ρ ($\frac{kg}{m^3}$)	V^o ($\frac{mL}{mol}$)	V^{ex} (mL)	file	date (ISO 8601)
2502	50.7	0.5026	2.043	1176	9.3	11.2	12	20070817T111600
2503	50.5	0.5012	2.037	1176	9.4	11.2	10	20070817T111000
3526	50.5	0.5304	2.156	1201	16.6	10.1	14	20070817T112800
3526	50.4	0.5312	2.159	1201	16.6	10.1	15	20070817T113100
4362	50.6	0.5538	2.252	1220	22.4	9.4	23	20070817T121100
4413	50.6	0.5544	2.254	1221	22.8	9.4	22	20070817T120800
4475	50.6	0.5576	2.267	1222	23.2	9.3	21	20070817T120500
4535	50.5	0.5571	2.265	1224	23.7	9.3	20	20070817T120200
4612	50.6	0.5593	2.274	1225	24.2	9.2	19	20070817T115800
4706	50.6	0.5624	2.287	1227	24.9	9.2	18	20070817T115500
4807	50.7	0.5660	2.301	1229	25.6	9.1	16	20070817T114800
4849	50.6	0.5677	2.308	1230	25.9	9.1	17	20070817T115200
T = 85.8 ^{o}C								
517	85.1	0.4294	1.744	1099	-16.2	24.6	31	20070817T133300
520	85.1	0.4295	1.744	1099	-16.2	24.6	32	20070817T133700
522	85.2	0.4296	1.745	1099	-16.2	24.6	33	20070817T134000
1050	86.7	0.4514	1.836	1116	-12.2	23.9	59	20070817T173600
1050	86.7	0.4515	1.836	1116	-12.2	23.9	60	20070817T174000
1885	84.3	0.4822	1.959	1142	-3.8	20.8	28	20070817T131900
1886	84.8	0.4818	1.957	1142	-3.0	21.0	29	20070817T132300
1886	84.9	0.4819	1.958	1142	-4.0	21.1	30	20070817T132600
2535	85.4	0.5043	2.048	1160	1.5	19.8	34	20070817T134700
2542	85.4	0.5040	2.047	1160	1.6	19.8	35	20070817T135300
2542	85.2	0.5038	2.047	1160	1.7	19.7	36	20070817T135700
4640	85.5	0.5612	2.279	1208	20.2	16.2	37	20070817T145900
4640	85.5	0.5623	2.284	1208	20.2	16.2	38	20070817T150300
4640	85.6	0.5613	2.280	1208	20.2	16.3	39	20070817T150600
4640	85.7	0.5613	2.280	1208	20.2	16.3	40	20070817T150900
5632	87.2	0.5893	2.397	1227	28.9	15.6	49	20070817T164500

Continued on next page

Table B.4: $MgSO_4$ (aq) 0.9965 ± 0.001 m

– continued from previous page

P (MPa)	T (°C)	f (GHz)	v ($\frac{km}{s}$)	ρ ($\frac{kg}{m^3}$)	V^o ($\frac{mL}{mol}$)	V^{ex} (mL)	file	date (ISO 8601)
5632	87.2	0.5894	2.397	1227	28.9	15.6	51	20070817T165100
5633	87.1	0.5830	2.373	1227	28.9	15.6	46	20070817T160500
5633	86.9	0.5893	2.397	1227	28.9	15.5	50	20070817T164800
5635	86.7	0.5903	2.398	1227	28.0	15.4	42	20070817T152900
5639	86.6	0.5878	2.388	1228	29.0	15.4	41	20070817T152700
6140	87.4	0.5998	2.439	1237	33.5	15.1	54	20070817T170700
6199	86.9	0.6029	2.452	1238	34.0	14.9	58	20070817T173000
6207	87.0	0.6003	2.441	1238	34.1	14.9	55	20070817T171800
6215	87.0	0.6023	2.449	1238	34.2	14.9	57	20070817T172600
6241	86.9	0.6035	2.454	1239	34.4	14.9	56	20070817T172300

$MgSO_4$ (aq) 1.5062 ± 0.004 m

P (MPa)	T (°C)	f (GHz)	v ($\frac{km}{s}$)	ρ ($\frac{kg}{m^3}$)	V^o ($\frac{mL}{mol}$)	V^{ex} (mL)	file	date (ISO 8601)
T = -10.3 °C								
1031	-10.2	0.4413	1.795	1207	-6.8	31.5	54	20070907T203600
1038	-10.4	0.4428	1.801	1207	-6.9	31.6	56	20070907T204300
1038	-10.5	0.4430	1.801	1207	-6.9	31.7	57	20070907T204700
1890	-10.0	0.4738	1.927	1232	1.0	31.1	53	20070907T202900
2745	-10.5	0.5026	2.044	1255	10.7	31.3	62	20070907T212700
2839	-10.6	0.5035	2.048	1257	11.6	31.4	59	20070907T210600
2855	-10.6	0.5045	2.052	1257	11.8	31.4	61	20070907T211900
3658	-10.3	0.5270	2.143	1276	20.1	31.7	64	20070907T214900
3740	-10.3	0.5286	2.150	1278	20.9	31.8	63	20070907T214200
4585	-10.4	0.5522	2.246	1296	29.6	32.8	72	20070907T231800
4591	-10.4	0.5543	2.254	1296	29.6	32.8	71	20070907T230900

Continued on next page

Table B.5: $MgSO_4$ (aq) 1.5062 ± 0.004 m

– continued from previous page

P (MPa)	T (°C)	f (GHz)	v ($\frac{km}{s}$)	ρ ($\frac{kg}{m^3}$)	V^o ($\frac{mL}{mol}$)	V^{ex} (mL)	file	date (ISO 8601)
4752	-10.4	0.5524	2.246	1299	31.3	33.0	67	20070907T221800
4852	-10.4	0.5584	2.271	1301	32.3	33.2	66	20070907T220800
4917	-10.3	0.5569	2.265	1303	32.0	33.2	65	20070907T220000
4981	-10.2	0.5613	2.283	1304	33.6	33.2	68	20070907T223000
5595	-10.5	0.5768	2.346	1316	39.0	34.5	74	20070907T233800
5603	-10.4	0.5751	2.339	1316	40.0	34.4	73	20070907T233100
5865	-10.3	0.5844	2.376	1321	42.7	34.9	70	20070907T225000
6007	-10.4	0.5872	2.388	1323	44.2	35.3	79	20070908T001300
6015	-10.4	0.5889	2.395	1323	44.3	35.3	78	20070908T000800
6022	-10.5	0.5884	2.393	1324	44.4	35.3	77	20070908T000400
6035	-10.5	0.5892	2.396	1324	44.5	35.4	76	20070907T235800
T = -9.9 to -0.5 °C								
1892	-9.9	0.4742	1.929	1232	2.0	31.0	52	20070907T202500
1895	-9.6	0.4721	1.920	1232	2.1	30.9	51	20070907T202100
1901	-8.8	0.4737	1.926	1232	2.4	30.6	50	20070907T201500
1905	-8.5	0.4739	1.927	1232	2.5	30.5	49	20070907T201200
1910	-8.2	0.4750	1.932	1232	2.6	30.4	48	20070907T200800
1914	-7.8	0.4752	1.932	1232	2.7	30.2	47	20070907T200500
1918	-7.3	0.4765	1.938	1232	2.9	29.0	46	20070907T200200
1930	-6.0	0.4765	1.938	1232	3.3	29.5	44	20070907T195300
1934	-5.5	0.4751	1.932	1232	3.4	29.3	43	20070907T195000
1938	-5.2	0.4779	1.943	1232	3.5	29.1	42	20070907T194700
1944	-4.7	0.4768	1.939	1232	3.7	28.9	41	20070907T194400
1948	-4.4	0.4781	1.944	1233	3.8	28.8	40	20070907T194000
1952	-4.2	0.4781	1.944	1233	3.9	28.7	39	20070907T193700
1958	-3.6	0.4786	1.946	1233	4.1	28.5	38	20070907T193300
1965	-3.2	0.4789	1.948	1233	4.2	28.3	37	20070907T192900
1977	-1.9	0.4801	1.953	1233	4.6	27.8	36	20070907T192200
1983	-1.3	0.4805	1.954	1233	4.8	27.5	35	20070907T191900

Continued on next page

Table B.5: $MgSO_4$ (aq) 1.5062 ± 0.004 m

– continued from previous page

P (MPa)	T (^{o}C)	f (GHz)	v ($\frac{km}{s}$)	ρ ($\frac{kg}{m^3}$)	V^o ($\frac{mL}{mol}$)	V^{ex} (mL)	file	date (ISO 8601)
5982	-2.0	0.5881	2.392	1320	42.0	30.5	82	20070908T004000
$T = 0.3$ °C								
409	0.3	0.4215	1.714	1184	-9.3	28.5	15	20070907T165500
409	0.3	0.4252	1.729	1184	-9.3	28.5	16	20070907T165900
409	0.2	0.4230	1.720	1184	-9.3	28.6	17	20070907T170300
409	0.1	0.4244	1.726	1185	-9.3	28.6	18	20070907T170600
410	0.0	0.4227	1.719	1185	-9.4	28.6	19	20070907T171000
999	0.1	0.4464	1.815	1204	-4.0	27.9	22	20070907T172700
1000	0.2	0.4467	1.817	1204	-4.0	27.9	21	20070907T172400
1007	0.1	0.4480	1.822	1204	-3.9	27.9	20	20070907T172000
2012	0.4	0.4818	1.960	1233	5.2	27.2	34	20070907T190400
2023	0.3	0.4841	1.971	1233	5.3	27.2	94	20070908T022000
2023	0.2	0.4833	1.968	1233	5.4	27.1	95	20070908T022400
2027	0.5	0.4820	1.960	1234	5.3	27.2	32	20070907T185700
2035	0.2	0.4821	1.961	1234	5.5	27.1	91	20070908T014900
2868	0.0	0.5094	2.071	1255	13.1	26.8	89	20070908T013600
2868	0.0	0.5089	2.070	1255	13.1	26.8	90	20070908T013900
3173	0.2	0.5184	2.108	1262	15.9	26.9	26	20070907T180200
3260	0.1	0.5211	2.119	1264	16.7	26.9	25	20070907T175700
3380	0.0	0.5243	2.132	1267	17.8	26.9	24	20070907T175200
3530	0.0	0.5275	2.145	1270	19.2	26.9	23	20070907T174800
4016	0.0	0.5415	2.202	1281	23.6	27.1	88	20070908T012700
4035	0.1	0.5419	2.204	1281	23.8	27.1	87	20070908T012400
4235	0.0	0.5453	2.217	1286	25.6	27.3	31	20070907T182400
4292	0.0	0.5483	2.230	1287	26.1	27.3	30	20070907T182100
4367	0.0	0.5496	2.235	1288	26.8	27.4	29	20070907T181800
4485	0.0	0.5524	2.247	1291	27.9	27.5	28	20070907T181400
5965	0.2	0.5881	2.392	1320	41.5	29.5	83	20070908T005200
6539	0.5	0.6030	2.452	1330	46.5	30.2	86	20070908T011400

Continued on next page

Table B.5: $MgSO_4$ (aq) 1.5062 ± 0.004 m

– continued from previous page

P (MPa)	T (°C)	f (GHz)	v ($\frac{km}{s}$)	ρ ($\frac{kg}{m^3}$)	V^o ($\frac{mL}{mol}$)	V^{ex} (mL)	file	date (ISO 8601)
6577	0.7	0.6031	2.453	1330	46.8	30.2	85	20070908T011100
6626	1.0	0.6031	2.453	1331	47.2	30.1	84	20070908T010800
T = 1.1 to 9.3 °C								
1023	6.0	0.4500	1.833	1203	-2.3	26.1	96	20070908T024500
1027	8.1	0.4504	1.834	1202	-1.8	25.4	97	20070908T024800
5988	4.8	0.5877	2.390	1318	40.6	27.1	81	20070908T003300
T = 9.9 °C								
318	10.3	0.4254	1.732	1178	-7.3	26.1	110	20070908T043400
320	10.3	0.4252	1.732	1178	-7.3	26.1	111	20070908T043700
1032	10.1	0.4518	1.840	1201	-1.4	24.0	98	20070908T025200
1110	9.5	0.4544	1.848	1204	0.9	25.0	14	20070907T161100
2074	9.3	0.4879	1.987	1231	7.1	23.0	100	20070908T031700
2076	10.0	0.4880	1.988	1231	7.2	23.8	99	20070908T030600
2621	10.1	0.5055	2.059	1245	11.7	23.4	101	20070908T032500
2965	10.4	0.5144	2.095	1253	14.6	23.1	102	20070908T033200
3927	10.3	0.5431	2.212	1275	22.5	23.0	103	20070908T034300
4688	10.4	0.5598	2.280	1291	28.8	23.3	106	20070908T040100
4760	10.4	0.5620	2.289	1292	29.4	23.3	105	20070908T035700
4869	10.4	0.5652	2.302	1295	30.3	23.4	104	20070908T035400
5625	10.3	0.5849	2.382	1309	36.6	24.1	109	20070908T042400
5658	10.3	0.5847	2.381	1310	36.8	24.2	108	20070908T042000
5707	10.4	0.5852	2.383	1311	37.2	24.2	107	20070908T041700
T = 10.5 to 22.1 °C								
1116	13.9	0.4565	1.856	1203	0.1	24.0	12	20070907T160200
1120	16.3	0.4576	1.861	1202	0.3	23.5	11	20070907T155900
1121	21.3	0.4589	1.866	1200	0.8	22.7	9	20070907T154800
1122	18.5	0.4590	1.867	1201	0.5	23.1	10	20070907T155500
2017	21.8	0.4906	1.997	1225	7.6	21.2	2	20070909T115900
2017	22.0	0.4906	1.996	1225	7.6	21.2	3	20070909T120200

Continued on next page

Table B.5: $MgSO_4$ (aq) 1.5062 ± 0.004 m

– continued from previous page

P (MPa)	T (^{o}C)	f (GHz)	v ($\frac{km}{s}$)	ρ ($\frac{kg}{m^3}$)	V^o ($\frac{mL}{mol}$)	V^{ex} (mL)	file	date (ISO 8601)
2866	22.0	0.5179	2.109	1246	13.0	20.2	3	20070911T140900
2873	21.9	0.5156	2.099	1246	14.0	20.2	2	20070911T140400
3027	22.0	0.5224	2.126	1250	15.2	20.1	5	20070909T121500
3068	22.0	0.5230	2.128	1251	15.5	20.0	4	20070909T121100
3922	22.0	0.5447	2.217	1270	21.9	19.6	6	20070909T122800
T = 22.1 ^{o}C								
500	22.2	0.4374	1.783	1180	-3.8	23.9	4	20070907T141700
500	22.2	0.4374	1.783	1180	-3.8	23.9	5	20070907T141700
1022	22.1	0.4577	1.866	1196	0.1	22.8	2	20070907T140100
1022	22.1	0.4578	1.866	1196	0.1	22.8	3	20070907T140400
2080	22.2	0.4939	2.013	1226	8.1	21.1	7	20070907T143800
2083	22.2	0.4946	2.016	1226	8.1	21.0	6	20070907T143400
3681	22.2	0.5384	2.191	1264	20.1	19.6	8	20070909T123900
3760	22.2	0.5404	2.199	1266	20.7	19.6	7	20070909T123400
5264	22.1	0.5810	2.364	1297	32.0	19.7	10	20070909T130300
5347	22.2	0.5817	2.367	1299	32.6	19.7	9	20070909T125900
T = 50.4 ^{o}C								
372	49.8	0.4379	1.782	1163	-5.5	25.7	26	20070911T213600
375	49.9	0.4372	1.779	1163	-5.5	25.8	27	20070911T214000
1196	49.0	0.4674	1.902	1189	0.4	23.0	22	20070911T194400
1197	49.0	0.4698	1.912	1189	0.4	23.0	21	20070911T193800
2034	49.1	0.4968	2.022	1212	6.3	20.8	19	20070911T191700
2034	49.0	0.4983	2.028	1212	6.3	20.8	20	20070911T192300
2991	49.2	0.5266	2.143	1236	12.0	18.8	23	20070911T211500
2991	49.5	0.5271	2.145	1236	12.9	18.8	24	20070911T211800
3640	49.2	0.5451	2.218	1250	17.5	17.7	18	20070911T190400
3685	49.0	0.5433	2.211	1251	17.9	17.6	17	20070911T185600
3737	49.2	0.5460	2.222	1253	18.2	17.5	16	20070911T185000
3747	51.7	0.5518	2.246	1251	17.0	17.7	13	20070911T181400

Continued on next page

Table B.5: $MgSO_4$ (aq) 1.5062 ± 0.004 m
– continued from previous page

P (MPa)	T (^{o}C)	f (GHz)	v ($\frac{km}{s}$)	ρ ($\frac{kg}{m^3}$)	V^o ($\frac{mL}{mol}$)	V^{ex} (mL)	file	date (ISO 8601)
4855	49.8	0.5756	2.342	1275	25.0	16.3	34	20070911T224400
4863	49.8	0.5769	2.348	1275	26.0	16.3	33	20070911T223300
4873	49.8	0.5802	2.361	1276	26.1	16.3	32	20070911T222400
4977	49.8	0.5785	2.354	1278	26.8	16.2	28	20070911T215700
5805	49.7	0.5982	2.438	1293	32.7	15.7	45	20070912T004800
5809	49.7	0.5971	2.433	1294	32.7	15.7	44	20070912T004400
6623	49.7	0.6146	2.505	1308	38.4	15.6	43	20070912T003200
6647	49.7	0.6152	2.507	1309	38.6	15.7	42	20070912T002900
6671	49.5	0.6183	2.520	1309	38.8	15.7	41	20070912T002700
6714	49.5	0.6177	2.517	1310	39.1	15.7	40	20070912T002300
T = 97.8 ^{o}C								
369	98.1	0.4335	1.767	1134	-25.0	54.2	52	20070912T020400
373	98.1	0.4334	1.766	1134	-24.0	54.2	53	20070912T020800
977	98.2	0.4589	1.870	1154	-18.9	51.3	55	20070912T021900
983	98.2	0.4585	1.869	1155	-18.8	51.2	54	20070912T021600
1950	98.1	0.4937	2.012	1183	-8.9	46.7	50	20070912T015400
1954	98.1	0.4944	2.015	1184	-8.9	46.6	51	20070912T015600
2991	98.2	0.5276	2.150	1210	1.7	42.5	57	20070912T023400
2992	98.2	0.5275	2.150	1210	1.7	42.5	56	20070912T023100
4002	98.0	0.5542	2.259	1233	12.0	38.8	49	20070912T014500
4004	97.4	0.5536	2.256	1234	12.2	38.3	47	20070912T013800
4004	97.7	0.5554	2.264	1234	12.1	38.6	48	20070912T014100
5005	98.3	0.5805	2.366	1254	22.2	36.1	59	20070912T025100
5010	98.2	0.5800	2.364	1254	22.3	36.0	58	20070912T024900

$MgSO_4$ (aq) 2.0137 ± 0.004 m

P (MPa)	T (°C)	f (GHz)	v ($\frac{km}{s}$)	ρ ($\frac{kg}{m^3}$)	V^o ($\frac{mL}{mol}$)	V^{ex} (mL)	file	date (ISO 8601)
T = 0.2 °C								
1023	0.2	0.4618	1.881	1252	-3.7	41.8	34	20070830T132700
1023	0.2	0.4637	1.889	1252	-3.7	41.8	35	20070830T133400
1972	0.1	0.4945	2.014	1278	4.9	40.8	29	20070830T124800
1974	0.1	0.4947	2.015	1278	4.9	40.8	30	20070830T125500
1975	0.2	0.4939	2.012	1278	4.0	40.7	31	20070830T130200
3236	0.3	0.5288	2.154	1308	16.5	40.3	38	20070830T140100
3336	0.3	0.5297	2.158	1311	17.4	40.3	37	20070830T135500
3449	0.4	0.5351	2.179	1313	18.4	40.3	36	20070830T134900
T = 10.3 °C								
516	10.7	0.4491	1.835	1233	-5.6	38.8	8	20070830T095400
516	10.4	0.4497	1.837	1234	-5.6	38.9	9	20070830T095900
517	10.3	0.4486	1.833	1234	-5.6	38.9	10	20070830T100200
1006	10.0	0.4661	1.904	1248	-1.6	37.9	12	20070830T101400
1007	10.0	0.4668	1.907	1248	-1.6	37.9	11	20070830T101100
1528	9.9	0.4832	1.974	1263	2.7	36.9	15	20070830T102700
1529	10.0	0.4845	1.979	1263	2.7	36.9	14	20070830T102300
1532	10.0	0.4840	1.977	1263	2.7	36.8	13	20070830T102000
2018	9.9	0.4995	2.041	1276	6.7	36.1	17	20070830T104200
2019	9.9	0.5013	2.048	1276	6.7	36.1	16	20070830T103900
2223	9.9	0.5059	2.066	1281	8.4	35.9	18	20070830T105200
2422	9.9	0.5108	2.087	1285	10.1	35.7	19	20070830T105800
3012	10.0	0.5281	2.157	1299	14.0	35.2	24	20070830T112400
3019	9.9	0.5283	2.158	1299	15.0	35.3	23	20070830T112100
3457	10.0	0.5401	2.206	1309	18.6	35.1	22	20070830T111400
3490	10.0	0.5387	2.201	1310	18.9	35.1	21	20070830T111100
3514	10.0	0.5414	2.212	1310	19.1	35.1	20	20070830T110800
T = 10.7 to 21.9 °C								
1697	21.5	0.4932	2.015	1262	5.1	32.0	2	20070830T081400

Continued on next page

Table B.6: $MgSO_4$ (aq) 2.0137 ± 0.004 m

– continued from previous page

P (MPa)	T (^{o}C)	f (GHz)	v ($\frac{km}{s}$)	ρ ($\frac{kg}{m^3}$)	V^o ($\frac{mL}{mol}$)	V^{ex} (mL)	file	date (ISO 8601)
1697	21.5	0.4935	2.016	1262	5.1	32.0	3	20070830T081700
T = 22.4 ^{o}C								
437	22.5	0.4497	1.829	1226	-4.3	36.3	5	20070827T200500
437	22.5	0.4498	1.829	1226	-4.3	36.3	6	20070827T200800
523	22.1	0.4513	1.844	1229	-3.7	36.1	6	20070830T084100
525	22.1	0.4526	1.849	1229	-3.7	36.0	7	20070830T084400
992	21.9	0.4705	1.908	1243	0.2	34.7	4	20070828T130200
993	22.0	0.4711	1.911	1243	0.1	34.7	5	20070828T130500
1088	22.6	0.4720	1.919	1245	0.6	34.3	4	20070827T200000
1089	22.5	0.4724	1.921	1245	0.6	34.3	3	20070827T195800
1493	22.8	0.4892	1.989	1256	3.7	33.2	9	20070827T203200
1502	22.4	0.4874	1.982	1257	3.7	33.2	8	20070827T201700
1508	22.6	0.4876	1.983	1257	3.8	33.2	7	20070827T201300
2005	22.0	0.5038	2.043	1270	7.5	32.2	6	20070828T131700
2005	22.1	0.5045	2.046	1270	7.5	32.2	7	20070828T131900
2005	22.0	0.5030	2.040	1270	7.5	32.2	8	20070828T132300
2495	22.4	0.5204	2.116	1282	11.2	31.2	10	20070827T204100
2570	22.2	0.5193	2.121	1284	11.7	31.2	5	20070830T083300
2572	22.1	0.5194	2.122	1284	11.8	31.2	4	20070830T083000
3022	22.1	0.5313	2.155	1294	15.1	30.6	9	20070828T133400
3022	22.0	0.5319	2.157	1294	15.1	30.6	10	20070828T134500
4046	22.1	0.5596	2.270	1316	22.9	29.8	11	20070828T135600
T = 50.5 ^{o}C								
499	50.0	0.4523	1.844	1215	-4.6	37.8	34	20070828T174100
500	50.0	0.4536	1.850	1215	-4.6	37.8	33	20070828T173600
990	50.0	0.4713	1.922	1230	-1.2	35.6	36	20070828T175500
995	50.0	0.4700	1.917	1230	-1.2	35.5	35	20070828T174900
2017	49.9	0.5040	2.055	1258	6.0	31.5	40	20070828T182400
2021	50.0	0.5053	2.061	1258	6.1	31.5	39	20070828T181900

Continued on next page

Table B.6: $MgSO_4$ (aq) 2.0137 ± 0.004 m

– continued from previous page

P (MPa)	T (°C)	f (GHz)	v ($\frac{km}{s}$)	ρ ($\frac{kg}{m^3}$)	V^o ($\frac{mL}{mol}$)	V^{ex} (mL)	file	date (ISO 8601)
2028	50.0	0.5037	2.054	1258	6.1	31.4	37	20070828T181000
2995	50.0	0.5313	2.166	1281	12.9	28.4	42	20070828T184000
3003	50.0	0.5310	2.165	1281	12.0	28.4	41	20070828T183500
4003	50.1	0.5586	2.278	1302	19.0	26.0	32	20070828T172100
4012	50.0	0.5592	2.280	1302	20.0	26.0	31	20070828T171200
4012	50.0	0.5588	2.279	1302	20.0	26.0	44	20070828T185600
4016	50.1	0.5579	2.275	1303	20.1	26.0	43	20070828T185000
4961	51.1	0.5830	2.377	1321	26.6	24.6	22	20070828T155900
4995	50.4	0.5844	2.383	1322	26.9	24.5	25	20070828T161500
5010	50.8	0.5844	2.383	1322	26.0	24.5	23	20070828T160500
5011	51.1	0.5855	2.387	1322	26.9	24.5	21	20070828T155600
5972	50.3	0.6041	2.464	1339	33.8	23.8	26	20070828T162500
6006	50.2	0.6044	2.464	1340	34.0	23.8	27	20070828T163200
6184	50.0	0.6085	2.482	1343	35.3	23.7	30	20070828T165900
6264	50.0	0.6092	2.484	1345	35.9	23.7	29	20070828T165100
6390	50.0	0.6129	2.499	1347	36.8	23.7	28	20070828T164300
T = 64.4 °C								
486	63.0	0.4544	1.851	1208	-7.6	43.3	47	20070828T192700
488	63.6	0.4546	1.851	1208	-7.8	43.7	48	20070828T193200
536	64.2	0.4518	1.840	1209	-7.6	43.8	63	20070828T215300
2005	65.5	0.5083	2.070	1250	2.9	37.3	51	20070828T194900
2011	65.0	0.5076	2.067	1250	3.1	36.0	50	20070828T194400
2014	64.6	0.5089	2.072	1250	3.2	36.7	49	20070828T194200
3515	65.8	0.5488	2.235	1285	14.2	31.6	53	20070828T200600
3525	65.7	0.5488	2.235	1285	14.3	31.6	52	20070828T200000
4552	65.7	0.5735	2.335	1306	21.0	28.7	55	20070828T202900
4594	65.8	0.5744	2.339	1307	22.3	28.6	54	20070828T202300
6303	65.5	0.6127	2.495	1338	35.1	25.8	58	20070828T205600
6399	65.7	0.6153	2.506	1340	35.8	25.7	57	20070828T205000

Continued on next page

Table B.6: $MgSO_4$ (aq) 2.0137 ± 0.004 m

– continued from previous page

P (MPa)	T (°C)	f (GHz)	v ($\frac{km}{s}$)	ρ ($\frac{kg}{m^3}$)	V^o ($\frac{mL}{mol}$)	V^{ex} (mL)	file	date (ISO 8601)
6720	65.8	0.6194	2.522	1345	38.3	25.5	56	20070828T204400
T = 94.3 °C								
538	94.4	0.4518	1.841	1189	-21.1	71.8	64	20070828T215600
1492	94.5	0.4878	1.987	1218	-11.8	65.4	66	20070828T220700
1495	94.4	0.4884	1.990	1218	-11.7	65.2	65	20070828T220300
2049	94.3	0.5075	2.067	1234	-6.3	61.6	62	20070828T214800
2051	94.0	0.5075	2.067	1234	-6.1	61.3	61	20070828T214500
2964	94.5	0.5365	2.185	1257	2.6	56.7	68	20070828T221800
2982	94.6	0.5356	2.182	1257	2.7	56.7	67	20070828T221400
3987	94.6	0.5570	2.269	1280	12.6	51.9	70	20070828T222800
3996	94.6	0.5556	2.263	1280	12.7	51.8	69	20070828T222500
4524	94.6	0.5775	2.352	1291	17.8	49.6	78	20070828T232800
4525	94.6	0.5773	2.352	1291	17.8	49.6	79	20070828T233100
5003	94.6	0.5826	2.373	1301	22.5	47.8	72	20070828T223800
5009	94.5	0.5822	2.372	1301	22.6	47.7	71	20070828T223500
5810	94.6	0.6026	2.455	1316	30.4	45.1	75	20070828T225900
5812	94.7	0.6022	2.453	1316	30.5	45.2	74	20070828T225600
5964	94.5	0.6052	2.465	1319	31.9	44.6	73	20070828T225000
6603	94.5	0.6152	2.506	1331	38.2	42.9	77	20070828T231900
6646	94.6	0.6160	2.509	1331	38.6	42.9	76	20070828T231300

Appendix C

REVISED HEAT FLOW ESTIMATES FOR EUROPA'S OCEAN USED IN THE CALCULATION OF THE TIME NEEDED TO MELT A ONE KILOMETER ICE SHELL

An estimate of ice thickness should be consistent with expected surface and bottom ice temperatures, at least in the simplification that the ice shell is not heated internally by tidal forces and cooling of the ice shell is entirely diffusive. Heat is transported by diffusion through the Europan ice shell. That is,

$$\frac{\delta T}{\delta t} = \kappa \frac{\delta^2 T}{\delta z^2} \tag{C.0}$$

where z denotes depth and κ is the thermal diffusivity of water ($\sim 10^{-7}$ m^2 s^{-1}). Thus, the diffusion time scale is $t \sim d^2/\kappa$, on the order of one million years for a O(1 km) thick ice shell. Heating in this region is determined by conduction (diffusion of heat):

$$Ht = \rho C_P d \Delta T \tag{C.0}$$

where d is the depth of the diffusive region and H is the heat production in W m^{-2}. Goodman et al. [2004] consider a broad range of global heat input to the base of Europa's ocean, for the range of extremes in which all or none of the tidal dissipation occurs in the rock underneath the ocean, at depth R: $F = 4\pi R^2 H = 0.1 - 100$ GW, or $H = 0.04 - 4$ mW m^{-2}, bracketing the estimates of O'Brien et al. [2002] and Thomson and Delaney [2001].

The difference in temperature between the top of the ice ($T_{surface} \sim 100$ K) and the bottom (melting temperature) is $T \sim 170$ K. For the lower heat flow estimate 0.04 (mW m^{-2}), the ice thickness needed for a liquid base is 200 km, twice our

assumed ocean depth, though only slightly thicker than H_2O layer thickness allowed by Galileo moment of inertia measurements [Anderson et al., 1998]. For the upper heat flow estimate, a self-consistent ice thickness is 4 km. The smallest heat flow that leads to melting ($\Delta T \sim 170$ K) within 100 km of Europa's surface is $H \sim 0.15$ mW m^{-2}. Therefore, we consider H between 0.15 and 4 mW m^{-2}.

Steven D. Vance

Education

Ph.D. Astrobiology and Geophysics, University of Washington, 2007
Thesis title: High Pressure and Low Temperature Equations of State for Aqueous Sulfate Solutions: Applications to the Search for Life in Extraterrestrial Oceans, with Particular Reference to Europa.

B.S. Physics, University of California, Santa Cruz, 2000
Thesis title: The role of methanol frost in particle sticking and the formation of planets in the early solar nebula.

Research Experience

NASA Postdoctoral Fellow — 2007–present
Chris Webster — Jet Propulsion Laboratory, Pasadena
Assisted with ground-based operation and developed scientific applications for the Mars Science Laboratory Tunable Laser Spectrometer. Investigated applications of new insights in physical chemistry to the structure and evolution of habitable planets.

Research Assistant — 2001–2007
J. Michael Brown and Evan Abramson — University of Washington, Seattle
Constructed and operated high-pressure instrumentation; collected and analyzed sound velocity data for aqueous solutions obtained by the method of impulsive stimulated scattering (ISS). Applied results to understanding physical processes in deep extraterrestrial oceans and hydrothermal systems.

Research Associate — 2003–2004
Jody Deming — Canadian Arctic Shelf Exchange Study
Prepared and inventoried shipboard laboratory on *CCGS* Amundsen while frozen into Franklin Bay, Northwest Territories, Canada; collected and preserved ice core samples for characterizing winter intra-ice bacterial populations.

Research Associate — 2003
Tilman Spohn — Institut für Planetologie, Münster
Reviewed hydrothermal systems literature and investigated means for modeling permeability of extraterrestrial seafloors.

Research Associate — 2001
Remington Stone — UCO/Lick Observatory
Operated Nickel reflector telescope for acquisition of optical SETI data. ~40 hours logged.

Research Assistant — 1998-2001
Frank Bridges — University of California, Santa Cruz
Designed and executed experiments investigating impact sticking of water- and methanol-frosted ices. Applied results to the problem of large-particle ($> cm$-size) formation in the early solar nebula.

Steven D. Vance

Teaching Experience

Founder and Facilitator — 2005-Present
UWAB Planetology Discussion Group — University of Washington, Seattle
Organized weekly reviews of selected journal articles pertaining to the formation and evolution of solar and extra-solar system objects.

Teaching Assistant — Winter 2004
Physics — University of Washington, Seattle
114/121: Waves/Mechanics. Taught three sections, approximately 20 students per section.

Visiting Scientist — 2002-2003
Project AstroBio — Seattle
Presented two guest lectures for a Seattle fifth grade class of approximately 30 students.

Tutor — 2002-2005
University Tutoring Service — Seattle
Taught three undergraduate or high-school students per year on average. Topics included algebra, trigonometry, calculus, physical chemistry and introductory physics.

Teaching Assistant — Spring-Summer, 2001
Physics Department — University of California, Santa Cruz
5B Labs: Wave motion in matter, including sound waves.

Mathematics and Physics Tutor — 1998-2001
Self-employed — University of California, Santa Cruz
Taught two undergraduate or high-school students per year on average. Topics included econometrics, calculus and introductory physics.

Service

American Geophysical Union Fall Meeting, 2006:

- Oral Session Chair, P31D, Once in a Blue Moon: The Surprising Diversity of Outer Planet Satellites I
- Poster Session Chair, P23E, Satellites, Rings, and Ices Posters,

Graduate Student Representative at Graduate Preliminary Examinations, Department of Earth and Space Sciences, University of Washington, Seattle, 2005-2006

Graduate Student Representative to Faculty, Department of Earth and Space Sciences, University of Washington, Seattle, 2004-2005

Awards and Honors

NASA Postdoctoral Fellowship, 2007-2008

Misch Fellowship, 2007

Stephens Graduate Support Grant, 2006

National Science Foundation IGERT/NASA Astrobiology Institute Grant, 2002-2005

Research support, University of Washington Alumni Grant, Winter and Spring, 200

Elks National Foundation Scholarship, 1996-2000 / Kern County Elks Scholarship, 1996

Howard and Mamie Nichols Scholarship, 1996-2000

Texaco Foundation Scholarship, 1996-2000

Steven D. Vance

Working Papers

Vance, S., J.M. Brown, E.H. Abramson and N. Castle, 2008. Equations of State for Aqueous MgSO4 to 2.0 m, 700 MPa from -20 to 100 °C. *in preparation for submission to Geochim. Cosmochim. Acta.*

Vance, S., J.M. Brown and E.H. Abramson, 2008. The Icy Satellite Interior Simulator, an Apparatus for Optical Measurements in Aqueous Systems in the range -20 to 100 °C and 700 MPa. *in preparation for submission to Rev. Sci Inst.*

Publications

Vance, S., J. Harnmeijer, J. Kimura, H. Hussmann, B. de Martin and J. M. Brown, 2007. Hydrothermal Systems in Small Ocean Planets. *Astrobiology, in press.*

Vance, S. 2005. Exploration & Characterization of Europa. *in* The Astrobiology Primer: An Outline of General Knowledge—Version 1, 2006. *Eds.* L.J. Mix, J.C. Armstrong, A.M. Mandell, A.C. Mosier, J. Raymond, S.N. Raymond, F.J. Stewart, K. von Braun, and O. Zhaxybayeva *Astrobiology* **6**, 735-813.

Vance, S. and J. M. Brown, 2005. Layering and Double-Diffusion Style Convection in Europa's Ocean. *Icarus* **177**, 506-514.

Vance, S., 2003. Signs of Liquid Water; Life on Jupiter's Moon Europa? *Planets & Life, A Newsletter of the Center for Astrobiology and Early Evolution* **5**, 4.

Oral Presentations

Vance, S. and J.M. Brown, 2007. Europan Ocean Sulfate Chemistry To 700 MPa From -20 to 100 °C. *Eos Trans. AGU, Fall Meet. Suppl.*, Abstract P52A-03

Vance, S., J. Harnmeijer and J. M. Brown 2005. Hydrothermal Systems in Europa's Seafloor. NASA Astrobiology Institute Annual Meeting, Boulder, CO.

Vance, S. and J. M. Brown 2005. Double-Diffusive Convection and Other Modes of Salinity-Modulated Heat and Material Transport in Europa's Ocean. LPSC XXXVI, Houston, TX.

Vance, S. and F. G. Bridges, 2003. Methanol Sticking and the Accretion of Centimeter-Size Particles in the Solar Nebula. *Meteoritics & Planetary Science* **38**, A141.

Poster Presentations

Vance, S., J. Harnmeijer, and J. M. Brown, 2006. The Depth of Fluid Circulation in Icy-Moon Hydrothermal Systems: Implications for Production of Heat and H_2 from Serpentinization. *Astrobiology* **6**, 217.

Vance, S., J. Harnmeijer, and J. M. Brown, 2005. Serpentinization-Driven Systems in the Seafloors of Icy Moons, *Eos Trans. AGU*, 86(52), Fall Meet. Suppl. Abstract P51D-0970.

Vance, S., and J. M. Brown 2004. Layering and Double-Diffusion Style Convection in Europa's Ocean. *Eos Trans. AGU*, **85**(47), Fall Meet. Suppl., Abstract P31A-0966.

Harnmeijer, J., and S. Vance, 2004. The Biopotential of Europa's Ocean: Contribution from Exogenous Sources. Bioastronomy Conference, Reykjavik, Iceland. *Astrobiology* **4**, 302.